

Charles University in Prague

Faculty of Science

Study program: Physical Chemistry



Mgr. Jakub Pastva

Preparation and characterization of new materials for metathesis and adsorption

Dissertation

Supervisor: Prof. Ing. Čejka Jiří, DrSc.

Prague, 2016

Univerzita Karlova v Praze

Přírodovědecká fakulta

Studijní program: Fyzikální chemie



Mgr. Jakub Pastva

Příprava a charakterizace nových materiálů pro metatéze a adsorpci

Disertační práce

Školitel: Prof. Ing. Čejka Jiří, DrSc.

Praha, 2016

Prohlášení:

Na disertační práci jsem pracoval v oddělení Syntézy a katalýzy na Ústavu fyzikální chemie J. Heyrovského, AV ČR.

Prohlašuji, že jsem závěrečnou práci zpracoval samostatně, a že jsem uvedl všechny použité informační zdroje a literaturu. Tato práce, ani její podstatná část, nebyla předložena k získání jiného nebo stejného akademického titulu.

V Praze, 29.9.2016

Podpis

Acknowledgements

This work was done at the Department of Synthesis and Catalysis of the J. Heyrovsky Institute of Physical Chemistry of the CAS, v. v. i. in Prague.

I would like to express my special thanks of gratitude to my supervisor Prof. Ing. Jiří Čejka, DrSc., for his valuable and constructive suggestions during the planning and development of this research work. His willingness to give his time so generously has been very much appreciated. Many thanks belong to RNDr. Hynek Balcar, CSc., my consultant, for his advices and assistance in keeping my progress on schedule. My grateful thanks are also extended to Dr. A. Zukal for his support over the years.

I would like to thank all people who helped me with the work, especially to Ing. N. Žilková for GC analysis, Dr. J. Pinkas, Dr. M. Lamač, and Dr. J. Dědeček for NMR spectroscopy, Doc. J. Sedláček from Charles University for SEC analysis, Dr. L. Brabec for recording SEM images. I also thank all the people from the group of Prof. Čejka for all kind of help, especially to Martin Kubů, Pavla Chlubná, Tushar Shinde, David Bek, and Michal Mazur.

Finally, I wish to thank my family for their support and encouragement throughout my study.

List of used symbols and abbreviations

| | |
|----------------------|---|
| A | adsorbed amount (cm ³ /g STP) |
| Å | Angstrom |
| ADMET | acyclic-diene metathesis |
| AlIB | allylbenzene |
| BET | Brunauer-Emmett-Teller method |
| BJH | Barrett-Joyner-Halenda method |
| Boc | <i>tert</i> -butyloxycarbonyl |
| Bu | butyl |
| C | concentration (mol/l) |
| CIT | (-)- β -citronellene |
| CM | cross-metathesis |
| COE | cyclooctene |
| Cy | cyclohexyl |
| <i>D</i> | average pore size diameter (nm) |
| Da | Dalton |
| DAB | <i>cis</i> -1,4-diacetoxy-2-butene |
| DAC | <i>tert</i> -butyl <i>N,N</i> -diallylcarbamate |
| DAF | <i>N,N</i> -diallyl-2,2,2-trifluoroacetamide |
| DEDAM | diethyl diallylmalonate |
| DHPETS | 2-(dicyclohexylphosphino)ethyltriethoxysilane |
| Et | ethyl |
| FID | flame ionization detector |
| FTIR | Fourier transform infrared spectroscopy |
| GC | gas chromatography |
| HexAc | 5-hexenyl acetate |
| ICP-MS | inductively coupled plasma mass spectrometry |
| <i>I_n</i> | polydispersity index |

| | |
|--------------|--|
| <i>i</i> -Pr | isopropyl |
| IUPAC | The International Union of Pure and Applied Chemistry |
| <i>K</i> | reaction rate constant |
| KJS | Kruk, Jaroniec and Sayari method |
| M_n | number average molecular weight |
| M_w | weight average molecular weight |
| MCM | Mobil Composition Matter |
| MMS | mesoporous molecular sieves |
| Me | methyl |
| MEOI | methyl oleate |
| NHC | <i>N</i> -heterocyclic carbene |
| NMR | nuclear magnetic resonance |
| OD | 1,7-octadiene |
| p/p_0 | relative pressure |
| Ph | phenyl |
| <i>ppm</i> | parts per million (= mg/kg) |
| PSA | pressure swing adsorption |
| R | alkyl |
| RCM | ring-closing metathesis |
| ROMP | ring-opening metathesis |
| RRM | ring-rearrangement metathesis |
| <i>rpm</i> | rotations per minute |
| RRM | ring-rearrangement metathesis |
| S_{BET} | BET area |
| SBA | Santa Barbara Amorphous |
| SEC | size-exclusion chromatography |
| SEM | scanning electron microscopy |
| SG-1, SG-2 | sol-gel materials n. 1 and 2 |
| SIMes | <i>N</i> -heterocyclic carbene, where S indicates a saturated backbone |

| | |
|----------|---|
| SM | self-metathesis |
| STP | standard temperature and pressure (0 °C, 101.325 kPa) |
| TBS | <i>tert</i> -butyldimethylsilyl |
| TEOS | tetraethyl orthosilicate |
| THF | tetrahydrofuran |
| TON | turnover number |
| Ts | methylbenzenesulfonamide |
| UV-Vis | ultraviolet–visible |
| V_{ME} | pore volume (cm ³ /g) |
| WHSV | weight hour space velocity |
| XPS | X-ray photoelectron spectroscopy |
| XRD | X-ray diffraction |
| Δ | chemical shift (ppm) |

List of publications

The Ph.D. thesis is based on the following publications:

- 1) Arnošt Zukal, Jakub Pastva, Jiří Čejka.
MgO-modified mesoporous silica's impregnated by potassium carbonate for carbon dioxide adsorption.
Microporous and Mesoporous Materials 167 (2013) 44 – 50.
- 2) Jakub Pastva, Jiří Čejka, Naděžda Žilková, Oto Mestek, Mojca Rangus, Hynek Balcar.
Hoveyda-Grubbs first generation type catalyst immobilized on mesoporous molecular sieves.
Journal of Molecular Catalysis A: Chemical 378 (2013) 184 – 192.
- 3) Jakub Pastva, Stefan J. Czarnocki, Jiří Čejka, Naděžda Žilková, Krzysztof Skowerski, Hynek Balcar.
Ru based complexes immobilized on mesoporous silica via quaternary ammonium tag.
ACS Catalysis 4 (2014) 3227 – 3236.

Further publications:

- 4) Michal Setnička, Pavel Čičmanec, Roman Bulánek, Arnošt Zukal, Jakub Pastva.
Hexagonal mesoporous titanosilicates as support for vanadium oxide - Promising catalysts for the oxidative dehydrogenation of n-butane.
Catalysis Today 204 (2013) 132 – 139.
- 5) Michal Setnička, Pavel Čičmanec, Roman Bulánek, Arnošt Zukal, Jakub Pastva.
Vanadium mesoporous silica catalyst prepared by direct synthesis as high performing catalyst in oxidative dehydrogenation of n-butane.
Catalysis Letters 144 (2014) 50 – 55.
- 6) Sabina Petrášová, Arnošt Zukal, Jiří Brus, Hynek Balcar, Jakub Pastva, Jiří Zedník, Jan Sedláček.
New hyper-crosslinked partly conjugated networks with tunable composition by spontaneous polymerization of ethynylpyridines with bis(bromomethyl)arenes: synthesis, spectral properties, and activity in CO₂ capture.
Macromolecular Chemistry and Physics 214 (2013) 2856 – 2866.

- 7) Krzysztof Skowerski, Jakub Pastva, Stefan J. Czarnocki, Jana Janošcová.
Exceptionally Stable and Efficient Solid Supported Hoveyda-Type Catalyst.
Organic Process Research and Development 19 (2015) 872–877.
- 8) Š. Botková, L. Čapek, M. Setnička, R. Bulánek, P. Čičmanec, A. Kalužová, J. Pastva, A. Zúkal.
VO_x species supported on Al₂O₃–SBA-15 prepared by the grafting of alumina onto SBA-15: structure and activity in the oxidative dehydrogenation of ethane.
Reaction Kinetics, Mechanisms and Catalysis 119 (2016) 319–333.

Abstract

The main objective of this work was to evidence versatile applications of ordered siliceous mesoporous materials, especially in adsorption and catalysis. For these reasons four mesoporous molecular sieves (SBA-15, SBA-16, MCM-41, and MCM-48) with different structures and textural properties have been chosen.

To show the possible application of mesoporous molecular sieves as a CO₂ adsorbent, magnesium oxide, and potassium carbonate were incorporated into SBA-15, SBA-16, and MCM-48 silicas. In order to avoid destruction of silica supports, a novel procedure based on the precipitation of magnesium acetate on the silica surface was developed. Subsequent *in situ* chemical conversion of magnesium acetate provided magnesium oxalate, while magnesium oxide was formed by calcination. To introduce potassium carbonate, silica modified with MgO was impregnated with potassium oxalate followed by its conversion to carbonate. All prepared mesoporous adsorbents preserved characteristic features of mesoporous molecular sieve (large surface areas, narrow pore size distributions). The comparison of carbon dioxide isotherms obtained on prepared samples revealed that their adsorption properties are influenced by the type of mesoporous structure. The SBA-15 silica containing magnesium oxide and promoted by potassium carbonate exhibited the steepest adsorption isotherm. The CO₂ adsorption capacity of this sample was higher than those of analogous samples prepared from SBA-16, and MCM-48. The amount adsorbed at 100 kPa and 20 °C increased in the order Mg/K-SBA-16 (10.3 cm³/g) < Mg/K-MCM-48 (12.7 cm³/g) < Mg/K-SBA-15 (18.8 cm³/g).

Mesoporous molecular sieves were used as supports for the preparation of new heterogeneous metathesis catalysts by immobilization of Ru alkylidenes (homogeneous catalysts highly active and tolerant towards a variety of functional groups in substrates). New heterogeneous catalysts for metathesis reactions were prepared either by immobilization *via* phosphine linkers or *via* non-covalent interactions. New catalysts were prepared by immobilization of the Hoveyda-Grubbs 1st generation-type catalyst (**RC-304**), and the Grubbs 2nd generation catalyst (**G-II**) onto the surface of mesoporous molecular sieves bearing dicyclohexylphosphine groups (PCy₂). The Hoveyda-Grubbs 2nd generation-type catalysts bearing a polar quaternary ammonium group in *N*-heterocyclic ligand were immobilized *via* non-covalent interaction onto the surface of mesoporous molecular sieves. The catalysts are bound to the silica surface by adsorption probably with a participation of surface silanol bonds.

UV-Vis spectroscopy, solid state NMR, X-ray powder diffraction and elemental analysis were used to determine structures of prepared heterogeneous catalysts. For textural characterization of the catalysts, nitrogen adsorption measurement was used. In all cases, the

mesoporous structure and morphology of the support remained unaffected by the immobilization process.

The activity of prepared catalysts was tested in various metathesis reactions. They were highly active in ring-closing metathesis (RCM) of 1,7-octadiene, diethyl diallylmalonate, *N,N*-diallyl-2,2,2-trifluoroacetamide, *tert*-butyl *N,N*-diallylcarbamate, (-)- β -citronellene, and allyl ether, self-metathesis and cross-metathesis (CM) of 5-hexenyl acetate, methyl 10-undecenoate, 1-decene, methyl oleate; allylbenzene with *cis*-1,4-diacetoxy-2-butene, and in ring-opening metathesis polymerization (ROMP) of cyclooctene. In many cases, high TONs (up to 16 000) at nearly 100 % selectivity were achieved. Depending on the support used, the catalyst activity was found to increase with increasing pore size of mesoporous molecular sieves.

All catalysts were easily separable from reaction mixtures, and in some cases they exhibited very low Ru leaching, enabling easy preparation of products with Ru content below 10 ppm (which is an acceptable level for pharmaceutical use). Successful catalyst reusing was achieved in most cases. These catalysts proved to have those properties: (i) preservation of high activity and selectivity of the parent homogeneous catalysts; (ii) easy catalyst separation; (iii) (multiple) catalyst reusing; and (iv) catalyst residue-free products.

Abstrakt

Hlavním cílem této práce bylo ukázat univerzální použití křemičitých mezoporézních materiálů s pravidelnou strukturou, zejména v adsorpci a katalýze. Z těchto důvodů byla zvolena čtyři mezoporézní molekulová síta (SBA-15, SBA-16, MCM-41 a MCM-48) s různou strukturou a texturními vlastnostmi.

Abychom dokázali, že molekulová síta jsou vhodná pro adsorpci CO₂, oxid hořečnatý a uhličitán draselný byly včleňovány (inkorporovány) do různých druhů silikátových materiálů: SBA-15, SBA-16 a MCM-48. K zamezení destrukce mezoporézního materiálu byl vyvinut nový proces přípravy založený na srážení octanu hořečnatého na silikátovém povrchu používaných molekulových sít. Chemická konverze (*in situ*) octanu hořečnatého poskytla šťavelan hořečnatý. Po kalcinaci takto modifikovaných materiálů bylo dosaženo vzniku oxidu hořečnatého na jejich povrchu. Silika obsahující MgO byla impregnována šťavelanem draselným, který byl následně přeměněn (konvertován) na uhličitán draselný. Všechny syntetizované adsorbenty si zachovaly charakteristické vlastnosti mezoporézních molekulových sít (velký objem a úzká distribuce velikosti pórů). Porovnáním adsorpčních izoterm CO₂ získaných na připravených materiálech vyplývá, že adsorpční vlastnosti těchto materiálů jsou závislé na typu mezoporézní struktury. Silika SBA-15 obsahující MgO s uhličitánem draselným vykazovala nejstrmější adsorpční izotermu. Adsorpční kapacita pro CO₂ tohoto vzorku byla větší než obdobně připravené vzorky z SBA-16 a MCM-48. Adsorbované množství CO₂ při tlaku 100 kPa a teplotě 20 °C vzrostlo v pořadí: Mg/K-SBA-16 (10,3 cm³/g) < Mg/K-MCM-48 (12,7 cm³/g) < Mg/K-SBA-15 (18,8 cm³/g).

Mezoporézní molekulová síta byla použita jako nosiče pro nové heterogenní metatezní katalyzátory, které byly připraveny imobilizací homogenních Ru alkylidenů (jenž jsou velmi aktivní a odolné vzhledem k velkému množství organických funkčních skupin). Nové heterogenní metatezní katalyzátory byly připraveny pomocí imobilizace přes fosfinový linker nebo cestou přímé nekovalentní interakce. Nově připravené katalyzátory byly připraveny imobilizací Ru alkylidenu Grubbs-Hoveyda první generace (**RC-304**) a Grubbs druhé generace (**G-II**) na povrchu mezoporézních molekulových sít obsahujících funkční skupiny dicyklohexylfosfinu (PCy₂). Alkyliden typu Grubbs-Hoveyda druhé generace mající polární kvartérní amoniovou skupinu v NHC ligandu byl také imobilizován na povrchu molekulových sít přímou cestou nekovalentní interakce (pravděpodobně se jedná o adsorpci s participací povrchových OH skupin použitých nosníků).

K určení struktury heterogenních katalyzátorů byly použity tyto fyzikálně chemické metody: UV-Vis spektroskopie, NMR spektroskopie pevné fáze, rentgenová difrakce a elementární analýza. Stanovení texturních vlastností heterogenních katalyzátorů bylo

provedeno pomocí adsorpce dusíku. Ve všech případech nově připravených heterogenních katalyzátorů byla zachována struktura a morfologie použitých mezoporezních sítí.

Připravené katalyzátory byly testovány v několika metatezních reakcích. Byly vysoce aktivní v RCM 1,7-oktadienu, diethyl diallylmalonátu, *N,N*-diallyl-2,2,2-trifluoroacetamidu, *tert*-butyl *N,N*-diallylcarbamátu, (-)- β -citronellenu a allyletheru; v self-metatezi 5-hexenylacetátu, metyl-10-undecenoátu, 1-decenu, metyloléátu, v cross-metatezi (CM) allylbenzenu s *cis*-1,4-diacetoxy-2-butene; a v ROMP cyklooktenu. V mnoha případech bylo dosaženo TON až 16 000 s prakticky 100 % selektivitou na žádané produkty. V závislosti na použitém nosiči, katalytická aktivita stoupala se zvětšující se velikostí pórů použitých mezoporezních molekulových sítí.

Všechny katalyzátory bylo možno snadno odseparovat z reakční směsi. V některých případech vykazovaly velmi nízký stupeň vymývání Ru do reakční směsi, čímž umožňovaly snadnou přípravu metatezních produktů s obsahem Ru nižším než 10 ppm (což je akceptovatelná úroveň pro farmaceutický průmysl). Ve většině případů byly katalyzátory úspěšně vícenásobně používány. Tyto katalyzátory vykazovaly následující vlastnosti: (i) vysoká aktivita a selektivita; (ii) jednoduchá separace katalyzátorů z reakční směsi; (iii) několikanásobné použití katalyzátorů; (iv) nízký obsah Ru v metatezních produktech.

Content

| | |
|--|----|
| 1. Aims of the thesis..... | 1 |
| 2. Introduction..... | 2 |
| 2.1. Molecular sieves..... | 2 |
| 2.1.1. Mesoporous molecular sieves..... | 2 |
| 2.2. Carbon dioxide..... | 6 |
| 2.2.1. Solid adsorbents..... | 7 |
| 2.3. Olefin metathesis..... | 11 |
| 2.2.1. Mechanism..... | 12 |
| 2.3.2. Types of olefin metathesis reactions..... | 13 |
| 2.3.3. Catalysts..... | 16 |
| 2.3.3.1. Ill-defined catalysts..... | 16 |
| 2.3.3.2. Well-defined catalysts..... | 17 |
| 2.3.4. Strategies for immobilizing Ru-alkylidenes complexes..... | 26 |
| 2.3.5. Application of MMS as support for metathesis catalysts..... | 34 |
| 3. Experimental part..... | 36 |
| 3.1. Applied chemicals..... | 36 |
| 3.1.1. List of chemicals..... | 36 |
| 3.1.2. Purification of solvents and substrates..... | 39 |
| 3.2. Synthesis of mesoporous molecular sieves..... | 40 |
| 3.2.1. Synthesis of SBA-15..... | 40 |
| 3.2.2. Synthesis of MCM-41..... | 40 |
| 3.2.3. Synthesis of MCM-48..... | 40 |
| 3.2.4. Synthesis of SBA-16..... | 40 |
| 3.2.5. Synthesis of SG-1 and SG-2..... | 41 |
| 3.3. Modifications of mesoporous molecular sieves..... | 41 |
| 3.3.1. Modification of mesoporous sieves for immobilization of metathesis catalysts..... | 41 |
| 3.3.2. Modification of mesoporous sieves for adsorption of carbon dioxide..... | 42 |
| 3.4. Preparation of the metathesis catalysts..... | 42 |
| 3.4.1. Immobilization of Ru alkylidenes <i>via</i> linker..... | 43 |

| | |
|---|----|
| 3.4.2. Immobilization of Ru alkylidenes <i>via</i> non covalent interaction..... | 43 |
| 3.4.3. Immobilization of Hoveyda–Grubbs alkylidenes on SG supports through the alkylidene ligand..... | 44 |
| 3.5. Characterization of prepared materials | 48 |
| 3.5.1. Characterization of the MMS, adsorbents and catalysts..... | 48 |
| 3.5.2. Characterization of substrates and products | 49 |
| 3.6. Catalysts testing..... | 50 |
| 3.6.1. Ring-closing metathesis..... | 50 |
| 3.6.2. Self-metathesis..... | 50 |
| 3.6.3. Cross-metathesis | 50 |
| 3.7. Catalytic data evaluation | 52 |
| 4. Results and discussion | 53 |
| 4.1. Characterization of the supports..... | 53 |
| 4.1.1. X-ray diffraction | 53 |
| 4.1.2. Textural characteristics..... | 53 |
| 4.1.3. Morphology of the particles | 55 |
| 4.2. Modification of mesoporous molecular sieves for CO ₂ adsorption..... | 56 |
| 4.2.1 Physicochemical properties of the samples | 56 |
| 4.2.2. Adsorption of carbon dioxide | 60 |
| 4.2.3 CO ₂ adsorbents summary | 62 |
| 4.3. Well-defined Ru catalysts immobilized on mesoporous molecular sieves | 63 |
| 4.3.1. Tested substrates in metathesis reactions | 63 |
| 4.3.2. Hoveyda-Grubbs type catalysts immobilized <i>via</i> exchange of L ligand..... | 63 |
| 4.3.2.1. Preparation and characterization of the catalysts | 64 |
| 4.3.2.2. Catalytic activity - influence of reaction conditions..... | 68 |
| 4.3.2.3. Catalysts activity in metathesis reactions of different types..... | 72 |
| 4.3.2.4. Filtration test, catalyst leaching and reusing | 78 |
| 4.3.2.5. Catalyst activity in metathesis reactions in flow reactor | 81 |
| 4.3.3. Grubbs type alkylidenes immobilized <i>via</i> exchange of L ligand | 85 |
| 4.3.4. Hoveyda–Grubbs alkylidenes immobilized on organic-inorganic hybrid silica material | 88 |

| | |
|---|-----|
| 4.3.5. Immobilization of Ru complexes <i>via</i> non covalent interaction | 90 |
| 4.3.5.1. Preparation and characterization of the catalysts | 90 |
| 4.3.5.2. Catalytic activity - influence of support | 91 |
| 4.3.5.3. Catalytic activity - influence of counter-anion | 93 |
| 4.3.5.4. Catalytic activity - influence of reaction conditions..... | 96 |
| 4.3.5.5. Catalytic activity - influence of solvent..... | 101 |
| 4.3.6. Metathesis summary | 103 |
| 5. Conclusions..... | 105 |
| 6. List of publications | 8 |
| 7. References..... | 106 |

1. Aims of the thesis

The Ph.D. thesis objectives can be summarized as follows:

1. Synthesis of high quality siliceous mesoporous molecular sieves SBA-15, SBA-16, MCM-41, and MCM-48.
2. Post-synthesis modification of mesoporous molecular sieves for adsorption of carbon dioxide.
3. Preparation of new type highly active and selective heterogeneous catalysts for olefin metathesis based on ruthenium complexes immobilized on mesoporous molecular sieves of various architecture and pore size.
4. New well-defined Ru metathesis catalysts immobilized on mesoporous molecular sieves characterization using physicochemical methods.
5. Testing of the activity and selectivity of new well-defined Ru metathesis catalysts immobilized on mesoporous molecular sieves in ring-closing metathesis (RCM) of 1,7-octadiene, diethyl diallylmalonate, *N,N*-diallyl-2,2,2-trifluoroacetamide, *tert*-butyl *N,N*-diallylcarbamate, (-)- β -citronellene, and allyl ether, self-metathesis, and cross-metathesis (CM) of 5-hexenyl acetate, methyl 10-undecenoate, 1-decene, methyl oleate; allylbenzene with *cis*-1,4-diacetoxy-2-butene, and in ring-opening metathesis polymerization (ROMP) of cyclooctene.
6. Ru leaching determination during the metathesis reactions, in order to test the possibility of catalyst reusing and to check the possibility of the catalyst application under flow conditions.

2. Introduction

2.1. Molecular sieves

Molecular sieves are a group of inorganic solid materials with regular pores or voids of uniform sizes. They are divided into different groups according to the size of their pores: (i) microporous, with pore diameter smaller than 2 nm (zeolites, active carbon); (ii) mesoporous, with pore diameter between 2 and 50 nm (siliceous molecular sieves, mesoporous oxides); (iii) or macroporous, with pore diameter greater than 50 nm (glass or rubbery macropolymer). In this chapter, mesoporous molecular sieves will be briefly discussed.

2.1.1. Mesoporous molecular sieves

Siliceous mesoporous molecular sieves are materials with regular structures, large BET areas (S_{BET}) (often higher than 1000 m²/g), high void volumes (up to 1 cm³/g), and pores in mesoporous region (diameter from 2 nm to 50 nm) with narrow pore size distribution [1]. The discovery of mesoporous molecular sieves opened new possibilities in many areas of chemistry and material science (adsorption, catalysis, drug delivery) [2]. Siliceous mesoporous molecular sieves (SBA-15, MCM-48) represent progressive supports for new heterogeneous catalysts for olefin metathesis and metathesis polymerization [3].

2.1.1.1. Preparation and characterisation

Mesoporous molecular sieves were described for the first time by Mobil Oil researchers in 1992. Typical mesoporous silica-based materials are M41S family, SBA series, and their related mesostructures [4]. The ordered mesoporous materials can be synthesized by the soft- or hard-templating way. In the first case, they are prepared in the presence of surfactants, forming micelles which play the role of mesopore-directing agents (siliceous mesoporous molecular sieves). In the hard-templating route, a preformed ordered mesoporous solid (porous silicas or carbon) is impregnated with liquid precursors of desired composition (metal oxide, inorganic non-oxide compound materials, pure metals, and carbons [5]). The subsequent carbonization of the composite material and removal of the mesoporous solid leads to the inverse replica materials of the mesoporous solid.

The mesoporous molecular sieves were investigated as: (i) adsorbents for removal of pollutants from liquid phase; (ii) adsorbents for gas separation, and purification; (iii) drug delivery systems; (iv) supports for the heterogenization of homogenous catalysts; and (v) catalysts or supports for bifunctional catalysts [4]. Four types of mesoporous molecular sieves were used in this work, namely MCM-41, MCM-48, SBA-15, and SBA-16 (Figure 2.1), which

can be modified in order to enhance their adsorption capacity for carbon dioxide and as support materials for highly active homogeneous metathesis catalysts.

The pore structure of MCM-41 consists of one-dimensional, cylindrical pores, which are organized in a hexagonal $p6mm$ structure with diameters ranging from 2 to 10 nm [6]. MCM-48 is the material with a 3-dimensional $Ia3d$ structure. The best representation of the structure is a gyroid minimal surface. The pore wall thickness of MCM-48 is about 0.8 to 1.0 nm. The pore size is also in the same range as for MCM-41 material. MCM-41 and MCM-48 are synthesized with cationic surfactants. Surfactants are tetraalkylammonium cations with long chain or di-*N*-quaternary cations. According to the synthesis conditions (silica to surfactant ratio, source of silica, composition of starting materials) leads to the formation of MCM-41 or MCM-48.[7].

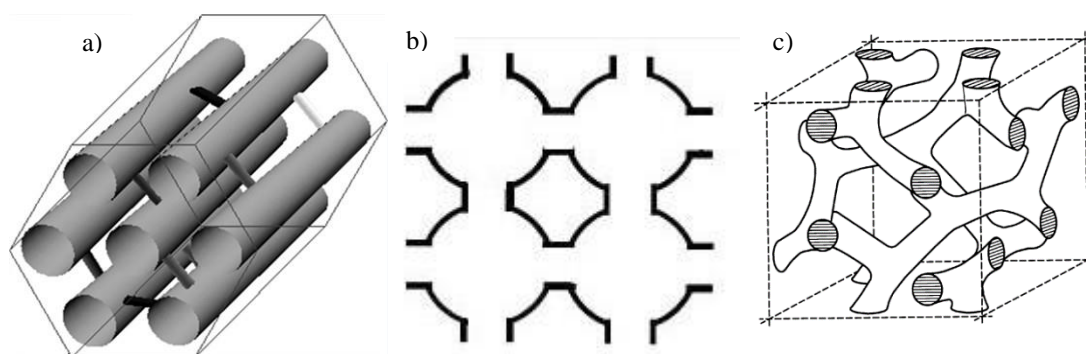
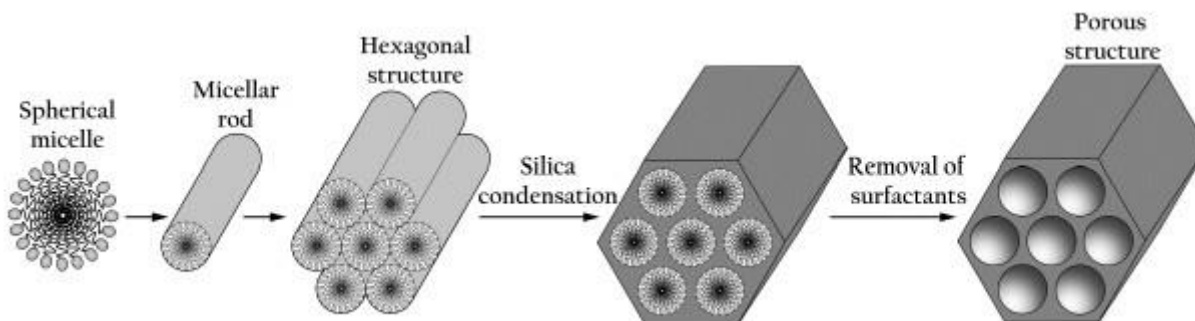


Figure 2.1. Structure of materials used (a – MCM-41 and SBA-15, b – SBA-16, and c – MCM-48; adapted from 4).

SBA-15 is mesoporous silica molecular sieve with parallel hexagonally arrayed cylindrical pores with the tuneable pore diameter of between 5 to 30 nm. The wall thickness is about 3 to 6 nm, which gives the material a higher hydrothermal and mechanical stability than, for instance, MCM-41 [8]. SBA-15 is synthesized by a self-assembly process under acidic conditions using the triblock copolymer Pluronic 123 ($\text{EO}_{20}\text{PO}_{70}\text{EO}_{20}$) as the template and tetraethyl orthosilicate (TEOS) as the silica source (Scheme 2.1).



Scheme 2.1. Illustration of the formation mechanism of SBA-15 (adapted from 4).

SBA-16 is a porous silica with large (5-15 nm) cage-like mesopores arranged in a three-dimensional cubic body-centered $Im\bar{3}m$ symmetry [9]. Like SBA-15, it is synthesized under acidic conditions using a non-ionic Pluronic surfactant. Each sphere is connected to eight neighbouring spheres. Thereby, the pore entrance size from one sphere to another is usually significantly smaller than the primary mesopore size, making this size the limiting factor for applications involving the intraparticle mass transfer. Desorption from this structure is dominated by so-called pore blocking [10].

There is no one universal analysis technique that provides all information necessary to characterize a porous material. For these reasons, multiple techniques must be combined to get a complex view. Such techniques are: (i) X-ray powder diffraction (XRD), (ii) scanning electron microscopy (SEM), and (iii) nitrogen adsorption. Electron microscopy provides a direct image of the porous structure, and enables us to evaluate the particle morphology [11]. Drawback of this method is that it shows a very small part of the porous structure. The basic structure parameters, which are related to the macroscopic amount of material, can be obtained by powder XRD, and adsorption measurement. X-ray powder diffraction (XRD) is technique primarily used for phase identification of a crystalline material and can provide information on unit cell dimensions. Ordered mesoporous materials have amorphous walls, but they possess a long-range order, which produces distinct diffraction patterns at angles in the range of $0^\circ < 2\theta < 5^\circ$, where the Bragg conditions are fulfilled [12]. From gas adsorption, we can determine pore volumes, pore diameters, and BET areas of porous materials. As a standard adsorption technique measurement of adsorption-desorption isotherms of N_2 at $-196^\circ C$ is used [13].

2.1.1.2. Properties important for catalysis and adsorption

Nowadays, increasing environmental concern resulted in the promotion of “green processes” such as substitution of traditional homogeneous catalysts by solid ones. The use of heterogeneous catalysts is desirable due to low energy routes to products, elimination on the

requirement for auxiliary species, and facilitating catalyst recovery to minimize waste generation during product isolation. Ordered mesoporous silica-based materials exhibit facile synthesis, well-characterized structure, extraordinary textural properties and a multitude of possibilities how to modify them, which makes these materials convenient for catalysis and adsorption [14]. The advantages of ordered mesoporous silicates are: (i) the possibility of controlling the pore size (minimizing diffusion limitation commonly observed for microporous materials) and structure of these materials during synthesis; (ii) the possibility of tailoring hydrophobic/hydrophilic properties of the catalyst surface; (iii) controlling the morphology of mesoporous silicates (thin film, fibres, tubes, spheres, or monolith); (iv) extraordinary hosting properties due to reactive surface OH groups.

In contrast with zeolites, which are widely used as catalysts in industry [15], ordered mesoporous silicas with considerably larger pores can overcome the major drawback of zeolitic materials: microporous nature of zeolites causing accessibility problems and diffusion limitations for large molecules. The larger pores of MMS open new possibilities for application in catalysis [16]. However, amorphous nature of ordered mesoporous silica has some important consequences on their properties in comparison with zeolite. The connectivity of the SiO_4 tetrahedra is often incomplete, giving rise to a large concentration of silanols, and together with the lack of crystallinity, it makes mesoporous silicas less stable towards the thermal, and hydrothermal treatments than zeolites. Ordered mesoporous silica-based materials have negligible catalytic activity due to framework neutrality in contrast of acid nature of zeolites [17]. They have to be functionalized in order to become catalytically active, either during synthesis or by post-synthesis functionalization (Figure 2.2.). The number of combinations of different modifications of ordered mesoporous materials is high (according www.sciencedirect.com, there is about 250 papers about modification of mesoporous silicas in 2015). The possible pathways of modification are schematically represented in Figure 2.2. [14].

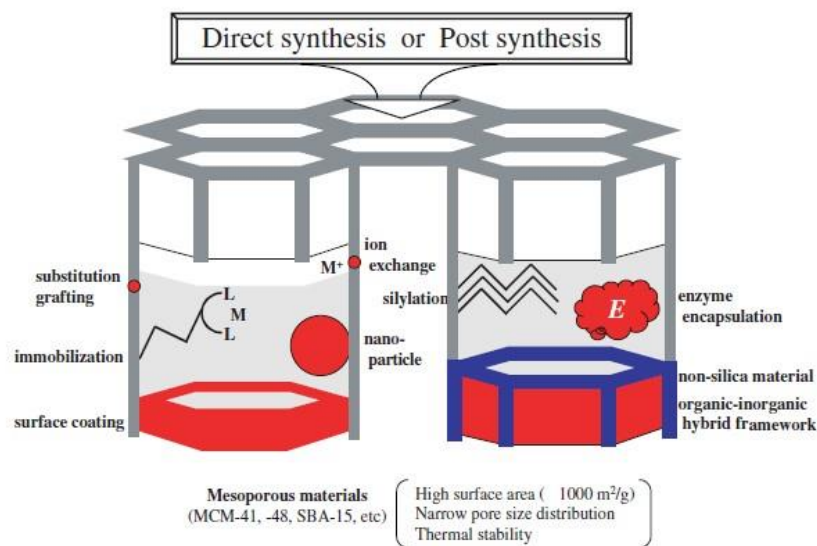


Figure 2.2. Schematic representation of the various methods for the functionalization of mesoporous materials (adapted from 14).

2.2. Carbon dioxide

Carbon dioxide (CO₂) is a colorless, odorless gas. It is a fundamental component of the Earth's carbon cycle; it is assimilated by plants, which in turn produce oxygen by photosynthesis [18].

Natural sources of atmospheric carbon dioxide are volcanic out-gassing, the combustion of organic matter, wildfires, and respiration process of living aerobic organisms. Human activities, such as the use of fossil fuels (coal, petroleum, and natural gas), power generation, and transportation are the source of carbon dioxide [19]. Carbon dioxide is the fourth most abundant gas in the atmosphere and is uniformly distributed over the surface of Earth, with a concentration of about 385 ppm [20]. The concentration of CO₂ in the atmosphere has seen continual increase of about 40 % since the Industrial Revolution [21]. Carbon dioxide is considered to be a major greenhouse gas that has a direct impact on the world's atmosphere [22]. Therefore, it is desirable to find an efficient and economic route to entrap CO₂ produced by various technological processes.

The most effective way to reduce the emission of CO₂ into the atmosphere would be to decrease the fossil fuel consumption. However, this solution is not applicable in practise, because our civilization is mainly driven by consumption of fossil fuels [23]. The strategies to reduce the emission of CO₂ are: (i) energy efficiency; (ii) energy conservation; (iii) fuel switching - get energy from renewable sources (wind, sun); (iv) conversion of CO₂ to useful chemicals; and (v) carbon dioxide capture and storage [24, 25].

Much attention has been paid to capture and storage of carbon dioxide (CCS) produced by power generation plants [26]. One of the most promising ways for CO₂ capture is adsorption on solids. Adsorption on solids can be less expensive and more energy efficient, in comparison to traditional liquid amine-based absorption processes. Generally, solid adsorbents for CO₂ can be divided into three classes: (i) inorganic porous materials including activated carbon, zeolites, and silicas; (ii) hydrotalcite materials, and basic oxides; and (iii) porous hybrid materials such as metal organic frameworks [27].

2.2.1. Solid adsorbents

According to the literature, good adsorbent should have following characteristics: (i) fast adsorption and desorption kinetics; (ii) high CO₂ capacity; (iii) operating window, including adsorption and desorption temperatures; (iv) regenerability and multi-cycle stability [22]. In this chapter, I will discuss the following solid adsorbents, which have been considered as CO₂ adsorbents including microporous and mesoporous materials: zeolites, metal organic frameworks, ordered mesoporous silicas, calcium and magnesium oxides.

Zeolites

Zeolites are microporous crystalline aluminosilicate minerals with a three-dimensional framework consisting of tetrahedral SiO₄ and AlO₄ connected by oxygen bridges. Two neighbouring tetrahedra are connected by one oxygen bridge [28]. The primary structural units, the SiO₄ and AlO₄ tetrahedra, are assembled into secondary building units like 4-, 5-, and 6-rings, double 4-, 5-, and 6-rings, *etc.* By the combination of the secondary building units, the three-dimensional framework is formed [29].

Due to the geometry and dimensionality of the zeolite channels, they can selectively admit molecules with diameters less than that of the pore window size, while those that are larger are sterically hindered [30]. Furthermore, only the reaction intermediates, which fit into the inner pores and channels of a particular zeolite can lead to products. In addition, only the products with smaller size than the pores, and the channels can exit the catalyst. This ‘molecular sieving’ effect has enabled the development of molecular size- or shape-selective applications in adsorption, separation, and catalysis. However, zeolites have one major drawback. Their microporous nature causes accessibility problems and diffusion limitations for large molecules, mainly in hydrocracking reactions [31]. The way to overcome the diffusion/access problem can be: (i) introduction of mesopores into zeolite crystals [32]; and (ii) preparation of pillared, and delaminated zeolites [33].

Generally, zeolites are promising CO₂ adsorbents at low temperature (< 200 °C). The CO₂ adsorption in various well-known zeolites has been extensively studied, included zeolites X, Y, β , ZSM, CHA, FER. To improve their CO₂ adsorption capacity and selectivity, several strategies were applied [34]: (i) isomorphous substitution in zeolites, which involves replacing the Si sites with various other metal ions (Fe, Ga, In, Ti, Sn, *etc.*), offering materials with different electronic and textural properties, and thus affecting adsorption and catalytic behavior [35]; (ii) cationic exchange influencing the electric field inside the pores as well as the available pore volume and providing a convenient mean for tuning the adsorptive properties of zeolites; (iii) impregnating or grafting various amines to increase the CO₂ capture capacity [35].

Metal-organic frameworks

Metal-organic frameworks (MOFs) are crystalline porous materials, in which organic molecule links metal-containing clusters through metal-ligand coordination bonds. The combination of organic and inorganic building blocks offers an almost infinite number of variations, enormous flexibility in the pore size, shape, and structure, moreover, myriad opportunities for functionalization and grafting. Owing to the success in controlling their functionality and structures, MOFs have received a growing attention in recent years for their potential applications in several technological areas such as: (i) gas adsorption; (ii) gas storage; and (iii) molecular separation [36].

Due to their structural features, MOFs can be used for CO₂ adsorption with pressures ranging from low pressure (<1.2 bar) to high pressure (60 - 70 bar). At high pressure of CO₂, MOFs can swell. This effect is called breathing and is associated with the change in the crystalline structure between an open form and a closed form. Such swollen MOFs possess higher surface areas and larger pore volume. Increasing surface areas and pore volumes of MOFs can enhance their CO₂ storage capabilities. At low pressures, CO₂ capacities depend on the heats of adsorption for CO₂ adsorbed in MOFs. Therefore, increasing the interaction strength between CO₂ molecules and the MOFs, such as introducing unsaturated metal centres, can help to increase the CO₂ capacities for MOFs [37]. To use MOFs for CO₂ adsorption in practice, two important issues have to be solved: (i) synthesis of MOFs in bulk with reasonable costs; (ii) and improvement of stability of MOFs toward water vapor, heat regeneration, and acidic gases.

Alkali and alkaline earth metal oxide

The acidic nature of CO₂ makes it very suitable for adsorption on basic sites of some metal oxides. Especially suitable are metal oxides with a low charge/radius ratio, which are more ionic in nature and contain more sites that are strongly basic. These materials include mainly alkaline metal oxides (Na₂O, K₂O) and alkaline earth metal oxides (CaO, MgO) [38]. Among the

variety of tested materials, CaO and MgO has attracted the most attention. Calcium oxide possesses high CO₂ adsorption capacity, is widely available, and its natural minerals. CaO can react stoichiometrically with CO₂ at high temperatures to form calcium carbonate (CaCO₃) which can be regenerated to CaO upon thermal decarbonation (above 900 °C in atmosphere pressure). However, research on the multi-adsorption cycles shows that the performance of CaO-based sorbent was difficult to keep as high as in the first cycle. The deactivation is due to the decrease of available surface area for carbonation, leading to an increasing thickness of CaCO₃ on CaO [39].

Magnesium oxide have been studied as a plausible CO₂ adsorbent mainly because of their lower energy requirements for regeneration comparing to calcium oxides. The CO₂ adsorption capacity of pure MgO is relatively small, due to the low specific surface area. It was found, that the CO₂ adsorption capacity of MgO is inherently correlated with its specific surface area, and that an increase in the specific surface area can improve the adsorption performance. As a result, the porous MgO synthesis with the high specific surface area, achieved by decreasing the particle size and increasing the active sites such as edges and corners on the crystalline structure has been recognized to be an effective way to increase the CO₂ adsorption capacity of MgO. Ruminski *et. al.* showed that CO₂ capacity of MgO nanocrystal increased with the increasing surface area of the particles [40]. Moon *et. al.* presented a new method to synthesize hierarchically nanoporous frameworks of nanocrystalline MgO by the thermal conversion of well-designed MOFs This material exhibits exceptional CO₂ adsorption capacity (9.2 wt. %) under conditions mimicking fluid gas [41].

However, despite the methods for preparation of porous MgO with the high specific surface area, the synthesis methods, containing multiple steps of processing the precursor are generally expensive and time-consuming. These drawbacks hinder the application of porous MgO in CO₂ adsorption [42].

Ordered mesoporous silicas as CO₂ adsorbents

Pure silica surfaces do not provide strong adsorption sites to interact strongly with CO₂ due to the fact that the hydroxyl groups on the silica surfaces fail to induce strong interactions with CO₂. However, modification of mesoporous silica with functional groups is an interesting way to adjust properties to increase the gas-adsorbent interactions. Widely used method to enhance CO₂ adsorption capacity of ordered mesoporous sieves is, the functionalization of the neutral surface with basic organic groups (preparation of organic-inorganic hybrid materials) or alkali metals.

Organic-inorganic hybrid materials are solid analogues of a liquids used in absorption processes. These materials are obtained by anchoring organic moieties onto mesoporous silica surface. Organic functionalization of the surface of mesoporous silica can be performed either by grafting various organic species onto the channel walls, or by co-synthesis based on the co-condensation of alkoxy silane and organosilane precursors in a templating environment. Compared with the grafting method, co-synthesis method can achieve higher loadings of organic functional groups and homogeneous surface coverage within a short preparation time. Typically, amines have been introduced into silica support such as MCM-41, or SBA-15 [43].

The advantages of combining amine and solid sorbents are: (i) avoid degradation of amines supported on solid, in contrast of amine solutions, in which amines degradate by evaporation; and (ii) lower pressure for gas recovery, and lower energy consumption for regeneration [44]. The first amine impregnated CO₂ adsorbent (polyethylenimine on MCM-41) was developed by Xu *et al.* in 2002. From that time, several studies have been reported for the synthesis of various amine-grafted mesoporous silicas for CO₂ capture. Tetraethylenepentamine, polyethylamine, polyvinyl pyridine, hexamethylenetetramine, and other amines were studied to enhance mesoporous silicas adsorption capacities of CO₂ [45].

Another way to increase CO₂ adsorption capacity of ordered mesoporous silicas is to modify them with alkali and alkaline earth metals. The incorporation of metal nanoparticles into mesoporous materials can be performed in a different way such as: (i) impregnation; (ii) co-condensation; and (iii) dispersion [46, 47].

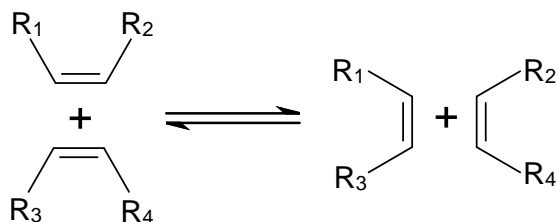
Song *et al.* synthesized Ca containing silica adsorbents and studied their performance in CO₂ adsorption at different temperatures. The results indicated that the CO₂ adsorption ability increased when Ca was incorporated into silica adsorbents, but decreased when the adsorption temperature increased [48]. Jang *et al.* prepared mesoporous magnesium oxide for CO₂ adsorption from mesoporous carbon CMK-3, which was used as an exotemplate. The basic mesoporous MgO showed a maximum CO₂ adsorption of 100 mg/g at 100 °C and nearly 80 mg/g at 25 °C. The reason for increasing CO₂ adsorption at elevated temperature is probably, that CO₂ is chemisorbed on mesoporous MgO [49]. Fernández *et al.* studied the CO₂ chemisorption using adsorbents CaO/SBA-15 and CaO/MCM-41. The maximum CO₂ adsorption capacity was 56.6 % mol CO₂/mol Ca [50]. Zhao *et al.* incorporated MgO into SBA-15 and MCM-41 by different methods of co-condensation and dispersion. To improve dispersion ability of Mg, the pre-synthesized powders of Na/Al-SBA-15 (or Na/Al-MCM-41) by co-condensation method were immersed in the MgAc₂ solution to exchange the cations. The unpaired electron defects caused by Al³⁺ tetra-coordination can effectively increase the amount of the highly dispersed MgO, and the CO₂ adsorption capacity increased from 9.4 cm³/g of pure silica SBA-15

to 30.24 cm³/g of MgO-SBA-15. In the case of MCM-41, the CO₂ adsorption capacity increased from 14.74 cm³/g of pure silica MCM-41 to 29.04 cm³/g of MgO-MCM-41, where dispersion of MgO was enhanced with the incorporation of ethane diamine [51]. Qiming *et al.* prepared MgO containing mesoporous silica by one-step synthesis (impregnation method). The surface area of MgO-SBA-15 greatly decreases from 769 m²/g to 177 m²/g compared with the original mesoporous silica. The MgO-modified mesoporous silica prepared by impregnating reaches CO₂ adsorption capacity of 15.55 cm³/g compared with the original mesoporous silica (10.35 cm³/g) [52].

In general, adsorption-desorption kinetics, adsorption-desorption temperature, adsorption capacity, adsorption selectivity, and regenerability (stability) should be considered for development of highly efficient solid CO₂ adsorbents [53]. Low temperature CO₂ adsorbents usually contain materials based on carbon, zeolites, MOFs, and alkali metal carbonates. The CO₂ adsorption capacity of synthetic zeolites and MOFs is high, but the cost of such materials is also high. The cyclic stability of the alkali metal carbonates and amine-based solid adsorbents is poor. The magnesium oxide is promising adsorbent due to the good adsorption capacity and low energy requirement for regeneration. MgO has lower surface area in comparison with other materials which is a limiting factor for widespread application as a sorbent. To overcome this limitation, MgO can be introduced into mesoporous molecular sieves. Such hybrid adsorbents benefit from thermal stability and large surface area of mesoporous silicas. There are environmental consequences too, as the preparation of MgO with large surface area requires a use of toxic chemicals. Approaches, which include promoting MgO into MMS *via* simple and more environmentally friendly route neglecting toxic solvent, can be considered as a promising candidates for large scale use [54].

2.3. Olefin metathesis

Olefin metathesis is considered as one of the most important reactions for the formation of carbon-carbon bonds having a wide range of applications in organic chemistry, polymer chemistry, and materials science (adhesives, flame retardants) [55]. Word metathesis comes from Greek's *meta* (change) and *tithemi* (place), which reflects the general mechanism of metathesis reaction (exchanging alkylidene fragments between two molecules of olefin). Metathesis consists of an alkene double bond cleavage followed by a redistribution of alkylidene fragments (Scheme 2.2.). In other words, olefin metathesis constitutes a catalytic method for both cleavage and forming C=C double bonds. Metathesis of alkenes has high activation energy and therefore proceeds only in the presence of transition metal catalysts [56]. Both homogeneous and heterogeneous catalysts can be employed. The most active ones are based on tungsten, molybdenum, rhenium and ruthenium compounds [57, 58].



Scheme 2.2. General scheme of olefin metathesis (R = alkyl, cycloalkyl, aryl).

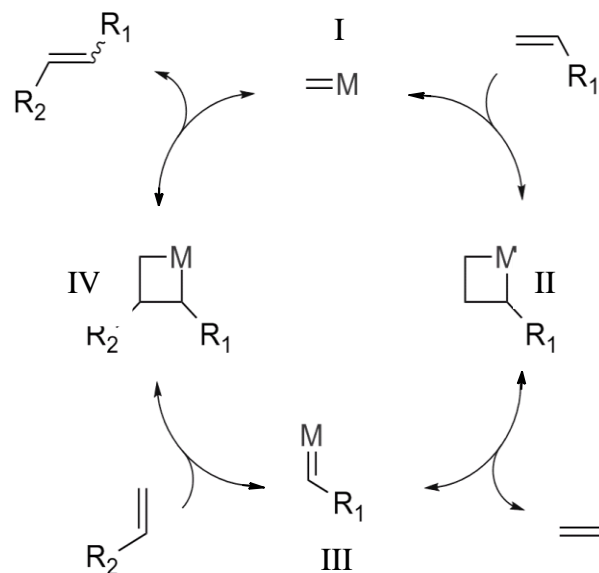
The alkene metathesis reactions are generally reversible and thermoneutral. The reactions result in an equilibrium with a statistical distribution of alkylidene fragments between reactants and products. A way to increase the product yield is based on Le Chatelier's principle by continuously removing one of the products from the reaction system in order to shift the equilibrium in favor of the desired product. This method is especially effective in the case of reactions in a liquid phase, where gaseous products (mainly ethylene) are formed and can be easily removed.

Metathesis reactions are divided in several important classes:

1. Alkene cross-metathesis (CM) and self-metathesis
2. Cycloalkene ring-opening metathesis (ROM) and ring-opening metathesis polymerization (ROMP)
3. Acyclic diene metathesis (ADMET)
4. Diene ring-closing metathesis (RCM)

2.2.1. Mechanism

Hérisson and Chauvin proposed the generally accepted mechanism (Scheme 2.3.) of alkene metathesis [59]. It is based on a metal-carbene species (a compound with a metal-carbon double bond, see **I** and **III** below) and a metallocyclobutane intermediate (**II** and **IV**). The catalytic cycle (Scheme 2.3.) involves the coordination of an olefinic substrate to a metal carbene **I**, to give metallocyclobutane intermediate **II**.

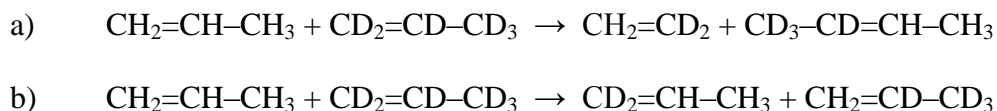


Scheme 2.3. Chauvin generally accepted mechanism of alkene metathesis.

This four-membered ring then fragments in the opposite direction to release ethylene and create a new metal carbene **III**, which reacts with olefinic substrate to form metallocyclobutane **IV**. Fragmentation of the resulting metallocyclobutane **IV** produces cross-metathesis product and regenerates the initial metal carbene, which re-enters the catalytic cycle [60].

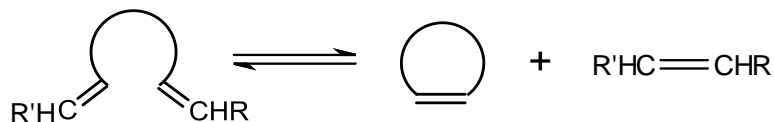
2.3.2. Types of olefin metathesis reactions

Self-metathesis is a reaction of two identical molecules forming metathesis products (Scheme 2.4.). In this case, two types of metathesis reaction can be recognized by using isotope labelled alkenes: (i) productive metathesis, where two new products are formed, and (ii) non-productive (degenerate) metathesis, where the metallacyclobutane intermediate is formed in such way, that the products of the reaction are the substrate molecules [61].



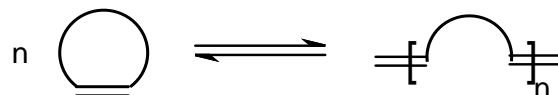
Scheme 2.4. Alkene metathesis of labelled and unlabelled propene: a) productive and b) non-productive metathesis ($\text{CD}_2=\text{CD}-\text{CD}_3$ is $[2-^{14}\text{C}]$ propene).

Ring-closing metathesis (RCM) is a variation of olefin metathesis that allows the closing of rings (*i. e.* construction of carbocyclic and heterocyclic ring systems). Ring closing metathesis occurs when a diene undergoes intramolecular metathesis, affording a cyclic olefin. On the other hand, ring-opening metathesis (ROM) takes place when a cyclic olefin reacts with another olefin, (Scheme 2.5.) [62].



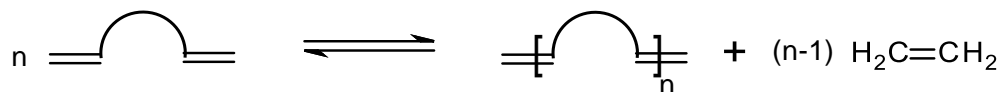
Scheme 2.5. Ring-closing metathesis (RCM) and ring-opening metathesis.

Ring-opening metathesis polymerization (ROMP) is a chain-growth polymerization, in which a cyclic olefin is converted to polymer (Scheme 2.6.). This process is usually accompanied by the release of ring strain, which provides the main driving force of the reaction. Some cycloalkenes, especially those with a high ring strain (norbornene, cyclobutene, cyclooctene, and dicyclopentadiene), can undergo ROMP under the formation of high-molecular-weight polyenes [63].



Scheme 2.6. Ring-opening metathesis polymerization (ROMP).

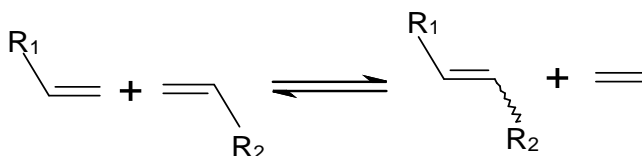
Acyclic diene metathesis (ADMET) is a type of step-growth, condensation reaction, (in contrast to the chain growth polymerization kinetics of ROMP), where terminal dienes are converted into unsaturated oligomers and/or polymers, yielding a molecule of ethylene in propagation step (Scheme 2.7.) [64]. Additionally, there are many metathesis pathways that do not lead to polymer formation, such as degenerate metathesis reactions and depolymerisation with ethylene. Each of these pathways occurs to some degree, and the elimination of gaseous ethylene from the polymerization is the driving force for the productive pathway [64].



Scheme 2.7. Acyclic diene metathesis (ADMET).

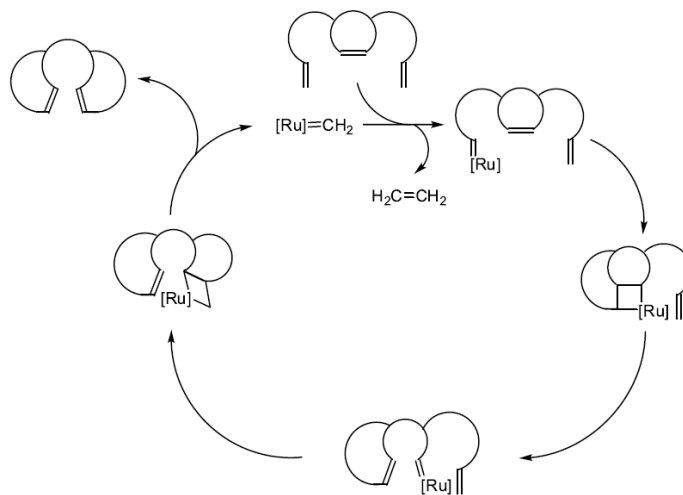
Olefin cross-metathesis (CM) (Scheme 2.8.) can be formally described as the intermolecular mutual exchange of alkylidene (or carbene) fragments between two olefins promoted by metal-carbene complexes [65]. The disadvantage of CM can be a low CM product selectivity, because self-metathesis of both starting olefins occurs in the system, too. Grubbs overcame this problem and found a general empirical model useful for the prediction of cross-metathesis selectivity. „A general ranking of olefin reactivity in CM is achieved by categorizing

olefins by their relative ability to undergo homodimerization via cross-metathesis and the susceptibility of their homodimers toward secondary metathesis reactions. Product selectivity can be achieved by suppressing the rate of homodimerization of one component and controlling the rate of secondary metathesis on the desired cross product. These rates can be controlled through the choice of olefins with significantly different activities, which can be modified by altering their steric and electronic properties through substituents, functionalities, or protecting groups. In addition, an appropriate choice of olefin metathesis catalyst is critical for product selectivity, regioselectivity, or chemoselectivity" [66].



Scheme 2.8. Cross-metathesis (CM).

The basic types of metathesis reaction can be combined into several metathesis steps (for example Scheme 2.9.). This type of olefin metathesis is called ring-rearrangement metathesis (RRM) [67]. The combinations of several metathesis transformations lead into a domino process, in which an endocyclic double bond of a cycloolefin reacts with an exocyclic alkene. These reversible processes are driven by a combination of thermodynamic factors (loss of ring strain, substitution pattern, or release of a volatile olefin) and kinetic effects such as the formation of a less-reactive carbene complex.



Scheme 2.9. The ring opening metathesis (ROM) and ring-closing metathesis (RCM) tandem coupling.

2.3.3. Catalysts

Metathesis of alkenes is a symmetry forbidden reaction and therefore proceeds only in the presence of transition metal catalysts. The reaction is catalysed by compounds of transition metals such as ruthenium (Grubbs-type alkylidene), tungsten, and molybdenum (Schrock-type alkylidene) [56]. These catalysts can be divided into homogenous and heterogeneous. They can be also divided into so-called ill-defined and well-defined catalysts. Ill-defined early metathesis catalysts are multicomponent systems consisting of transition metal compounds and main group metal compounds as co-catalysts. Modern well-defined catalysts contain stable transition-metal alkylidenes or metallacyclobutanes [68]. The majority of metathesis catalysts can be applied in several metathesis reactions; however, there is no universal catalyst that, would achieve high activity for all types of metathesis reactions.

2.3.3.1. Ill-defined catalysts

Ill-defined metathesis catalysts are multicomponent systems consisting of transition-metal complexes without an alkylidene ligand. The active metal alkylidene is formed *in situ* by the addition of a carbene source (alkyl aluminium, alkyl lithium, or alkyl stannane). Although, these ill-defined systems were used in the early stage, before well-defined catalysts were invented, they are still used. The advantages of these catalysts compared to the well-defined ones are: (i) they are generally cheaper and readily commercially available; or (ii) can be easily prepared from commercially available compounds [69].

In contrast to the well-defined catalysts, the activity of ill-defined catalysts cannot be fully controlled. Because the nature of catalytically active centre is not known [70]. They also suffer from poor functional group tolerance [71]. The first metathesis reaction was reported in the 1950's, when chemists from Du Pont, Standard Oil, and Phillips Petroleum found that propylene was transformed to ethylene and 2-butenes [72]. The reaction was catalysed by molybdenum in the form of metal, oxide or $\text{Mo}(\text{CO})_6$ supported on alumina. In 1960, the first polymerization of norbornene by the catalyst system $\text{WCl}_6/\text{AlEt}_2\text{Cl}$ was reported [73]. In 1965, Natta reported polymerization of cyclobutene and 3-methylcyclobutene by ring opening on RuCl_3 [74]. In the end of the 1960s, industry used: (i) WO_3/SiO_2 or Ziegler-Natta derived systems such as WCl_6 (or MoCl_5) + $\text{AlX}_n\text{R}_{3-n}$ ($n = 1, 2, 3$) catalysts for the transformation of propylene to ethylene and butenes; (ii) or polymerization of cyclopentene catalysed by system $\text{WCl}_6 + \text{AlEt}_3$ [75].

Nowadays, ill-defined catalyst systems are used in industry for large scale productions. In the Phillips triolefin process a heterogeneous WO_3/SiO_2 catalyst is used to convert propylene to ethylene and 2-butene [76]. The neohexene process consists of cross metathesis of the dimer of

isobutene to produce 3,3-dimethylbut-1-ene over catalyst mixture of WO_3/SiO_2 and MgO in ratio 1:3 [77]. The Shell Higher Olefins Process is another important large scale process. The process was developed for the conversion of ethylene to C10-C14 internal olefins, but can be modified to obtain linear olefins of any desired range [76]. It involves 4 steps: (i) ethylene oligomerization; (ii) isomerization of α -olefins into internal olefins; (iii) metathesis; and (iv) recycle (the byproducts of the process are only linear olefins, they can be recycled by isomerization and metathesis). The metathesis step gives a broad mixture of linear internal olefins, of which 10-15 % are in the desired range.

2.3.3.2. Well-defined catalysts

Schrock isolated the first stable metal-alkylidene complex $[\text{Ta}(\text{CH}_2\text{CMe}_3)_3(=\text{CHCMe}_3)]$ with the high oxidation state of Ta in the middle of 1970s [78]. Prepared alkylidene complex did not catalyse metathesis of olefins. Later, Schrock and co-workers prepared well-defined tantalum-alkylidene complex, $[\text{Ta}(=\text{CHC}(\text{CH}_3)_3)\text{Cl}(\text{PMe}_3)(\text{O}-\text{C}(\text{CH}_3)_3)_2]$, which catalysed metathesis of *cis*-2-pentene [79]. The reason why this complex catalysed the metathesis reaction, whereas the other tantalum alkylidene complexes failed, was the presence of ancillary alkoxide ligand in the catalyst. Alkoxide ligand stabilizes reactive mononuclear species toward bimolecular decomposition reactions. Based on this success, Schrock *at al.* prepared a whole family of molybdenum and tungsten-alkylidene complexes active in alkene metathesis [80].

The first reported ruthenium-carbene complex $[\text{RuCp}\{=\text{C}(\text{Me})\text{OMe}\}(\text{CO})(\text{PCy}_3)][\text{PF}_6]$ was prepared in 1971 by Green's group at Oxford. This complex was not active in metathesis reaction, because it is 18-electron coordinatively saturated complex of Fisher-type. In the 1988, Grubbs reported polymerization of 7-oxanorbornene by RuCl_3 or $[\text{Ru}(\text{H}_2\text{O})_6(\text{OTs})_2]$ (OTs = toluene sulfonate) [81]. Then, Grubbs reported the first well-defined ruthenium-carbene complex (Figure 2.3.) that promoted ROMP of low-strain olefins and RCM of functionalized dienes [82].

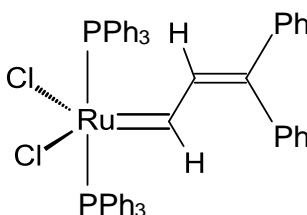


Figure 2.3. The first well-defined Ru metathesis catalyst.

The discovery of stable transition metal alkylidene complexes inspired the development of a new family of “well-defined” metathesis catalysts with high activities and tolerance to a broad spectrum of functional groups. Well-defined metathesis catalysts are those that: (i) are essentially identical to the active species in terms of metal oxidation state and ligand

coordination sphere in the catalytic reaction; and (ii) are stable enough to be characterized by physicochemical methods [83]. The most popular metathesis catalysts are tungsten and molybdenum alkylidene complexes developed by Schrock and ruthenium alkylidene complexes developed by Grubbs. W, Mo, and Ru alkylidenes give the good balance between activity and functional group tolerance. Table 2.1. shows a general trend of the inverse relationship between the functional group tolerance and the activity for different catalysts (more active catalysts are, more sensitive they are to functional groups). Farther to the left, titanium and tungsten catalysts are the most sensitive to ketones and esters. In comparison, molybdenum catalysts are more reactive toward olefins, although they also react with aldehydes and other polar or protic groups. Farther to the right, ruthenium reacts preferentially with carbon-carbon double bonds over most other species, which makes these catalysts unusually stable toward alcohols, amides, aldehydes, and carboxylic acids [84].

Table 2.1. Functional group tolerance of olefin metathesis catalysts (adapted from 84).

| <i>Titanium</i> | <i>Tungsten</i> | <i>Rhenium</i> | <i>Ruthenium</i> | |
|-----------------|-----------------|----------------|------------------|---|
| Acids | Acids | Acids | Olefins | ↑ Increasing order of reactivity |
| Alcohol, water | Alcohol, water | Alcohol, water | Acids | |
| Aldehydes | Aldehydes | Aldehydes | Alcohol, water | |
| Ketones | Ketones | Olefins | Aldehydes | |
| Esters, amides | Olefins | Ketones | Ketones | |
| Olefins | Esters, amides | Esters, amides | Esters, amides | |

→
Functional group tolerance

2.3.3.2.1. Schrock-type carbene complexes

Molybdenum and tungsten high oxidation state carbene complexes reported by Schrock and co-workers [85] are highly active toward a broad range of substrates, suitable for different type of metathesis reactions, and several of them have been made commercially available (Figure 2.4.) [86]. In contrast to Ru alkylidenes, Mo and W alkylidenes are more sensitive to oxygen and moisture or even to impurities present in the solvent. Moreover, these catalysts have lower functional group tolerance than Grubbs-type alkylidenes.

The metal in a Schrock alkylidene is electrophilic, and is stabilized by electron-donating ligands as well as back-bonding from an occupied *p*-orbital of the carbenic carbon atom. This results in a strong metal-carbon double bond.

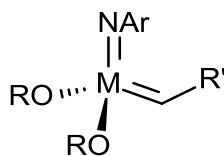


Figure 2.4. General formula of the family of Schrock metathesis catalysts (M = Mo or W; R, R' are bulky substituents, Ar is aromatic substituent).

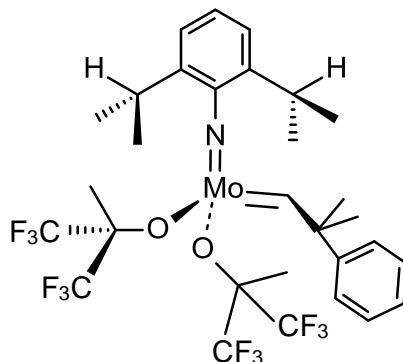
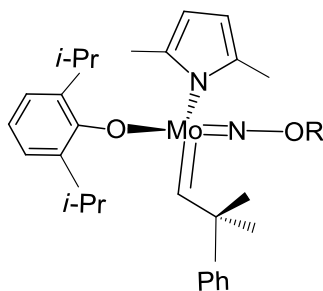


Figure 2.5. Schrock catalyst commercially available.

The basic type of alkylidenes (Figure 2.5.) features two alkoxide ligands and an imido ligand. The high activity of these imido alkylidene complexes has led to the development of various analogous W-, Mo-alkylidene systems, which can exhibit extremely high stereoselectivity, depending on their ligand environment. When the alkoxide ligands are replaced with an enantiomerically enriched chelating biphenolate or naphtholate ligands, a chiral complex is generated. These chiral catalysts are enantioselective, which was shown *e.g.* in asymmetric RCM of achiral trienes [87]. Based on these results, monoalkoxide monopyrrolyl ligands were introduced into Mo-alkylidene complexes (Figure 2.6). These types of catalysts display higher activity than classical Schrock-type alkylidenes or chiral W, Mo-alkylidenes previously mentioned [88].



R = *t*-Bu, *i*-Pr, Ar, *i*-Pr_{F6}, *t*-Bu_{F6}

Figure 2.6. Chiral Mo based metathesis catalysts.

In 2009, Schrock and Hoveyda introduced the first Mo-based Z-selective metathesis catalyst (Figure 2.7.) [89]. The origin of the Z-selectivity arises from the flexibility of introduced binaphthyl-type aryloxy ligand. The ligand can freely rotate in the metallacyclobutane intermediate, which directs the R-groups of the olefinic substrate in the metallacyclobutane toward the smaller arylimido ligand and favours the formation of Z-alkene. The catalyst is effective in CM of alkenes [90].

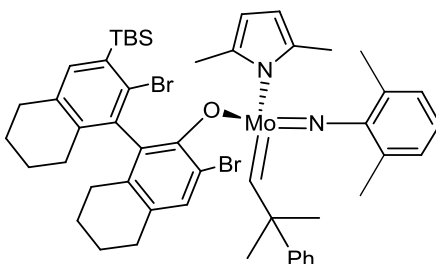
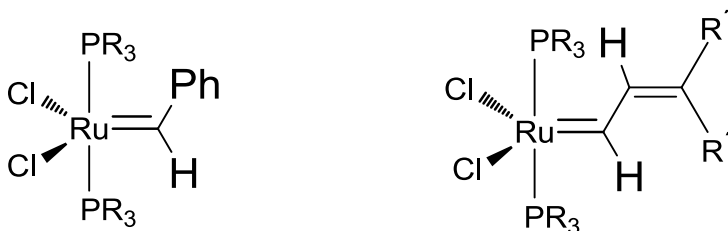


Figure 2.7. Z-selective Mo based metathesis catalyst.

2.3.3.2.2. Grubbs-type carbene complexes

The well-defined ruthenium carbene complexes developed by Grubbs and co-workers in 1992 are the first well-defined ruthenium metathesis catalysts (Figure 2.8.), which show good activity and selectivity to acyclic and cyclic olefins. These carbenes show remarkable tolerance towards various organic functional groups, air, and moisture stability, which makes these catalysts suitable for organic and polymer synthesis [91, 92, 93].



R = *i*-Pr, Ph, Cy

R = Ph, Cy, R' = Ph, CH₃

Figure 2.8. The well-defined ruthenium carbene complexes developed by Grubbs.

In 1995, Grubbs and co-workers reported the new type of well-defined Ru carbene complexes [Ru(=CHPh)Cl₂(PR₃)₂], R = Ph, or Cy (cyclohexyl) [94], which were much more active than the earliest catalysts. Ru carbene with Cy [Ru(=CHPh)Cl₂(Cy)₃] has been commercialized and is known as Grubbs 1st generation catalyst (Figure 2.9.). The catalyst is easily prepared in a one-pot synthesis from RuCl₂(PPh₃)₃, phenyldiazomethane, and tricyclohexylphosphine and it is the precursor for other Grubbs-type catalysts. The Grubbs 1st

generation catalyst has been widely used for ring-opening metathesis polymerization, ring-closing metathesis, ethenolysis, cross-metathesis of terminal olefins, and the preparation of 1,3-dienes *via* enyne metathesis.

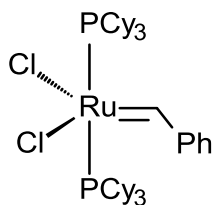


Figure 2.9. Grubbs 1st generation catalyst.

This catalyst has commercial potential, for example: ethenolysis of feedstocks derived from bio-renewable seed oils [95] and the manufacture of macrocyclic hepatitis C therapeutics [96]. However, the application of this catalyst is limited, because Grubbs 1st generation catalyst suffers from reduced activity in contrast to the more sensitive but highly active Schrock catalyst. This catalyst showed low activity in the transformation of trisubstituted olefins in ring-closing metathesis and over the transformation of hindered and electron deficient substrates in cross-metathesis. Many of the limitations of the Grubbs 1st generation catalyst were overcome by preparation of Grubbs 2nd generation catalyst.

The discovery of the Grubbs 2nd generation catalyst in 1999 led to a more active catalyst, reasonably stable toward H₂O, O₂, and minor impurities with high functional group tolerance [97]. This catalyst has been widely used in areas of fine chemicals and pharmaceutical synthesis [98]. The first example of this catalyst is shown in Figure 2.10. The one phosphine ligand in Grubbs 1st generation catalyst is exchanged with NHC ligand (1,3-dimesitylimidazol-2-ylidene), which increases the catalyst activity. The Ru centre in Grubbs 2nd generation catalyst prefer the coordination of olefinic substrates over rebinding of phosphine ligand [86].

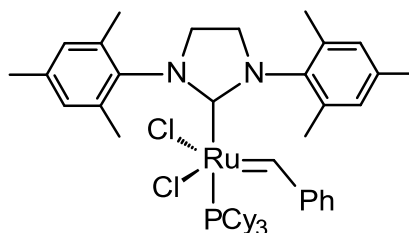
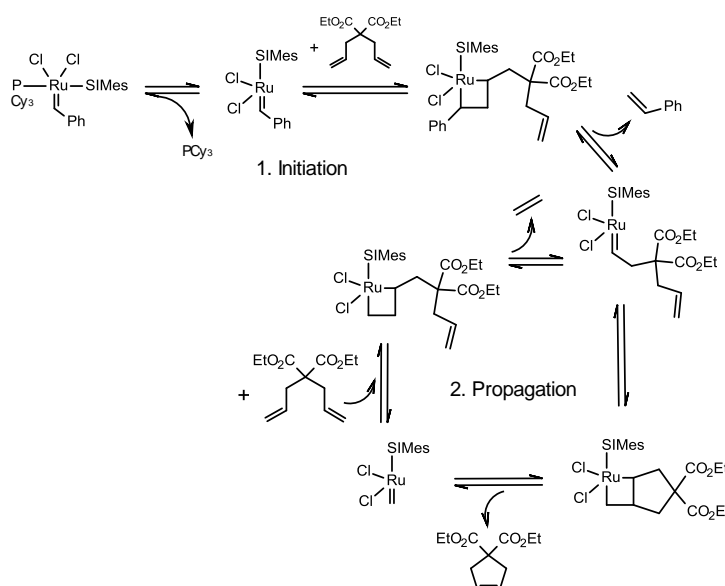


Figure 2.10. Grubbs 2nd generation catalyst.

The initiation step of metathesis reaction promoted by Grubbs 1st and 2nd generation catalysts (Scheme 2.10.) can proceed in two competing pathways. The first one is dissociation mechanism, where PCy₃ ligand is released from Ru alkylidene to form a 14-electron active species (which is a dominant one). This active species can be either re-trapped by free PCy₃ with regeneration of starting alkylidenes, or bound to substrates. This is followed by the creation of metallacyclobutane ring, and a propagation step of metathesis reaction forming product olefins. After finishing catalytic cycle (propagation step), the Ru alkylidene is regenerated by coordination of initially released phosphine linker [99]. The initiation step can also proceed as an associative mechanism, in which alkene binds to the metal centre to yield an 18-electron intermediate before the loss of a ligand followed by [2+2] cycloaddition.

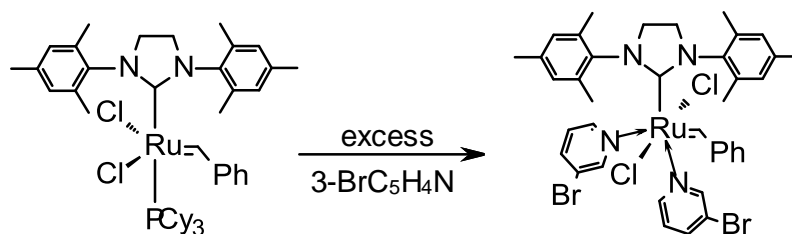


Scheme 2.10. Grubbs second generation catalyst cycle in ring-closing metathesis.

Grubbs *et al.* showed that the initiation step in the case of the second generation catalyst proceeds more slowly than in the case of the first generation catalyst, and that the higher activity is due to the higher affinity of Grubbs 2nd generation catalyst to coordinate olefinic substrates in the presence of free phosphine [100].

From the Grubbs 2nd generation catalyst, a new type of Ru-alkylidenes was prepared (known as Grubbs 3rd generation catalyst) by a simple exchange of phosphine ligand with more labile 3-bromo-pyridine ligands (Scheme 2.11.) [101]. It is an extremely active metathesis catalyst due to fast initiation (about 4000 times faster than in the case of Grubbs 2nd generation catalyst), caused by rapid dissociation of electron-deficient 3-bromo-pyridine ligand. This feature

makes the catalyst effective in CM of acrylonitrile, which usually does not undergo metathesis with Grubbs 2nd generation catalyst.



Scheme 2.11. Grubbs 3rd gen. catalyst prepared from Grubbs 2nd gen. catalyst.

A new class of ruthenium metathesis catalysts has been introduced by Hoveyda and co-workers in 1999 [102]. So-called Hoveyda-Grubbs catalysts (Figure 2.11.) contain chelating benzylidene ether ligand, and in the case of the second generation Hoveyda-Grubbs catalyst a phosphine-free structure is formed.

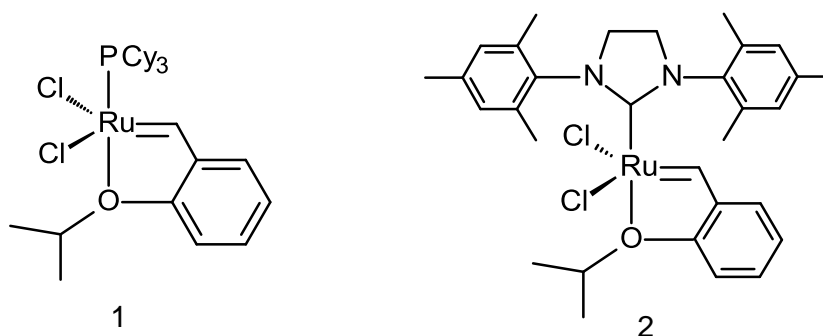
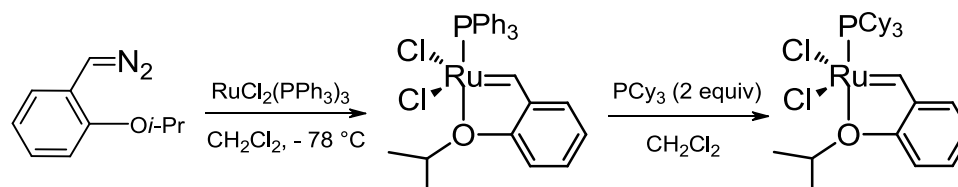


Figure 2.11. A new class of ruthenium metathesis catalysts presented in 1999.

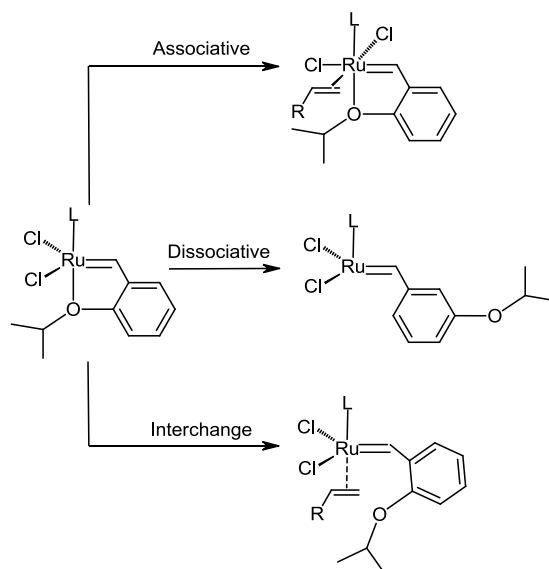
The Hoveyda-Grubbs 1st generation catalyst (1, Figure 2.11.) was prepared, when 2-isopropoxystyrene was treated with one equivalent Grubbs 1st generation catalyst. To avoid the use of stoichiometric amounts of Grubbs 1st generation catalyst Hoveyda *et al.* used a two step single-vessel synthetic route, where alkoxyphenyldiazomethane reacted with $\text{RuCl}_2(\text{PPh}_3)_3$ (Scheme 2.12.) [103].



Scheme 2.12. Hoveyda-Grubbs 1st generation catalyst prepared via single-vessel synthetic route.

The activity of the Ru-carbene 1 (Figure 2.11) is similar to the Grubbs 1st generation catalyst. This aryl-ether chelate complex offers the advantage that the same active species as in the case of the Grubbs 1st generation catalyst are formed, while the catalyst is exceptionally robust and recyclable: it is recovered in high yield after a reaction by air-driven silica gel chromatography (air pressure is used to speed up flow of solvent, which decreases the time for purification of product). The convenience of possible recovery after the reaction should be assigned to a release/return mechanism. The isopropoxystyrene, which decoordinates during metathesis, can react again with a Ru-intermediate to regenerate the original catalyst [104].

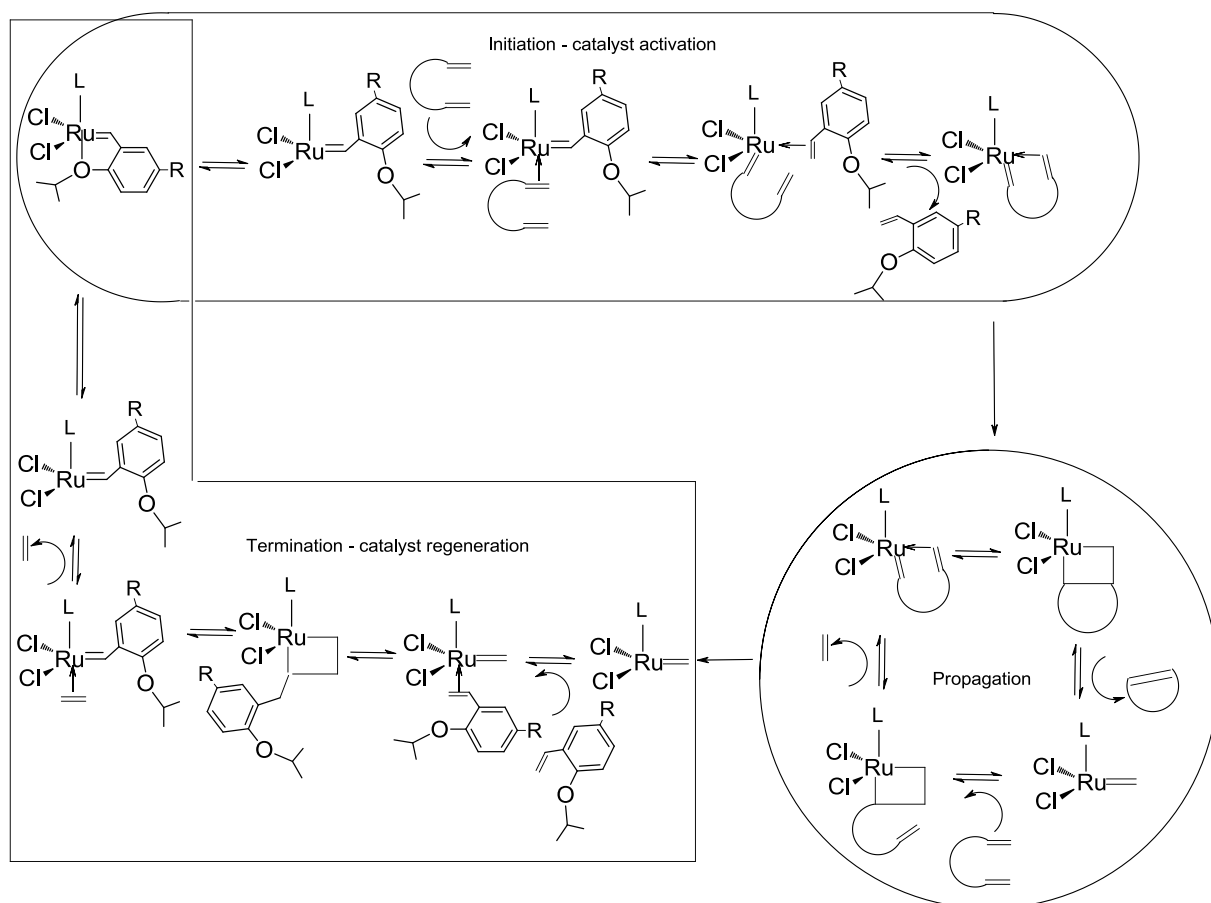
The initiation step of Hoveyda-Grubbs catalysts, unlike that of the Grubbs catalysts, does not involve the loss of PCy₃ ligand, but the creation of 14-electron active Ru-carbene species is achieved by three different initiation steps (Scheme 2.13.) [105]. Hoveyda proposed that catalyst activation takes place through a dissociation of styrene ether [102]. Experiments suggested that in some cases initiation step can be different. Associative coordination of olefin molecule on the metal centre can occur before dissociation of the styrene ether. Plenio and co-workers proposed an interchange mechanism, in which the coordination of incoming olefin occurs simultaneously with the dissociation of the styrene ether [105]. The preference for one of the possible modes of catalyst activation critically depends on the steric and electronic properties of the respective ruthenium complexes and the olefin employed for the metathesis reaction [106].



Scheme 2.13. Three mechanisms for Hoveyda-Grubbs type catalysts activation.

Then metathesis cycle occurred by loading the alkenes onto active catalytic species and releasing of isopropoxystyrene (Scheme 2.14.) [107, 108]. After several propagation cycles of the metathesis reaction, the catalyst can be regenerated by recaption of the initially released

isopropoxystyrene [109]. The absence of dissociation of phosphine ligand during metathesis cycle has advantage for heterogenization of the Hoveyda-Grubbs 1st generation complex by exchanging phosphine ligands. Such immobilized Ru alkylidene is firmly bonded to the support during metathesis reactions.



Scheme 2.14. Hoveyda-Grubbs catalysts cycle in ring-closing metathesis reaction.

The Hoveyda-Grubbs 2nd generation catalyst was prepared in two different ways. Hoveyda and co-workers synthesized this catalyst from the corresponding Grubbs 2nd generation catalyst by the addition of the isopropoxystyrene in the presence of phosphine scavenger CuCl [110]. Blechert *et al.* prepared this catalyst from Hoveyda-Grubbs 1st generation catalyst by addition of NHC ligand [111]. Such complex does not contain phosphines and is extremely air and moisture stable. Grubbs *et al.* showed that under optimized conditions, catalyst loadings as low as 25 ppm can lead to 100 % conversion in the ring-closing metathesis of diethyl diallylmalonate [112].

2.3.4. Strategies for immobilizing Ru-alkylidenes complexes

Immobilization of the well-defined Ru-alkylidenes on solid supports provides a combination of benefits of homogeneous and heterogeneous catalysts. The use of supported catalysts has generally several benefits: (i) stabilization of highly active homogeneous complexes; (ii) easy removal of the catalyst from the reaction products; (iii) the possibility of recycling the expensive catalysts; (iv) low catalyst residues in the products; and (v) the possibility of continuous-flow processes [113].

The commonly applied process for immobilization of homogeneous catalysts is anchoring the catalysts on the surface of solid supports with a large surface area [114]. There are several methods for the immobilization of frequently used Ru-alkylidenes (Grubbs and Hoveyda-Grubbs complexes) on siliceous solids supports. The simplest method is the direct interaction of the alkylidene complexes with the support surface. In the literature, there are several reports on the immobilization of Hoveyda-Grubbs 2nd generation alkylidene using this way [115, 116, 117]. The details about the interaction mode are not known: adsorption and/or hydrogen bonds can be assumed.

The most frequently used immobilization methods consist of the exchange reaction between complex ligands and suitable reactive groups on the surface under formation of covalently bound organometallic species [118]. To create proper reactive groups on the surface, special molecules (linkers) are used. For Ru alkylidenes (Grubbs and Hoveyda-Grubbs complexes), the exchanges of X ligands [119, 120], L ligands [121, 122], and alkylidene ligands [123, 124] have been used. In many cases, this method required elaborate synthesis of special linkers.

2.3.4.1. Immobilization *via* non-covalent interactions

Direct immobilization of ruthenium-alkylidenes on the surface of a solid support is a convenient method, because it does not require special linker molecule. Simple immobilizations of Hoveyda-Grubbs catalysts were reported several times in the literature. Immobilized catalysts were prepared by mixing Hoveyda-Grubbs catalysts with dried silica [125] or siliceous mesoporous molecular sieves [116, 117, 126]. There is not strong evidence about the type of the interaction of Ru-alkylidene with the surface of the supported materials used. Most likely physical adsorption and/or hydrogen bond can be assumed. High activity was found for the catalysts prepared in this way. However, it seems that their application is limited by the polarity of solvent used. In the nonpolar systems, they can operate as true heterogeneous catalysts, with low Ru leaching. On the contrary, in the polar systems, the possibility of significant Ru leaching needs to be taken into account.

In the same way, complex $\text{RuCl}_2(\text{p-cymene})(\text{PCy}_3)$ was immobilized on mesoporous molecular sieves MCM-41 and SBA-15 and on conventional silica [127]. These catalysts were active in ROMP of norbornene, and cyclooctene in toluene.

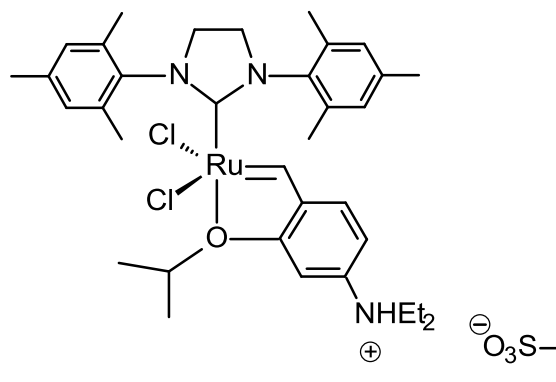


Figure 2.12. Hoveyda-Grubbs catalyst immobilized *via* ionic interaction.

Another example of immobilization of Ru alkylidenes *via* non-covalent interactions is the ionic interaction between Ru complex and a support material. For the first time, this new strategy was described by Grela and co-workers [128]. They immobilized Hoveyda-Grubbs 2nd generation catalyst modified with NEt_2 substituent on 2-isopropoxybenzylidene ligand on the support containing SO_3H groups (Figure 2.12.). The promoted quarternized amino group plays two roles: (i) an anchor for immobilization; and (ii) activation of the catalysts after protonation (the switch of electron donating to electron withdrawing effect occurs). This catalyst was active in CM of allylestrone with acrylic acid derivatives to form a new 17- β -hydroxysteroid dehydrogenase type 1 inhibitor [129]. This estradiol-synthesizing enzyme is mainly responsible for the conversion of estrone to the potent estrogen estradiol. It is a key player in controlling the tissue levels of estrogen estradiol. It is, therefore, an attractive target in estradiol dependent diseases such as breast cancer or endometriosis [130].

2.3.4.2. Immobilization *via* X-ligands

Generally, in complexes, there are three groups of ligands: (i) L ligands; (ii) X ligands; and (iii) Z ligands. X-ligands are radical type ligands, they bring one electron or an odd number of electrons to the metal, but they require one valence electron from the metal to form the metal-ligand bond. The interaction M-X leads to the covalent bond, where each partner brings one electron to form the bond electron pair [131].

Mol *et al.* described this strategy for immobilization of Ru-alkylidenes. They used the ability of anionic ligand to create strong bond with ruthenium during the entire catalytic cycle.

The authors replaced the chloride ligand in Grubbs 1st generation catalyst with carboxylic group as linker molecule supported on polystyrene resin (Figure 2.13.) [120]. Such immobilized catalyst was active in self-metathesis of internal alkenes and in RCM.

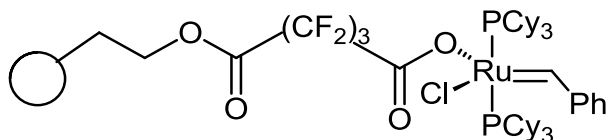


Figure 2.13. The first immobilized Ru-alkylidene metathesis catalyst *via* X ligand.

Immobilization of the Grubbs 2nd generation catalyst on silica and monolith supports *via* exchange of one chlorine ligand was introduced by Buchmeiser [132]. The surface of supported materials was modified with two polymerizable, carboxylate-containing ligands, *exo,exo*-7-oxanorborn-2-ene-5,6-dicarboxylic anhydride and 7-oxanorborn-2-ene-5,6-carboxylic acid and was then converted into the di-silver salt by treatment with $\text{Ag}(\text{NH}_3)_2\text{NO}_3$. Halogen exchange of the starting compounds with the Ru alkylidene was carried out at elevated temperature to form the new heterogeneous catalysts. Prepared catalysts were active in RCM of diethyl diallylmalonate, 1,7-octadiene, diallyldiphenylsilane, methyl *trans*-3-pentenoate, diallyl ether, *N,N*-diallyltrifluoroacetamide, and *t*-butyl *N,N*-diallylcarbamate. In the case of RCM of diethyl diallylmalonate, and 1,7-octadiene, TONs reached close to 1000. These heterogeneous catalysts showed low leaching (Ru leaching in all RCM experiments was ≤ 3.5 ppm) and can be used in monolith-based flow-through reactors. The same group presented immobilized tetrahydropyrimidin-2-ylidenes based complexes (Figure 2.14.) on different polymeric supports [133]. Buchmeiser's group also immobilized Grubbs 2nd generation catalyst by fluorinated carboxylates onto hydroxymethylpolystyrene support [134].

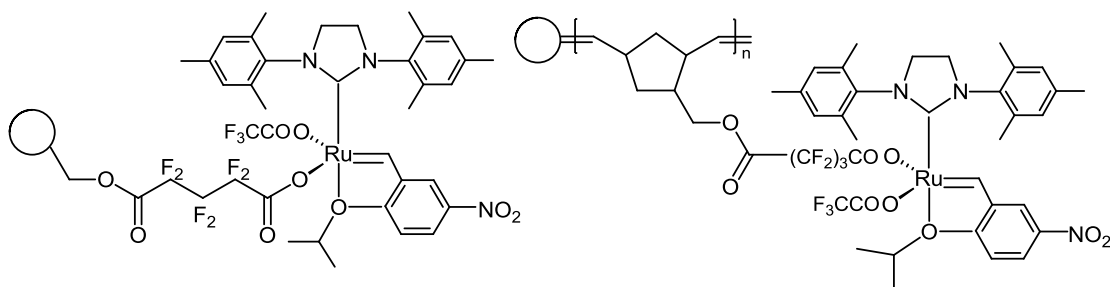


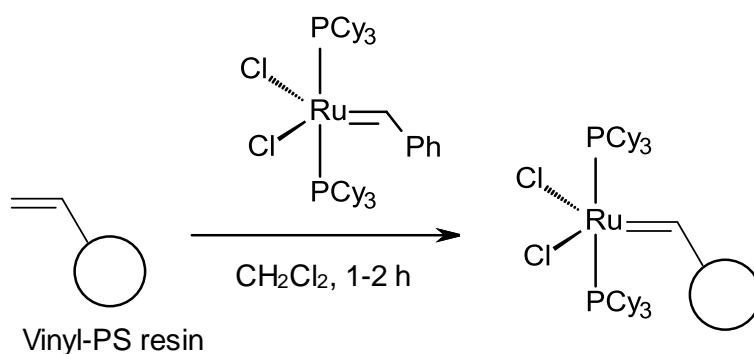
Figure 2.14. Hydroxymethyl-Merrifield resin supported catalyst and monolith supported catalyst.

Blechert *et al.* reported the first stable mono- (Figure 2.15.) and di-substituted fluorocarboxylate ruthenium alkylidenes [119]. These homogeneous catalysts were immobilized onto silica gel. After heterogenization, free OH groups on the silica surface were capped by dimethoxydimethylsilane.

2.3.4.3. Immobilization *via* alkylidene ligand

A most widely used method for immobilization of Ru-alkylidenes is *via* alkylidene ligand. Catalysts prepared by this method are so-called boomerang catalysts. Because the initiation step of the metathesis reaction involves exchange of alkylidenes. It is believed, that after propagation steps of metathesis, the released Ru species can be re-attached to the support (release-return or boomerang mechanism). During the initiation step of the reaction, the active catalyst species are released into a liquid phase (*i.e.* propagation steps occur in a liquid phase as in the case of homogeneous catalysts). In the case of effective return of soluble active species to the support materials, the catalyst combines features of heterogeneous catalyst (easy separation) with features of homogeneous catalyst (higher turnover frequency) [139].

The first supported so-called boomerang catalyst has been introduced by Barrett and co-workers [140]. The ruthenium catalyst was attached onto vinyl polystyrene resin through the exchange of its alkylidene ligand with vinyl groups (Scheme 2.15.). Later, Hoveyda and Grela provided evidence in favor of release-return mechanism with Hoveyda-Grubbs catalysts operating under high catalyst loading conditions (5 mol %). The Grela's explanation was that during the metathesis reaction, the whole amount of Hoveyda-Grubbs catalyst was involved in the catalytic cycle and was then regenerated by the release-return mechanism [141, 142]. On the other hand, Plenio investigated this topic using a fluorophore-tagged Hoveyda-Grubbs complex. They used 0.2 mol % of catalyst and did not find any evidence for release-return mechanism in RCM reactions in the Grubbs-Hoveyda type complexes. They actually believe that the re-isolation of Grubbs-Hoveyda complex is due to incomplete activation (initiation) of the initial catalyst [143].



Scheme 2.15. The 1st immobilized boomerang catalyst.

2.3.4.4. Immobilization *via* L-ligand

L ligands, donating two electrons to an empty orbital on the central atoms, are derived from charge-neutral precursors and are represented by amines, phosphines, CO, N₂, and alkenes

[144]. In the case of Ru-alkylidene metathesis complexes, L ligands are phosphine, pyridine, ethers, and NHC-carbenes.

Heterogenization *via* N-heterocyclic carbenes is one of the most frequently applied routes for immobilization of Ru-alkylidene metathesis catalysts. NHC ligands are strong donors and weak π -acceptors, which can lead to a very strong bond between NHC ligand and metal. Furthermore, it's easy to tune steric and electronic properties of the NHC ligand by modification of nitrogen and of the backbone carbon atoms. By tuning the properties of the NHC ligand one can control the activity and selectivity of NHC catalysts [145]. The advantage of this immobilization method is a strong bond between the catalyst and the support. Prepared catalysts showed a low leaching of Ru and could be used repeatedly. On the contrary, immobilization *via* NHC ligand required organic synthesis of functionalized NHC ligand.

The first immobilized catalyst *via* NHC ligand was introduced by Blechert *et al.* [146]. As a support, they used 4-(poly(styrene-*co*-divinylbenzene)methyloxymethyl)-1,3-dimesityl-4,5-dihydroimidazolin-2-ylidene, which then reacted with $\text{RuCl}_2(\text{PCy}_3)_2(=\text{CHPh})$ to create heterogenized catalysts (Figure 2.17.). This heterogeneous catalyst was successfully used in various metathesis reactions, typically in RCM reactions, which were completed in 12–18 h at 45 °C in CH_2Cl_2 and molar ratio substrate/Ru = 20.

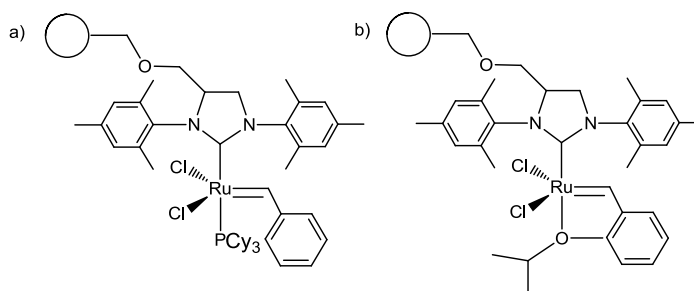


Figure 2.17. The first Grubbs (a) and Hoveyda-Grubbs (b) catalysts immobilized through NHC ligand.

Since this time, several types of supported Ru-alkylidenes *via* NHC ligand have been reported. Buchmeiser's group reported a number of supported catalysts on monolithic materials [147]. NHC containing Ru-alkylidenes were also immobilized on silica materials [148, 149]. Another strategy was to attach Ru-alkylidenes to a water soluble support (poly(ethylene glycol) conjugated with N-heterocyclic carbene ligand) [150], to overcome moderate activity of heterogenized catalysts connected with solids supports.

Sol-gel synthesis represents different methodology for preparing hybrid solid NHC metathesis ruthenium catalysts. The sol-gel hydrolytic condensation of suitable alkoxy silanes is

a convenient method for preparation of hybrid organic materials with targeted properties. The group of prof. Pleixats was interested in the synthesis of supported Hoveyda-Grubbs catalysts *via* sol-gel procedure with suitably modified ligands [151]. They introduced Hoveyda-Grubbs 2nd generation catalyst supported *via* NHC ligand prepared by sol-gel method [152]. This bisilylated supported catalyst (Figure 2.18.) was active in RCM of different dienes, in enyne metathesis and CM of styrene. Catalyst was successfully reused 5 times (during the first three runs without any significant drop of substrate conversion - decrease from 99 % to 89 %).

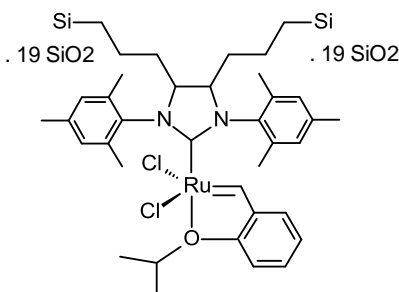
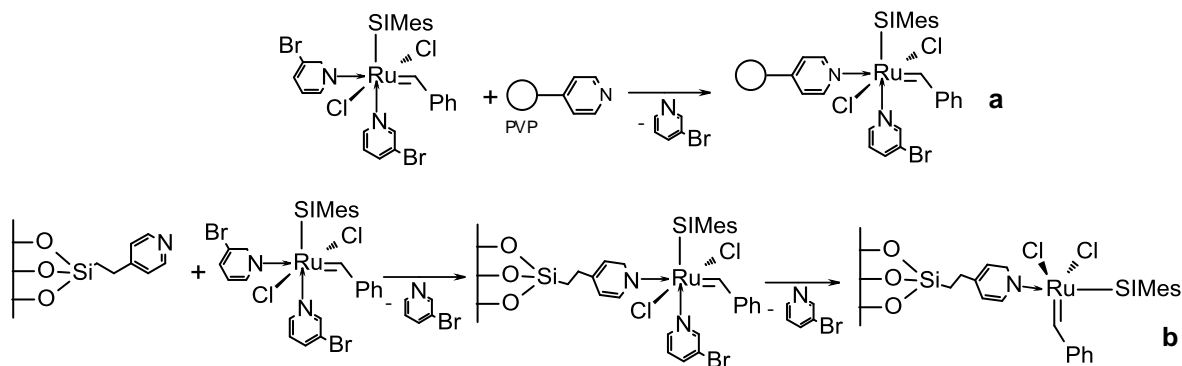


Figure 2.18. Hoveyda-Grubbs 2nd generation catalyst heterogenized *via* direct sol-gel method.

Grela and co-workers described a new concept of immobilization of Grubbs 3rd generation catalyst to polyvinyl pyridine [153]. The immobilization was achieved by ligand exchange (Scheme 2.16., catalyst **a**) resulting in a new type of grafted metathesis catalyst. The catalyst showed a good chemical reactivity in RCM, enyne, and CM reactions of various substrates.

The possibility of immobilization of Grubbs 3rd generation catalyst *via* pyridine ligands was tried also by Bek *et al.* [104]. They used mesoporous molecular sieves SBA-15 and MCM-41 (Scheme 2.16., catalyst **b**) as a supports, which were modified on their surface with the linker containing pyridine end groups. The catalyst was unstable, fast decomposition took place without complete conversion of metathesis substrates. On the other hand, catalyst showed negligible leaching of ruthenium species (0.18 %).



Scheme 2.16. Grubbs 3rd generation catalyst immobilized *via* pyridine linkers with two different ways.

The first example of immobilized Grubbs catalyst *via* phosphine ligands was reported by Grubbs *et al.* [154], who attached catalyst on a polystyrene support (Figure 2.19.). Prepared catalyst was active in self-metathesis of *cis*-2-pentene and ROMP of norbornene. In comparison with homogeneous analogue, it was found to be two orders of magnitude less active, probably because of chelation effect of both attached phosphine ligands. According to the mechanism of initiation, the phosphine ligand has to dissociate to form 14-electron active species, followed by coordination of olefin substrate or re-capture of free phosphine. The presence of a high concentration of phosphine on the support strongly favors phosphine re-capture, which slows down the rate of the metathesis.

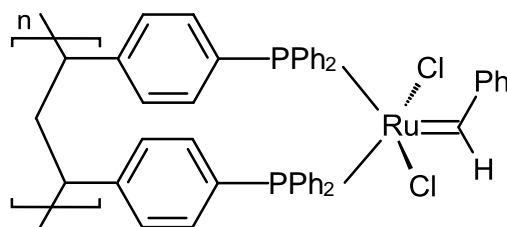


Figure 2.19. The first immobilized Grubbs 1st generation catalyst *via* phosphine ligands.

Later, the Grubbs 1st generation catalyst (Figure 2.20.) was immobilized through one phosphine ligand only [155]. Mesoporous molecular sieve MCM-41 was used as a solid support, which was then modified by phosphine ligands. Prepared catalysts showed activity in ROMP of norbornene (yield up to 70 %) and in RCM of diallylamine and diethyl diallylmalonate (catalysts TON's about 20). The cyclohexyl analogue was also active in the aqueous environment.

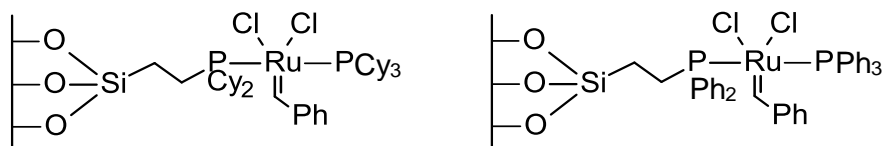
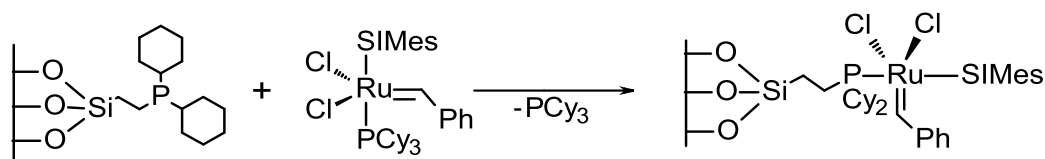


Figure 2.20. The Grubbs 1st generation catalyst immobilized through phosphine linker onto mesoporous molecular sieves MCM-41.

Exchange of tricyclohexylphosphine ligand of the Grubbs 2nd generation catalyst with the phosphine groups anchored on the SBA-15 support (Scheme 2.17.) was reported by Bek *et al.* [104]. Prepared catalyst was successfully applied in RCM of diethyl diallylmalonate (catalyst achieved TON's nearly 2000), (-)- β -citronellene, linalool, and diallyl phthalate; metathesis of methyl oleate, and CM of allylbenzene with 1,4-diacetoxy-2-butene and 5-hexenyl acetate with methyl acrylate. TONs achieved in these reactions were from 200 to 500. The catalyst exhibited high stability and selectivity in all tested reactions. The leaching of the catalyst was in the range from 1.6 % to 7.7 % of starting amount Ru in the catalyst, according to reaction conditions (Ru leaching was increased with increasing of the reaction temperature).



Scheme 2.17. The Grubbs 2nd generation catalyst immobilization on SBA-15 and MCM-41 modified with PCy₂ linkers.

2.3.5. Application of MMS as support for metathesis catalysts

2.3.5.1. W, Mo and Re oxides supported on MMS

Since the discovery of ordered mesoporous silicas, ill-defined metathesis catalysts were effectively immobilized onto these materials [3]. W, Re and Mo oxide catalysts were prepared from metal precursors by thermal spreading method [156]. These compounds reacted with surface OH groups under formation of metal oxide species covalently bound to the surface. The support architecture and pore size did not change substantially up to the relatively high loading.

The first MoO₃ supported catalyst on mesoporous silicas was reported by Ookoshi in 1998 provided very good activity in 1-octene metathesis with respect to all previously known MoO₃ based catalysts [157]. Improvement of catalyst activity of MoO₃ immobilized on MCM-41, MCM-48, and SBA-15 in metathesis of 1-octene was reported later [158].

Generally, good dispersion of metal oxide species on the surface of the support is considered to be a crucial factor for obtaining a highly active catalyst. Mesoporous molecular sieves having high BET areas can provide a better dispersion than ordinary silica. Moreover, the activity increased with increasing pore diameter of used mesoporous supports.

2.3.5.2. W, Mo, Re and Ru organometallic complexes on MMS

A number of protocols were developed for heterogenization of Ru alkylidenes. All possible ligands around Ru were modified in order to prepare heterogeneous catalyst. In about 20 years this effort did not lead to any efficient heterogeneous metathesis catalyst. Prepared catalysts showed low activity and stability in metathesis of terminal alkenes. The crucial step for the preparation of heterogeneous catalysts, which can provide high TONs in metathesis and work for long period of time without losing their activity, is stabilization of active, propagating species (Ru leaching during the propagation step into liquid phase can lead to the bimetallic decomposition). If heterogeneous catalysts are used under flow conditions, the leaching of active species can be a problem, it can dramatically reduce the productive time of such catalysts. To avoid the Ru leaching, the heterogenization should be realized through L ligand (active species can be attached to the support during the propagating step). Also, bulky L ligand stabilizes the active species and decreases intermolecular decomposition [159]. Finally, for the development of hybrid metathesis catalysts, the choice of support material is important. Suitable support material should enable fast diffusions of alkenes to and from catalytic centres and has large surface area for proper site isolation of Ru alkylidenes. Those conditions are fulfilled by mesoporous molecular sieves [3].

3. Experimental part

The first part of the chapter is focused on the synthesis of mesoporous molecular sieves. Three types of supports were prepared: (i) SBA-15, and MCM-41 with hexagonal channel-like structures and mesopore diameters 6.2 and 4.0 nm, respectively; (ii) SBA-16 of a cage-like body-centered cubic structure with pore cage diameter 7.4 nm and pore entrance diameter 4.7 nm; and (iii) MCM-48 of a three-dimensional interconnected cubic pore structure with mesopores of 6.0 nm. The supports were modified: (i) with ruthenium complexes using immobilization methods; and (ii) with magnesium oxide using incipient wetness method as it is explained in Chapter 3.3., and 3.4. The prepared materials were characterized by spectroscopic and physico-chemical techniques as mentioned in Chapter 3.5. All prepared heterogeneous metathesis catalysts were tested in several types of metathesis reactions of various substrates (Chapter 3.6.).

3.1. Applied chemicals

3.1.1. List of chemicals

Table 3.1. Solvents used.

| <i>Chemical name</i> | <i>M/g·mol⁻¹</i> | <i>Purity</i> | <i>Supplier</i> |
|---|-----------------------------|---------------|-----------------|
| <i>CAS number</i> | <i>ρ/g·cm⁻³</i> | <i>%</i> | |
| Methanol | 32.04 | p.a., | Lach-Ner |
| 67-56-1 | 0.7910 | ≥99.5 | |
| tetrahydrofuran (THF) | 72.11 | min. 99.9 | Sigma-Aldrich |
| 109-99-9 | 0.887 | | |
| Dichloromethane | 84.93 | p.a., | Lach-Ner |
| 75-09-2 | 1.33 | ≥ 99.5 | |
| Toluene | 92.14 | p.a., | Lach-Ner |
| 108-88-3 | 0.867 | ≥99 | |
| ethyl acetate | 88.11 | ≥99.7 | Fluka |
| 141-78-6 | 0.902 | | |
| chloroform d, 99.8 % D | 120.38 | - | Chemotrade |
| 865-49-6 | 1.5 | | |
| dichloromethane d₂ 99.6 % D | 86.94 | - | ISOSAR GMBH |
| 1665-00-5 | 1.362 | | |

Table 3.2. Chemicals used for the synthesis of heterogeneous catalysts and reaction substrates.

| <i>Chemical name</i> | <i>M/g·mol⁻¹</i> | <i>Purity</i> | <i>Supplier</i> |
|---|-----------------------------|---------------|--|
| <i>CAS number</i> | <i>ρ/g·cm⁻³</i> | <i>%</i> | |
| 2-(dicyclohexylphosphino)ethyltriethoxysilane (DHPETS) | 388.6 | | |
| 55289-47-9 | 0.986 | 95 | ABCR |
| Hexamethyldisilazane | 161.4 | | |
| 999-97-3 | 0.774 | ≥97 | Fluka |
| (-)-β-citronellene (CIT) | 138.25 | | |
| 10281-56-8 | 0.761 | ≥90 | Sigma-Aldrich |
| cis-cyclooctene (COE) | 110.2 | | |
| 931-87-3 | 0.846 | 95 | Janssen Chimica |
| N, N-Diallyl-2,2,2-trifluoroacetamide (DAF) | 193.17 | | |
| 14618-49-6 | 1.13 | 98 | Sigma-Aldrich |
| diethyl diallylmalonate (DEDAM) | 240.3 | | |
| 3195-24-2 | 0.994 | 98 | Sigma-Aldrich |
| 1,7-octadiene (OD) | 110.12 | | |
| 3710-30-3 | 0.74 | ≥97 | Fluka |
| 5-hexenyl acetate (HexAc) | 142.2 | | |
| 5048-26-0 | 0.883 | 97 | Sigma-Aldrich |
| cis-1,4-diacetoxy-2-butene (DAB) | 172.18 | | |
| 25260-60-0 | 1.08 | 95 | Sigma-Aldrich |
| n-nonane | 128.2 | | |
| 111-84-2 | 0.718 | ≥ 98.5 | BHD Chemicals |
| ethyl vinyl ether | 72.11 | | |
| 109-92-2 | 0.754 | 99 | Sigma-Aldrich |
| tert-butyl N, N-diallyl-carbamate (DAC) | 197.28 | | |
| 151259-38-0 | 0.914 | 98 | Sigma-Aldrich |
| Allylbenzene | 118.18 | | |
| 300-57-2 | 0.892 | 98 | Sigma-Aldrich |
| methyl oleate | 296.49 | | Research Inst. of Inorg. |
| 112-62-9 | 0.873 | 94 | Chem., a.s. Czech Republic |
| methyl 10-undecenoate | 200.32 | | |
| 111-81-9 | 0.872 | 96 | Sigma-Aldrich |
| 1-decene | 140.27 | | |
| 872-05-9 | 0.741 | 98 | Sigma-Aldrich |
| Hoveyda-Grubbs Catalyst 1st Generation (RC-304) | 707.74 | | |
| 918871-44-0 | - | - | Zhannan Pharma |
| AquaMet catalysts (X-HG-Cl) | 803.31 | | |
| 1414707-08-6 | - | | Apeiron Catalysts Sp. z o.o. Wrocław, Poland |
| Dichloro[1,3-Bis(2-methylphenyl)-2-imidazolidinylidene](benzylidene)(tricyclohexylphosphine)ruthenium(II) (G-II-tolyl) | 927429-60-5 | 792.88 | - |
| | | | Sigma-Aldrich |

Table 3.3. Chemical used for the synthesis of mesoporous molecular sieves and MgO modification.

| <i>Chemical name</i> <i>CAS number</i> | <i>M/g·mol⁻¹</i> <i>ρ/g·cm⁻³</i> | <i>Purity</i> <i>%</i> | <i>Supplier</i> |
|--|---|---------------------------|-----------------|
| Pluronic P123, poly(ethylene glycol)-block-poly(propylene glycol)-block-poly(ethylene glycol), (EO:PO:EO = 20:70:20) 9003-11-6 | average M_n =5800 Da 1.018 | - | Sigma-Aldrich |
| tetraethyl orthosilicate (TEOS) 78-10-4 | 208.33 0.933 | 98 | Sigma-Aldrich |
| <i>n</i>-heptane 142-82-5 | 100.20 0.684 | 99 | Sigma-Aldrich |
| hydrochloric acid | 36.46 1.2 | 37 | Penta |
| 1-methyl-3-octylimidazolium chloride 64697-40-1 | 230.78 1.01 | >97 | Sigma-Aldrich |
| hexadecyltrimethylammonium bromide 57-09-0 | 364.45 - | >98 | Sigma-Aldrich |
| sodium silicate | - 1.39 | - | Sigma-Aldrich |
| <i>n</i>-butanol 71-36-3 | 74.12 0.81 | 99 | Sigma-Aldrich |
| Pluronic F127 (Polyoxypropylenepolyoxyethylene Block Copolymer) 9003-11-6 | average M_n = 12 500 Da | - | Sigma-Aldrich |
| magnesium acetate tetrahydrate 16674-78-5 | 214.45 1.45 | 98 | Sigma-Aldrich |
| oxalic acid 144-62-7 | 90.03 1.90 | ≥99 | Sigma-Aldrich |
| potassium hydroxide 1310-58-3 | 56.11 2.04 | ≥85 | Lach-Ner |
| Styrylethyltrimethoxysilane 134000-44-5 | 266.64 1.02 | 92 | ABCR |
| Triethoxyvinylsilane 78-08-0 | 190.32 0.911 | 97 | Sigma-Aldrich |

Table 3.4. Other chemicals and materials used.

| <i>Chemical name</i> | <i>M/g·mol-1</i> | <i>Purity</i> | <i>Supplier</i> |
|--|------------------|---------------|------------------|
| <i>CAS number</i> | <i>ρ/g·cm-3</i> | <i>%</i> | |
| argon | 39.95 | 99.999 | Messer Technogas |
| 7440-37-1 | - | | |
| 2,6-di-tert-butyl-p-cresol | 220.36 | >99 | Fluka |
| 128-37-0 | - | | |
| calcium chloride, anhydrous | 110.98 | - | Lachema |
| 10043-52-4 | 2.15 | | |
| sodium sulfate, anhydrous | 142.04 | ≥99 | Fluka |
| 7757-82-6 | - | | |
| sodium | 22.99 | - | Fluka |
| 7440-23-5 | 0.968 | | |
| Silicagel 40 (Merck) | 60.08 | - | Merck |
| 112926-00-8 | - | | |

3.1.2. Purification of solvents and substrates

All solvents used for preparations of the catalysts and catalytic experiments were purified by fractional distillation.

Toluene: was dried overnight with anhydrous Na₂SO₄ and then distilled with Na. Distilled toluene was stored over the molecular sieve of type 4A.

Dichloromethane: was dried overnight with anhydrous CaCl₂ and then distilled with P₂O₅. Distilled dichloromethane was stored in a flask under Ar atmosphere in dark.

Tetrahydrofuran: was dried overnight with molecular sieve type 4A and then refluxed with Na and benzophenone till the color of THF in distillation flask changed to dark blue. Distilled THF was stored in a flask under Ar. For reactions freshly distilled THF was used.

Ethyl acetate: was dried overnight with anhydrous P₂O₅ and then distilled with CaH₂. Distilled ethyl acetate was stored over the molecular sieve of type 4A.

All substrates used for metathesis reactions were purified by passing through a short column of activated alumina before the addition into the reactor.

3.2. Synthesis of mesoporous molecular sieves

Mesoporous silicas were prepared *via* hydrothermal synthesis. Reaction mixtures were prepared in 1 L autoclavable Nalgene bottles. After the synthesis, the solid product was recovered by filtration, thoroughly washed with distilled water and dried overnight in air. Structure-directing agents were removed by calcination in air carried out at 540 °C for 8 h with a temperature ramp of 1 °C/min.

3.2.1. Synthesis of SBA-15

Synthesis of siliceous SBA-15 was carried out according to the procedure described in ref. [2]. 24 g of Pluronic P123 was dissolved in the solution of 774 mL of distilled water and 126 mL of 2 M hydrochloric acid. The reaction mixture was stirred for 24 h at 35 °C. Then 54 mL of tetraethyl orthosilicate (TEOS) was added. The synthesis mixture was vigorously stirred at 35 °C for 5 min and subsequently aged under static conditions for 24 h at 35 °C and 48 h at 97 °C.

3.2.2. Synthesis of MCM-41

MCM-41 was synthesized by the homogeneous precipitation method, described in ref. [160]. In a typical synthesis of MCM-41, 3 g of 1-methyl-3-octylimidazolium chloride and 1 g of hexadecyltrimethylammonium bromide together with 4 g of Na₂SiO₃ was dissolved in 900 mL of distilled water under vigorous stirring, resulting in a clear solution. Afterward, 15 mL of ethyl acetate was quickly added, the mixture was homogenized and the stirring was stopped. The reaction mixture was allowed to stand at ambient temperature for 5 h and then heated at 90 °C for 72 h in a polypropylene bottle.

3.2.3. Synthesis of MCM-48

Synthesis of siliceous mesoporous MCM-48 based on the modification of the method described in ref. [161] was carried out in the following way: 20 g of Pluronic P123 and 33.5 mL of hydrochloric acid (37 %) were dissolved in 720 mL of distilled water to form a clear solution. 24.7 mL of *n*-butanol was added; afterward, the mixture was stirred at 35 °C for 3 h. Then, 46.1 mL of TEOS was added; afterward, the mixture was stirred at 35 °C for 2 h. Finally, the reaction mixture was aged without stirring for 24 h at 35 °C and 24 h at 95 °C.

3.2.4. Synthesis of SBA-16

In the typical synthesis [162] 3.27 g of Pluronic P123, 10.21 g of Pluronic F127 and 91 mL of hydrochloric acid (37 %) were dissolved in 550 mL of distilled water to form a clear solution.

50 mL of TEOS was added, and the mixture was stirred for 5 min. The reaction mixture was then aged without stirring for 24 h at 35 °C and 24 h at 95 °C.

3.2.5 Synthesis of SG-1 and SG-2

Synthesis of **SG-1** based on the modification of the method described in ref. [152] was carried out as follows: solution of TEOS (4.5 mL) and triethoxyvinylsilane (105 μ L) in dry and degassed EtOH (10 mL) was prepared in a 25 mL flask. To this solution, a solution of NH_4F (105 μ L), and water (1.0 mL) in dry EtOH (10 mL) was added under stirring. The final mixture was stirred at room temperature for 5 min and then stirring was stopped. A gel was formed after 1 h and was aged for 6 days at room temperature under argon atmosphere. At this time, the gel was pulverized, filtered, washed with dry EtOH (3 x 10 mL), dry CH_2Cl_2 (2 x 10 mL), and finally dried overnight at 50 °C under vacuum. The final solid was crushed to obtain material **SG-1**. **SG-2** was prepared in the same way, but instead of the triethoxyvinylsilane, styrylethyltrimethoxysilane was used.

3.3. Modifications of mesoporous molecular sieves

3.3.1 Modification of mesoporous sieves for immobilization of metathesis catalysts

Mesoporous molecular sieves were modified with phosphine linker containing triethoxysilane group. All modifications were performed at room temperature in a Schlenk tube under Ar atmosphere.

Typical modification of SBA-15: 15 mL of toluene was added to 900 mg of SBA-15 (predried under vacuum at 300 °C for 3 h) in a Schlenk tube, then 650 μ L of 2-(dicyclohexylphosphine)ethyltriethoxysilane was added, and the mixture was stirred for 23 h at 60 °C. Supernatant was filtered off and the modified SBA-15 (**M1**) was 4 times washed under the argon atmosphere with 10 ml of toluene and dichloromethane and finally the rest of solvent was removed by drying of the modified SBA-15 in vacuum at room temperature. All other modifications (**M2** - **M4**) were performed in a similar way (Table 3.5.). The modified sieves were stored in Schlenk tubes under argon atmosphere.

Preparation of **M5**: 500 mg of **M1** was suspended in 15 ml of toluene and 6.7 g of hexamethyldisilazane was added. The mixture was stirred for 23 h at 60 °C. Supernatant was filtered off and the modified SBA-15 (**M5**) was 4 times washed under the argon atmosphere with 10 ml of toluene and dichloromethane. Finally, the rest of solvent was removed by drying of the modified SBA-15 in vacuum at room temperature.

Table 3.5. List of sieves modified.

| <i>Sample</i> | <i>m(sieves), mg</i> | <i>Amount of a linker</i> | <i>P content in modified samples, wt. %</i> |
|---------------|----------------------|---|---|
| M1 | 900 (SBA-15) | 0.6 g DHPETS | 1.29 |
| M2 | 1000 (SBA-16) | 0.6 g DHPETS | 1.46 |
| M3 | 950 (MCM-48) | 0.6 g DHPETS | 1.33 |
| M4 | 900 (MCM-41) | 0.6 g DHPETS | ND ^a |
| M5 | 500 (SBA-15) | 0.6 g DHPETS, 6.7 g hexamethyldisilazane | ND |

^a not determined

reaction conditions: 15 mL toluene, reaction time 24 h, temperature = 60 °C

DHPETS = 2-(dicyclohexylphosphino)ethyltriethoxysilane

3.3.2. Modification of mesoporous sieves for adsorption of carbon dioxide

Magnesium oxide-grafted materials were prepared from purely siliceous SBA-15 mesoporous molecular sieve synthesized as reported earlier (Chapter 3.2.). To prepare magnesium oxides-grafted material, 2 g of the SBA-15 silica were added to a solution containing 5 mL of ethanol, 5 mL of distilled water and 2 g of magnesium acetate tetrahydrate. This mixture was filtered after 5 min and dried at 60-90 °C for 1 h. The sample was dried at 115 °C for 8 min. The dried composite was soaked in 10 mL of oxalic acid solution (30 g oxalic acid in 100 mL of ethanol) for 5-10 min. The powder was filtered, dried at 75 °C, and calcined in air at 300 °C for 10 h (temperature ramp of 1 °C/min). Magnesium oxides-grafted materials were impregnated with potassium oxalate: 0.5 g of MgO-SBA-15 was soaked in 3 ml of 0.5 M solution of potassium oxalate (4.5 g oxalic acid, and 5.02 g KOH in 100 mL of distilled water) overnight. Samples were dried by vacuum filtration at room temperature. Calcination was carried out in air at 300 °C for 6 h (temperature ramp of 1 °C/min).

3.4. Preparation of the metathesis catalysts

Dried siliceous supports were used for the preparation of the catalysts. The supports were dried in Schlenk tubes under vacuum at 300 °C for 3 h (temperature ramp of 10 °C/min) to

remove water adsorbed on the surface of the supports. Preparation of the catalysts was carried out in a Schlenk tube under the argon atmosphere. All manipulations with the catalysts were performed under the argon atmosphere. Structures of used well-defined homogeneous Ru catalysts are displayed in the Figure 3.1. Prepared catalysts are displayed in Table 3.6.

3.4.1. Immobilization of Ru alkylidenes *via* linker

3.4.1.1. Immobilization of well-defined Ru alkylidenes *via* exchange of PCy₃ ligands

Catalysts **C01**, **C02**, **C03**, and **C04**, were prepared by immobilization of Hoveyda-Grubbs-type catalysts on siliceous supports *via* 2-(dicyclohexylphosphino)ethyltriethoxysilane linker.

Immobilization of **RC-304** complex on SBA-15, SBA-16, MCM-41, and MCM-48 was performed according to the previously published procedure [104].

Preparation of **C01**: 1.2 g of linker modified SBA-15 (**M1**) was suspended in 13 mL of dry toluene and 109.2 mg **RC-304** was added. The suspension was stirred at room temperature for 24 h. The product was several times washed with toluene and CH₂Cl₂. The product **C01** was dried in vacuum. 1.07 wt. % loading of Ru was determined using ICP-MS.

Preparation of **C01a**: 320 mg of linker-modified SBA-15 (**M5**) was suspended in 15 ml of dry toluene and 29.1 mg **RC-304** was added. The suspension was stirred at room temperature for 24 h. The product was several times washed with toluene and CH₂Cl₂. The product **C01a** was dried in vacuum. The Ru loading was 0.83 wt. % (determined by ICP-MS).

Preparation of catalysts **C02** – **C04** was done in the same way like preparation of catalyst **C01**, the amounts of sieves and Ru complexes are given in Table 3.7.

Catalyst **C13** was prepared by immobilization of the Grubbs 2nd generation catalyst (**G-II-tolyl**) on SBA-15 *via* 2-(dicyclohexylphosphino)ethyltriethoxysilane linker. Preparation of catalyst **C13** was performed in toluene at room temperature under argon atmosphere. 300 mg of linker modified SBA-15 (**M1**) was suspended in 15 mL of dry toluene and 26.6 mg **G-II-tolyl** was added. The suspension was stirred at room temperature for 24 h. The product was several times washed with toluene and CH₂Cl₂. The product **C13** was dried in vacuum. 0.66 wt. % loading of Ru was determined using ICP-MS.

3.4.2. Immobilization of Ru alkylidenes *via* non covalent interaction

Preparation of catalyst **C05** was performed in CH₂Cl₂ at room temperature under argon atmosphere. In a typical preparation, 1000 mg of SBA-15 (pre-dried under vacuum at 300 °C for 3 h) was dissolved with 15 mL of CH₂Cl₂ in a Schlenk tube, then 103 mg of **Cl-HG-II** was

added, and the mixture was stirred for 3 h at 25 °C. The product was 2 times washed under the argon atmosphere with 10 mL of CH₂Cl₂ and the rest of CH₂Cl₂ was removed by drying of the **C05** in vacuum at room temperature. The preparation of **C06**, **C07**, and **C08 – C10** (from **X-HG-II**, where X = I, BF₄⁻, and PF₆⁻) was done in the same way (amounts of sieves and complexes are given in Table 3.7.).

Preparation of catalyst **C11** was performed in toluene at room temperature under argon atmosphere. 300 mg of SBA-15 (pre-dried under vacuum at 300 °C for 3 h) was mixed with 15 mL of toluene in a Schlenk tube, then 28 mg of **RC-304** was added, and the mixture was stirred at 25 °C for 23 h. The product was 2 times washed under the argon atmosphere with 10 mL of toluene and 2 times with 10 mL of CH₂Cl₂. The product **C11** was dried in vacuum. 0.48 wt. % loading of Ru was determined using ICP-MS.

3.4.3. Immobilization of Hoveyda–Grubbs alkylidenes on SG supports through the alkylidene ligand

Preparation of catalyst **SG01** was performed in toluene at room temperature under argon atmosphere. In a typical preparation, 150 mg of SG-1 (pre-dried under vacuum at 100 °C for 6 h) was mixed with 15 mL of toluene in a Schlenk tube, then 14 mg of **RC-304** was added, and the mixture was stirred at 25 °C for 23 h. The product was four times washed with toluene and CH₂Cl₂. The preparation of **SG02** was made in the same way. **SG01** was prepared with Ru loading of 0.33 wt. %, and **SG02** with 0.44 wt. %.

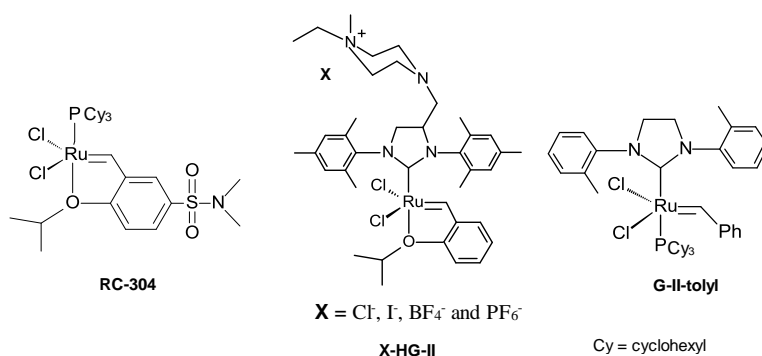
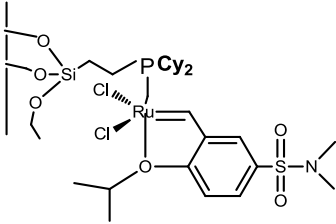
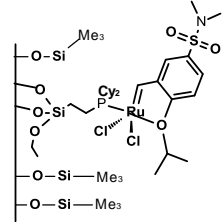
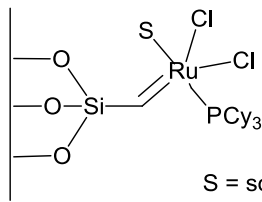
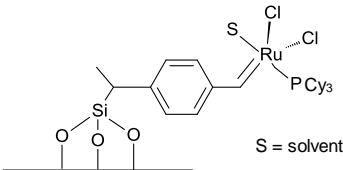
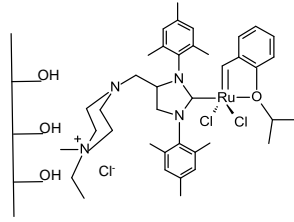
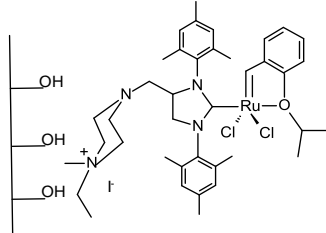


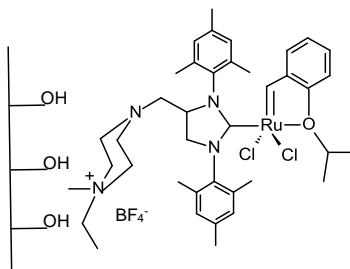
Figure 3.1. Structure of well-defined homogeneous Ru catalysts used in this work.

Table 3.6. Structures of catalysts prepared by immobilization of well-defined Ru alkylidenes.

| <i>Catalyst</i> | <i>Used supports</i> | <i>Structure</i> |
|-------------------------|----------------------|---|
| C01 | SBA-15 |  <p>Cy = cyclohexyl</p> |
| C02 | SBA-16 | |
| C03 | MCM-48 | |
| C04 | MCM-41 | |
| C01a | SBA-15 |  |
| SG01^a | - |  <p>S = solvent</p> |
| SG02^a | - |  <p>S = solvent</p> |
| C05^a | SBA-15 |  |
| C06^a | MCM-41 | |
| C07^a | silica | |
| C08^a | SBA-15 |  |

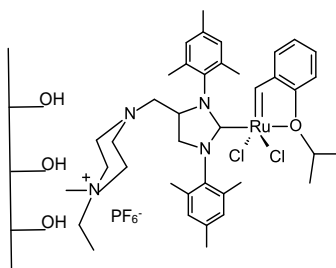
C09^a

SBA-15



C10^a

SBA-15



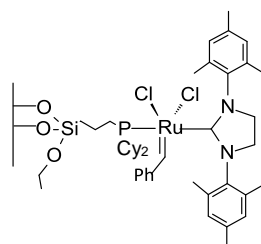
C11

SBA-15

RC-304 physisorbed on SBA-15

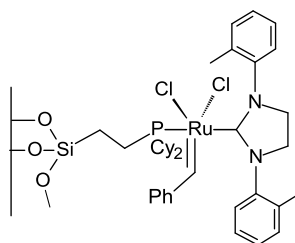
C12^b

SBA-15



C13

SBA-15



^a proposed structure, catalysts were not be fully characterized

^b catalyst prepared in our laboratory by D. Bek, described in ref. 104

Table 3.7. Supports and Ru alkylidenes used for the preparation of the catalysts.

| <i>Catalyst</i> | <i>Used supports</i> | <i>Weight of P modified sieves mg</i> | <i>Weight of sieves mg</i> | <i>Weight of alkylidenes applied mg</i> | <i>Catalyst Ru content wt. %</i> | <i>f</i> |
|-----------------|----------------------|---------------------------------------|----------------------------|---|----------------------------------|----------|
| C01 | SBA-15 | 1200 (M1) | - | 109.2 | 1.07 | 0.83 |
| C01a | SBA-15 | 500 (M5) | - | 29.1 | 0.83 | 0.64 |
| C02 | SBA-16 | 340 (M2) | - | 47.6 | 0.95 | 0.48 |
| C03 | MCM-48 | 720 (M3) | - | 65.5 | 1.01 | 0.78 |
| C04 | MCM-41 | 550 (M4) | - | 50.3 | 1.06 | 0.82 |
| C05 | SBA-15 | - | 1000 | 103.0 | 1.17 | 0.99 |
| C06 | MCM-41 | - | 500 | 51.5 | 1.17 | 0.99 |
| C07 | Silica | - | 500 | 51.5 | 0.92 | 0.76 |
| C08 | SBA-15 | - | 500 | 51.5 | 1.12 | 0.95 |
| C09 | SBA-15 | - | 500 | 51.5 | 1.15 | 0.97 |
| C10 | SBA-15 | - | 500 | 51.5 | 1.09 | 0.93 |
| C11 | SBA-15 | - | 300 | 28.0 | 0.48 | 0.41 |
| C13 | SBA-15 | - | 300 | 29.6 | 0.66 | 0.56 |

\bar{f} = fraction of Ru captured on the support

3.5. Characterization of prepared materials

3.5.1. Characterization of the MMS, adsorbents and catalysts

Adsorption isotherms of nitrogen at $-196\text{ }^{\circ}\text{C}$ (*i.e.*, 77.35 K) on materials under study were determined using an ASAP 2020 (Micromeritics) instrument. In order to attain sufficient accuracy in the accumulation of the adsorption data, this instrument was equipped with pressure transducers covering the 133 Pa , 1.33 kPa , and 133 kPa ranges. Before each sorption measurement, each sample was degassed. Starting at ambient temperature the sample was degassed at $110\text{ }^{\circ}\text{C}$ (temperature ramp of $0.5\text{ }^{\circ}\text{C min}^{-1}$) until the residual pressure of 1 Pa was attained. In the case of silica materials bearing organic molecules, the samples were outgassed at $110\text{ }^{\circ}\text{C}$ under turbomolecular pump vacuum for 8 h. After one 1 h delay at $110\text{ }^{\circ}\text{C}$, in the case of CO_2 adsorbents, the temperature was further increased for (heating ramp of $1\text{ }^{\circ}\text{C/min}$) to $300\text{ }^{\circ}\text{C}$. The samples were also outgassed at this temperature under turbomolecular pump vacuum for 8 h.

The Iso-Therm thermostat (e-Lab Services, Czech Republic) maintaining temperature of the sample with accuracy of $\pm 0.01\text{ }^{\circ}\text{C}$ was used for the measurement of carbon dioxide adsorption at 0 , 20 , 40 , and $60\text{ }^{\circ}\text{C}$. (The exact temperature of each measurement was determined using platinum resistance thermometer.) As adsorption isotherms of carbon dioxide were measured on the same sample immediately after nitrogen adsorption measurement, the degas procedure was performed at $300\text{ }^{\circ}\text{C}$ for 8 h under turbomolecular pump vacuum. These conditions were also applied when carbon dioxide adsorption measurement was repeated at another temperature.

X-ray powder diffraction (XRD) data were obtained on a Bruker AXS D8 Advance diffractometer with a graphite monochromator and a position sensitive detector Vantec-1 using $\text{Cu K}\alpha$ radiation (at 40 kV and 30 mA) in Bragg-Brentano geometry.

^{31}P MAS (Magic-Angle Spinning) and ^{29}Si MAS nuclear magnetic resonance (NMR) spectra were recorded on a 500 MHz (11.7 T) Wide Bore Agilent NMR system using an Agilent $3.2\text{ mm T3 HXY MAS Solids NMR Probe}$ and zirconia rotors. Sample rotation frequencies for ^{29}Si cross-polarization (CP MAS) experiments were 10 kHz while for ^{31}P MAS experiments were 20 kHz . Recycle delays and number of transients for ^{31}P MAS were 30 s and 400 s , and for ^{29}Si CP MAS were 5 s and 10000 s . The chemical shifts reported were expressed relative to TMS and 80 \% solution of H_3PO_4 for ^{29}Si and ^{31}P signals, respectively. The measurements were done in Erlangen Catalysis Resource Center (ECRC), Erlangen, Germany.

Photoelectron spectra of the samples were measured using an ESCA 310 (Scienta, Sweden) spectrometer equipped with a hemispherical electron analyser operated in a fixed transmission

mode. Monochromatic Al K α radiation was used for electron excitation. The spectra were recorded at room temperature. The Si 2p, O 1s, Cl 2p, P 2p, P 2s, C 1s, and Ru 3d photoelectrons were measured. Sample charging was corrected using the Si 2p peak at 103.4 eV as an internal standard. For overlapping C 1s and Ru 3d lines, the contributions of individual components were determined by curve fitting.

The morphology of mesoporous molecular sieve particles was examined by scanning electron microscopy (SEM) on a JEOL, JSM-5500LV microscope.

UV-Vis spectra of homogeneous catalysts were recorded using a Perkin-Elmer Lambda 950 spectrometer.

FTIR spectra were recorded on FTIR spectrometer Nicolet Avatar 320 in KBr pellets with DTGS-KBr detector and a cell with NaCl windows connected to vacuum apparatus. IR spectra were recorded at room temperature with resolution of 1 cm⁻¹ by collecting 32 scans for a single spectrum.

Size-exclusion chromatography (SEC) measurements were carried out on a Watrex Chromatograph fitted with a differential refractometer Shodex RI 101. A series of two PL-gel columns (mixed-B and mixed-C, Polymer Laboratories, Bristol, UK) and tetrahydrofuran (THF) (flow rate 0.7 mL/min) were used. Weight average molecular weight, M_w , and number average molecular weight, M_n , relative to polystyrene standards are reported. The measurements were performed at the Department of Physical and Macromolecular Chemistry, Faculty of Science, Charles University in Prague.

Determination of magnesia species, ruthenium, and phosphorus was performed at the Institute of Analytical Chemistry, ICT, Prague using inductively coupled plasma mass spectrometry (ICP-MS) using an Elan DRC-e (Perkin Elmer, Concord, Canada) spectrometer, equipped with a concentric PTFE nebulizer, a cyclonic spray chamber and a high efficiency quartz torch. Before measurement, the liquid samples were evaporated to dryness and mineralized with HNO₃ in UniClever microwave decomposition unit (Plazmatronika-Service, Wroclaw, Poland). Solid samples were decomposed with the mixture of HF and HNO₃ (1:3 v/v). The estimation error was 5 %.

3.5.2. Characterization of substrates and products

A high-resolution gas chromatography Agilent 6890 with DB-5 column (length: 50 m, inner diameter: 320 μ m, stationary phase thickness: 1 μ m) was used for the product analysis. *n*-nonane was used as an internal standard for quantitative evaluation. Individual products were identified

by GC-MS. GC-MS measurements were performed on a Thermo Focus DSQ using the capillary column Thermo TR-5MS (length 15 m \times film thickness 0.25 mm internal diameter \times 0.25 mm).

^1H (300 MHz) and ^{13}C (75 MHz) NMR spectra were recorded on a Varian Mercury 300 spectrometer in tetrahydrofuran d_8 , dichloromethane d_2 , chloroform d or benzene d_6 at 25 °C. Chemical shifts (δ , ppm) are given relative to the solvent signals. The measurements were performed at the Institute of Macromolecular Chemistry of the ASCR, v. v. i. in Prague, Czech Republic.

Size-exclusion chromatography (SEC) measurements of ROMP products were carried out in the way already described (*vide supra*).

3.6. Catalysts testing

All catalytic experiments and manipulations with catalysts were carried out under argon atmosphere. Reactions in a batch reactor were carried out by standard Schlenk tube technique; reactions in a flow system were carried out in home-made flow reactor. Samples from all reactions were terminated by terminating agent ethyl vinyl ether, the samples were centrifuged, and the supernatant analysed by GC.

3.6.1. Ring-closing metathesis

In a typical RCM experiment, 8.1 mg of the catalyst **C01** was placed into the reactor, then 1.3 mL of toluene was added and the suspension was heated to 50 °C in an oil bath. Then, 30 μL of 1,7-octadiene (molar ratio Ru/1,7-octadiene = 1:250, c^0 (1,7-octadiene) = 0.15 mol/L) was added under stirring. Samples (0.1 mL of the reaction mixture) were taken at given time intervals after 1,7-octadiene addition.

3.6.2. Self-metathesis

In a metathesis of 5-hexenyl acetate (HexAc), 10.7 mg of **C01** was placed into the reactor, then 1.1 mL of toluene was added and the suspension was heated to 80 °C in an oil bath. Then, 15 μL of *n*-nonane (internal standard) and 28.0 μL of HexAc (molar ratio Ru/HexAc = 1:250, c^0 (HexAc) = 0.15 mol/L) were added under stirring.

3.6.3. Cross-metathesis

In a typical cross-metathesis (CM) experiment, 22.0 mg of catalyst **C01** was placed into the reactor, then 2.5 mL of toluene was added, and the suspension was heated to 80 °C in an oil bath. Then the mixture of 74 μL of allylbenzene (AllB), 179 μL of *cis*-1,4-diacetoxy-2-butene

(DAB) (molar ratio AlIB/Ru = 40, c^0 (AlIB) = 0.2 mol/L, c^0 (DAB) = 0.3 mol/L) and 70 μ L of *n*-nonane (internal standard) was added under stirring. During metathesis experiments samples (0.1 mL) were taken at given intervals after substrate(s) addition.

3.6.4. ROMP

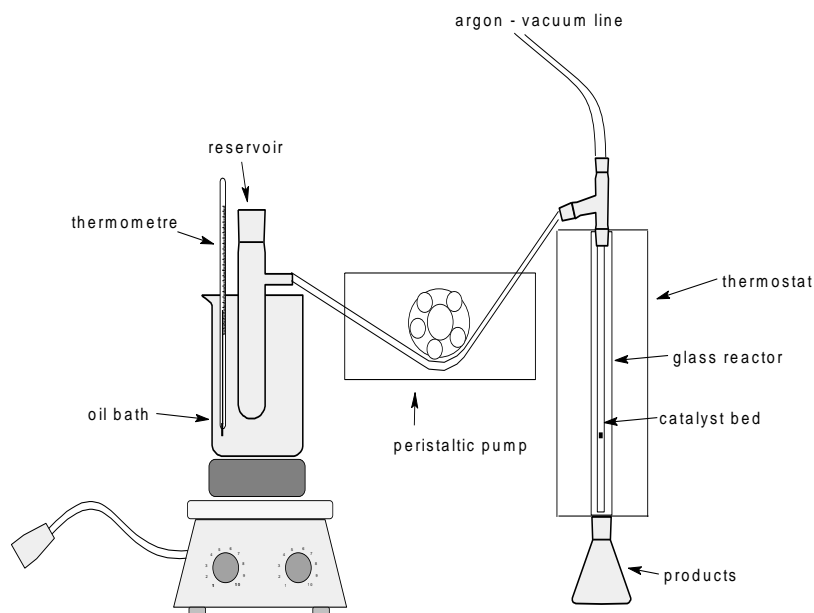
ROMP of cyclooctene (COE) was performed with the **C01** catalyst. In a typical experiment, 20 mg of the catalyst **C01** was placed into the reactor, 1 mL of toluene was added and the suspension was heated to 80 °C in an oil bath. Then 140 μ L of COE (molar ratio Ru/COE = 1:500, c^0 (COE) = 0.8 mol/L) was added and the reaction mixture was stirred for 3 h. Reaction was terminated by addition of 0.1 mL of ethyl vinyl ether, after 10 min the reaction mixture was cooled, catalyst separated by centrifugation and poly(COE) was precipitated by pouring into 10 mL of methanol containing a small amount of antioxidant 2,6-di-tert-butyl-p-cresol. The polymer was dried in a vacuum oven at 60 °C to the constant weight.

3.6.5. Flow reactions

The experimental set up of the home-made reactor for metathesis reactions under the flow conditions was designed according to Scheme 3.1. The mixture of solvent and metathesis substrate was stirred and heated to desired temperature in a Schlenk tube under the argon atmosphere. The tubular glass reactor previously loaded with the catalyst was fixed into the thermostat in a vertical position, and heated to the reaction temperature. The flow was from the top to the bottom. Then, mixture of reactant olefins was sent to the glass catalyst bed by a peristaltic pump. After passing the catalyst the reaction mixture was collected at given intervals and analysed by GC.

All flow reactions were performed with the **C01** catalyst. For the typical flow reaction, the catalysts bed was filled with 63 mg of **C01** catalyst and heated to the reaction temperature. Solution of 20 mL of toluene and 445 μ L of 1,7-octadiene was placed into a Schlenk tube and heated to a desired temperature in an oil bath (molar ratio Ru:1,7-octadiene = 1:250, c^0 (1,7-octadiene) = 0.15 mol/L). Samples (0.1 mL) were taken at given intervals in the outlet of the flow reactor.

WHSV was calculated as the weight of feed per hour per unit weight of catalyst loaded in the reactor.



Scheme 3.1. The experimental set up of the home-made reactor.

3.7. Catalytic data evaluation

In the case of RCM of 1,7-octadiene and (-)- β -citronellene internal standard was not used, because it was found unnecessary. For DEDAM, it was experimentally verified that addition of an internal standard (*n*-nonane) was also not necessary. In this case, the molar amounts of substrate and products used for calculation of the conversion were determined from the areas of corresponding peaks in GC chromatogram under the assumption that ratios of weight amounts are equal to ratios of peak areas.

n-nonane was used as an internal standard for determination of substrate conversion, whenever required (DAC, DAF, 5-hexenyl acetate, methyl 10-undecenoate, methyl oleate) using calibration curves, which were experimentally determined for all substrates used.

In the case of ROMP, the polymer yields were determined gravimetrically as follows: the weight of the dry polymer was divided by the weight of the monomer used for the reaction and multiplied by 100.

4. Results and discussion

4.1. Characterization of the supports

After calcination, the prepared mesoporous molecular sieves were characterized by nitrogen adsorption, X-ray diffraction, and scanning electron microscopy.

4.1.1. X-ray diffraction

Prepared mesoporous molecular sieves were checked by X-ray powder diffraction (XRD) at low angles. Well-developed diffraction lines confirmed the ordered hexagonal mesoporous structure of SBA-15, MCM-41 and ordered cubic mesoporous structure of SBA-16 and MCM-48. Figure 4.1. displays typical XRD patterns of SBA-15, SBA-16, MCM-41, and MCM-48.

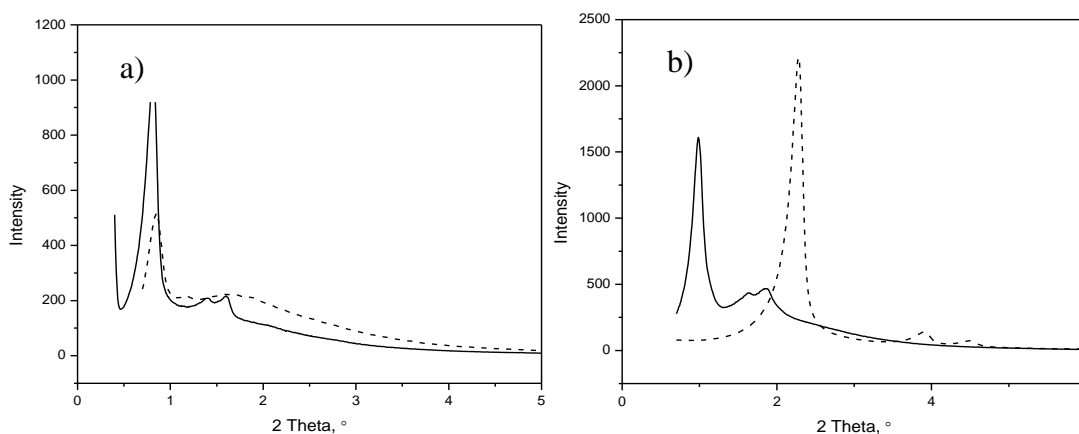


Figure 4.1. a) XRD patterns of SBA-15 (full line), and SBA-16 (dashed line); b) MCM-48 (full line), and MCM-41 (dashed line).

4.1.2. Textural characteristics

Nitrogen adsorption isotherms for all supports SBA-15, SBA-16, MCM-41, and MCM-48 (Figure 4.2.) confirmed mesoporous character according to the IUPAC classification. The BET area S_{BET} was evaluated using adsorption data in a relative pressure range from 0.05 to 0.25. The volume of mesopores (V_{ME}) and average pore diameter (D_{ME}) for the supports were evaluated from desorption branch of hysteresis loop using BJH algorithm. Textural parameters of prepared mesoporous molecular sieves are characterized by $S_{BET} = 756 - 972 \text{ m}^2/\text{g}$, $V_{ME} = 0.6 - 1.1 \text{ cm}^3/\text{g}$ and $D_{ME} = 4.0 - 6.2 \text{ nm}$. The isotherms of SBA-15 and MCM-48 featured hysteresis loops of H1 type with sharp adsorption/desorption branches at relative pressure p/p_0 of 0.68/0.75 and 0.70/0.77, respectively. The steepness of both adsorption and desorption branches is indicative of a narrow mesopore size distribution. The adsorption isotherm of SBA-16 has hysteresis loop of

type H2 according to the IUPAC classification with steep desorption branch at p/p_0 of 0.45. This type of hysteresis loop is characteristic for mesoporous materials with narrow pore entrances. There is a correlation between the shape of hysteresis loop and the texture of mesoporous materials. With increasing pore size the shift of hysteresis loop to higher p/p_0 is observed (Figure 4.2). Table 4.1. lists textural data of siliceous supports under study. Narrow mesopore size distributions of used sieves are seen in Figure 4.3. Silicagel 40 is the exception, which possesses broad pore size distribution.

Table 4.1. Used mesoporous molecular sieves characteristics.

| Support | S_{BET} (m ² /g) | V_{ME} (cm ³ /g) | D_{ME} (nm) |
|--------------|-------------------------------|-------------------------------|-----------------------------------|
| SBA-15 | 766 | 1.03 | 6.2 |
| SBA-16 | 796 | 0.61 | 7.4 ^a 4.7 ^b |
| MCM-48 | 756 | 0.91 | 6.2 |
| MCM-41 | 972 | 1.14 | 4.0 |
| Silicagel 40 | 559 | 0.47 | 4.6 |

^a Pore cage diameter

^b Pore entrance diameter

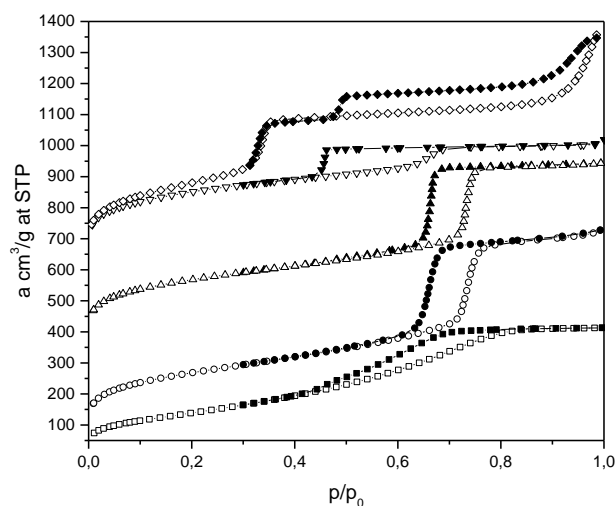


Figure 4.2. Nitrogen adsorption and desorption isotherms of Silicagel 40 (■), SBA-15 (●), SBA-16 (▼), MCM-41 (◆), and MCM-48 (▲). For clarity 50, 350, 600, and 700 cm³/g (STP) was added to the adsorption isotherms of SBA-15, MCM-48, MCM-41, and SBA-16 respectively. Open symbols are used for adsorption branches of the isotherms, filled symbols for desorption branches of the isotherms.

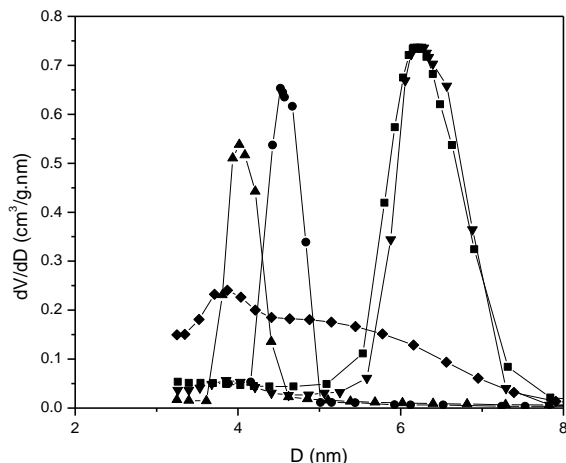


Figure 4.3. Pore size distribution for SBA-15 (■), SBA-16 (●), MCM-41 (▲), MCM-48 (▼), and Silicagel 40 (◆).

4.1.3. Morphology of the particles

The morphology of catalyst particles was investigated using scanning electron microscopy (SEM) (Figure 4.4.). Very narrow particle size distribution was observed in the case of SBA-15, where estimated average particle sizes were about 1 μm and in the case of SBA-16 with the same average particle size. MCM-41 shows particle size between 2 - 5 μm . In the case of MCM-48, wide particle sizes were observed with an estimated average particle size from 10 μm to almost 50 μm .

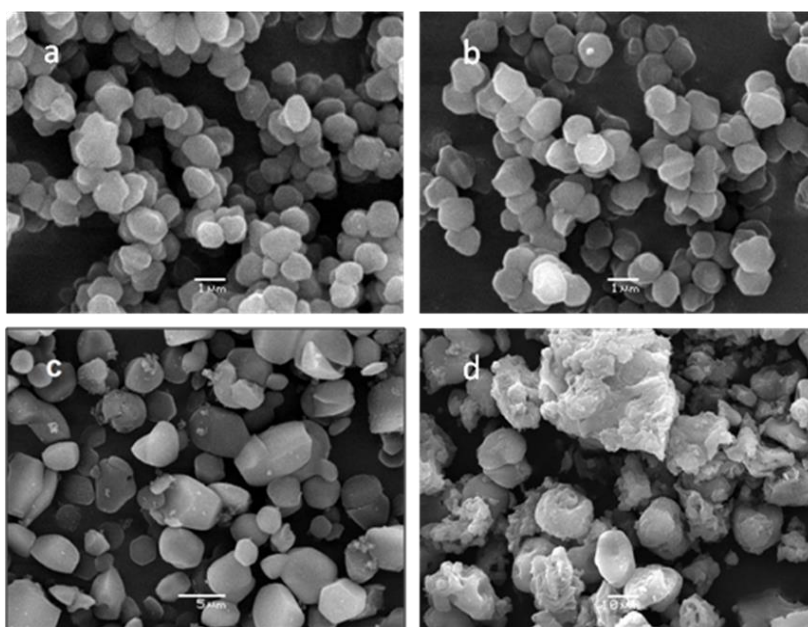


Figure 4.4. SEM images of a) SBA-15, b) SBA-16, c) MCM-41, and d) MCM-48.

4.2. Modification of mesoporous molecular sieves for CO₂ adsorption

In this contribution, we have promoted magnesium oxide containing mesoporous silicas (SBA-15, SBA-16, and MCM-48) with potassium carbonate. For that purpose, a novel procedure for the preparation of mesoporous Mg-SBA-15, Mg-SBA-16, and Mg-MCM-48 adsorbents with further introduction of potassium cations was developed to enhance the adsorption capacity over CO₂.

The application of common synthesis procedures such as impregnation with solutions of magnesium acetate, magnesium nitrate, sodium or potassium carbonate or bicarbonate was unsuccessful leading to a collapse of the mesoporous system observed after drying and calcination of the sample. To introduce magnesium oxide or alkali metal carbonate on the inner surface of mesoporous silica without destruction of the parent porous system, a special method was developed. This procedure, similar to the template synthesis of macroporous solids suggested by Stein *et al.* [163], is based on the precipitation of metal salts on the mesoporous silica surface and subsequent chemical conversion of the inorganic precursor. It is well-known that magnesium oxalate decomposes directly before melting to form magnesium oxide. Because magnesium oxalate is insoluble in water or ethanol, we performed in situ chemical reaction by introducing the solution of oxalic acid into the silica containing magnesium acetate. Similarly, we introduced potassium carbonate into silica pores: MgO/silica was impregnated with potassium oxalate solution followed by its conversion to carbonate.

4.2.1 Physicochemical properties of the samples

Figure 4.5. gives the low-angle XRD pattern of parent SBA-15, Mg-SBA-15, and K/Mg-SBA-15. Three diffraction peaks can be indexed as (100), (110), and (200) reflections, respectively. These diffraction peaks are associated with space group $p6mm$, which is characteristic of SBA-15 [8]. That means all samples of Mg-SBA-15, and K/Mg-SBA-15 have mesoporous structures, and the introduction of MgO and potassium cations does not destroy the mesoporous structure of SBA-15. This can be confirmed by N₂ adsorption characterization. The introduction of MgO and potassium cations to SBA-16 and MCM-48 also does not destroy their mesoporous structures.

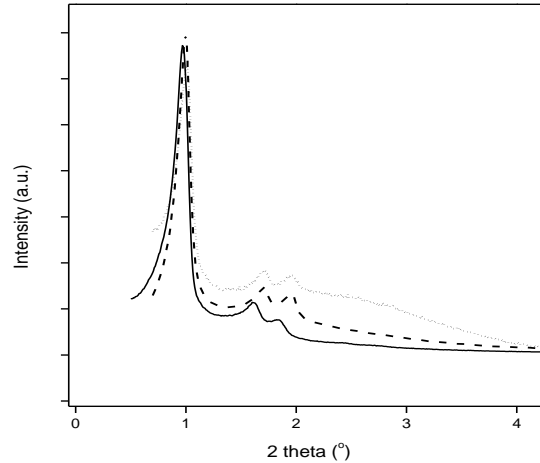


Figure 4.5. XRD patterns of SBA-15 (full line), Mg-SBA-15 (dashed line), and K/Mg-SBA-15 (dotted line).

The SEM investigation of the starting sample SBA-15 and Mg-SBA-15 samples has revealed aggregates with the diameter approximately about 1 μm with regular particle morphology, and without any presence of other phases (Figure 4.6.). The particle morphology was preserved after the introducing of MgO into SBA-15 (Figure 4.6.).

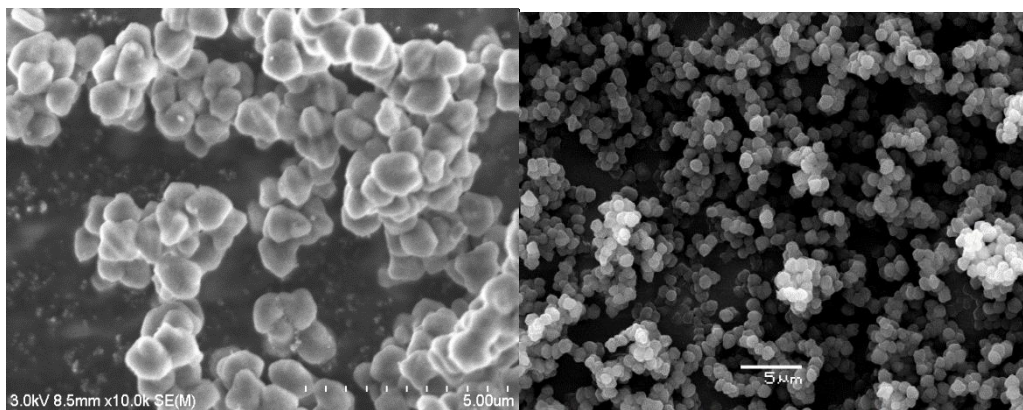


Figure 4.6. SEM images of the samples SBA-15 and Mg-SBA-15.

Figure 4.7. displays the nitrogen adsorption isotherms of SBA-15, MgO-modified SBA-15 support, and Mg/K-SBA-15. The textural parameters of support materials were summarized in Table 4.2. All supports exhibit type IV isotherm according to the IUPAC classification [164], which is characteristic for mesoporous materials. The isotherms of pure silica SBA-15, and Mg-SBA-15 displayed a sharp increase in the nitrogen uptake in the relative pressure (p/p_0) range of 0.60 - 0.75 with a characteristic H1-type hysteresis loop, corresponding to the presence of typical uniform mesopores with 1D open “cylindrical-shaped” channel [165]. However, the hysteresis loops of Mg-SBA-15 and K/Mg-SBA-15 were dramatically smaller than that of SBA-15, which

was due to the impregnation of MgO particles in SBA-15. The pore size of MgO-modified SBA-15 was homogeneous and distributed in the range of 8 - 9 nm.

Table 4.2. Chemical composition and textural characteristics of used materials.

| <i>Sample code</i> | <i>MgO</i> (mg/g) | <i>K₂CO₃</i> (mg/g) | <i>S_{BET}</i> (m ² /g) | <i>V_{ME}</i> (cm ³ /g) | <i>D_{ME}</i> (nm) | <i>a₁₀^a</i> (cm ³ /g <i>STP</i>) | <i>a₁₀₀^b</i> (cm ³ /g <i>STP</i>) |
|--------------------|----------------------|--|---|---|-------------------------------|---|--|
| SBA-15 | - | - | 660 | 1.03 | 10.2 | 2.0 | 16.5 |
| Mg-SBA-15 | 38 | - | 464 | 0.65 | 9.2 | 1.7 | 12.2 |
| K/Mg-SBA-15 | 38 | 43 | 257 | 0.49 | 8.7 | 7.8 | 18.8 |
| SBA-16 | - | - | 710 | 0.53 | 7.7 | 2.5 | 20.6 |
| Mg-SBA-16 | 20 | - | 489 | 0.41 | 7.4 | 3.0 | 16.6 |
| K/Mg-SBA-16 | 20 | 27 | 273 | 0.27 | 7.1 | 2.9 | 10.3 |
| MCM-48 | - | - | 867 | 1.06 | 11.1 | 2.5 | 20.1 |
| Mg-MCM-48 | 39 | - | 530 | 0.74 | 10.7 | 3.2 | 16.7 |
| K/Mg-MCM-48 | 39 | 49 | 318 | 0.52 | 10.1 | 3.7 | 12.7 |

The *BET* area (Table 4.2.) was evaluated using adsorption data in a relative pressure range from 0.05 to 0.25 (Figure 4.7.). While the structure-directing agent was removed from the as-synthesized SBA-15 by calcination, the shrinking of the silica pore walls occurred. As a consequence, the micropore volume determined using the α_s -plot was negligible.

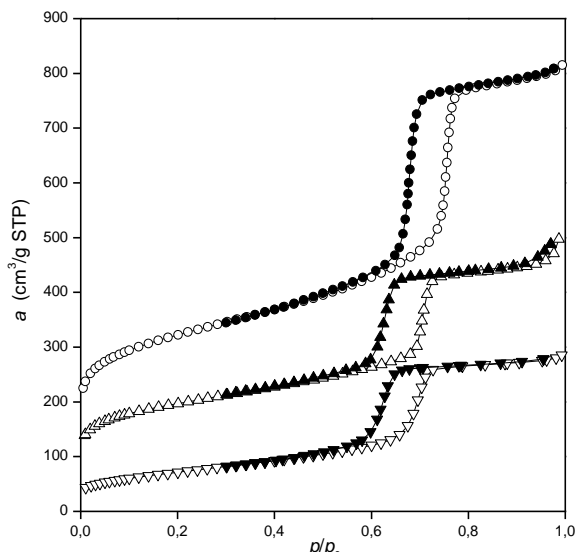


Figure 4.7. Nitrogen adsorption and desorption isotherms of SBA-15 (○), Mg-SBA-15 (△), and K/Mg-SBA-15 (▽). For clarity 70, and 150 cm³/g (STP) was added to the adsorption isotherms of Mg-SBA-15, and K/Mg-SBA-15 respectively. Open symbols are used for adsorption branches of the isotherms, filled symbols for desorption branches of the isotherms.

The mesopore volume and mesopore distributions of the SBA-15, Mg-SBA-15, and alkali-metal modified samples were determined using the Kruk, Jaroniec, and Sayari (KJS) method [166] based on the BJH algorithm calibrated to accurately reproduce the pore diameter and volume. The inspection of these data reveals that due to the modification of MgO, mesopore volume decreases from 1.03 cm³ g⁻¹ to 0.65 cm³ g⁻¹; an additional slight decrease in V_{ME} occurs due to the alkali metal cation exchange. Insertion of MgO also causes a small decrease in the mesopore diameter from 10.2 nm to 9.2 nm, which is further constant for ion-exchanged molecular sieves. The same trend was observed for all modified samples based on SBA-16 and MCM-48.

The decrease in the pore volume and surface area due to post-synthesis modifications of parent silicas is not proportional to the mass of deposited compounds. With respect to the relatively small mass of deposited compounds, the reduction of surface area would be much lower if these compounds would be located exclusively on the external surface of the particles. The strong reduction of surface area indicates that deposited MgO are located inside the particles. The mentioned changes in the textural parameters are similar to those observed with grafting of alumina on SBA-15 [167]. Although the complete explanation was not suggested yet, it is obvious that the smoothing of the mesopore surface can play an important role. It was shown in ref. [168] that the mesopores of the SBA-15 silica are surrounded by a corona due to the roughness of their surface. The filling of corona with aluminium oxide results in a gradual

smoothing of the surface and leads to a decrease in surface area [169]. A similar effect can be expected when introducing MgO into SBA-15 silicas.

4.2.2. Adsorption of carbon dioxide

Adsorption isotherms of carbon dioxide at 20 °C displayed in Figure 4.8. show distinct differences in the adsorption properties of parent siliceous SBA-15, Mg-SBA-15, and K/Mg-SBA-15. Isotherms recorded on SBA-15, and Mg-SBA-15 indicate that in the low pressure region these materials do not interact very strongly with CO₂ because the surface hydroxyl groups are not able to induce sufficiently strong interaction and real adsorption sites are missing. The weak interaction of CO₂ with the surface of Al-SBA-15 silica was also reported [170]. In addition, the size of the pores is too large to influence the adsorption by the effect “from the top” as recently described by Nachtigall *et al.* [171, 172], which is really important in the case of CO₂ adsorption in microporous zeolites. The CO₂ isotherms on modified samples exhibit nonlinear concave decreasing course typical for adsorption of CO₂ on inorganic materials (zeolites, mesoporous adsorbents, hydrotalcite-like compounds). The steepness of these isotherms and the CO₂ adsorption capacity are characterized by the amounts a_{10} and a_{100} adsorbed at 10 and 100 kPa, respectively.

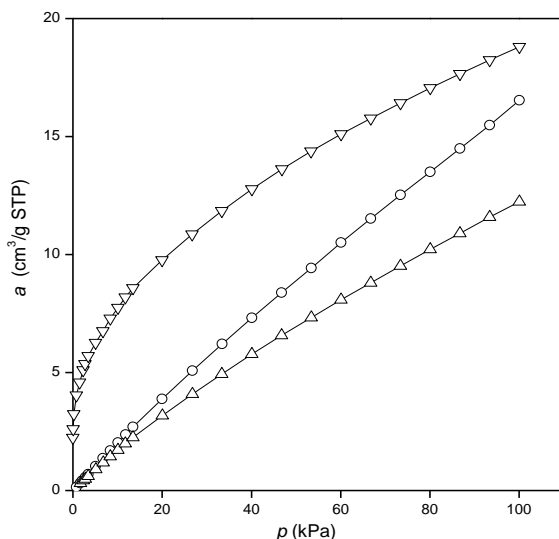


Figure 4.8. Adsorption isotherms of carbon dioxide at 20 °C on SBA-15 (○), Mg-SBA-15 (△), K/Mg-SBA-15 (▽).

It can be summarized that adsorbent based on the SBA-15 silica shows adsorption capacity higher than adsorbents based on SBA-16 or MCM-48. The behaviour of K/Mg-SBA-15 is similar to amine-modified SBA-15 materials, which also exhibit high adsorption enthalpies at low CO₂ coverage [173].

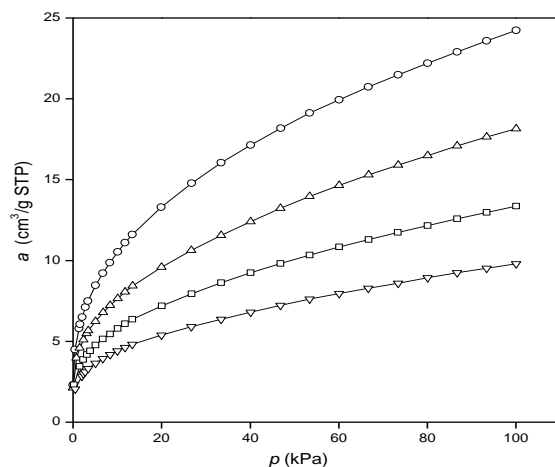


Figure 4.9. Adsorption isotherms of carbon dioxide at 0 °C (○), 20 °C (△), 40 °C (□), and 60 °C (▽) on K/Mg-SBA-15

Due to the temperature dependence of CO₂ adsorption isotherms, we can evaluate the isosteric heat of adsorption (Q_{st}), which is characteristic of adsorbate - adsorbent interaction. Its calculation requires precise knowledge of the adsorption isosteres; for this reason, adsorption isotherms at four temperatures in the interval 0 °C - 60 °C (Figure 4.9.) were chosen for precise determination of isosteric adsorption heat. Adsorption isosteres (Figure 4.10.) were calculated from isotherms using a polynomial interpolation procedure in coordinates $\log p$ vs. $1/T$ corresponding to a series of adsorbed amounts $a = 4, 5, 6, \dots, 20 \text{ cm}^3/\text{g STP}$.

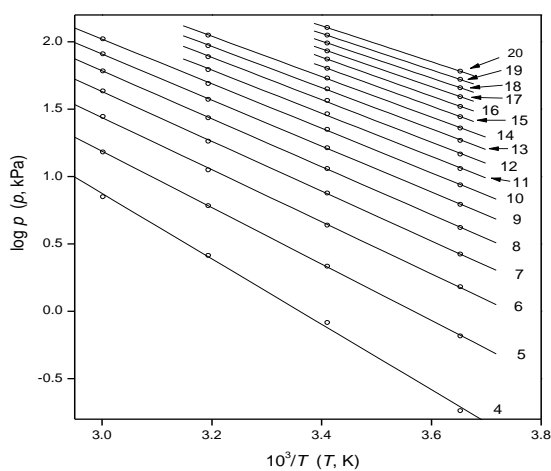


Figure 4.10. Adsorption isosteres of carbon dioxide on sample K/Mg-SBA-15. Points were calculated by numerical interpolation of adsorption isotherms, lines represent linear fit.

All isosteres are marked with corresponding amount adsorbed in $\text{cm}^3/\text{g STP}$.

Isosteric adsorption heats Q_{st} were then determined from the slopes of adsorption isosteres using Clausius–Clapeyron equation:

$$[\partial(\log p)/\partial(1/T)]_a = - Q_{st}/2.303 R,$$

where R is gas constant, T is thermodynamic temperature, p is pressure and a is amount adsorbed in $\text{cm}^3/\text{g STP}$. The adsorption isosteres in coordinates $\log p$ vs. $1/T$ were linear (Figure 4.10.), isosteric adsorption heats did not depend on temperature; it depends only on the amount adsorbed. Dependences of isosteric adsorption heats Q_{st} on the amount of CO_2 adsorbed are presented in Fig. 4.11. Low values of Q_{st} for SBA-15 and Mg-SBA-15 (maximal values about 27 kJ/mol for both samples) indicate a weak interaction of CO_2 molecule with the materials without potassium cations. Mg-SBA-15 sample promoted with potassium cations showed maximal values of Q_{st} of 46.5 kJ/mol for the small amount adsorbed. It is comparable with isosteric heats found for different alkali-metal exchanged low-silica zeolites, which is in the range from 40 to 50 kJ/mol [174].

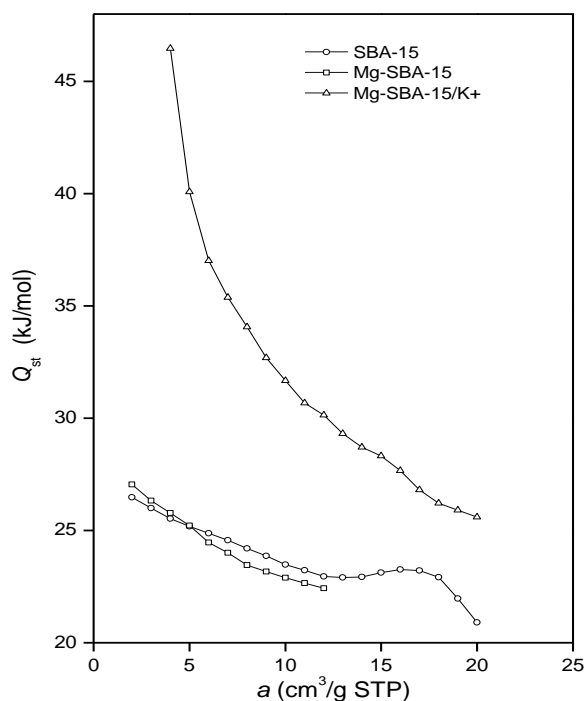


Figure 4.11. Isosteric adsorption heats of CO_2 on samples SBA-15 (\circ), MgO-SBA-15 (\square), and K/Mg-SBA-15 (\triangle).

4.2.3 CO_2 adsorbents summary

A new method was developed to introduce magnesium oxide and potassium carbonate into the different structure types of mesoporous silica (SBA-15, SBA-16, MCM-48) without causing a collapse of their porous systems. This procedure is based on the precipitation of

magnesium acetate on the silica surface and its subsequent chemical conversion to magnesium oxalate, which decomposes directly to magnesium oxide. To introduce potassium carbonate, MgO-modified silica was impregnated with potassium oxalate followed by conversion to carbonate. The adsorption properties of prepared materials modified by magnesium oxide and promoted with potassium carbonate are influenced by the type of mesoporous structure. The SBA-15 silica with MgO and promoted by potassium carbonate exhibited the steepest adsorption isotherm. The CO₂ adsorption capacity of this sample was higher than that of analogous samples prepared from SBA-16, and MCM-48 silicas.

4.3. Well-defined Ru catalysts immobilized on mesoporous molecular sieves

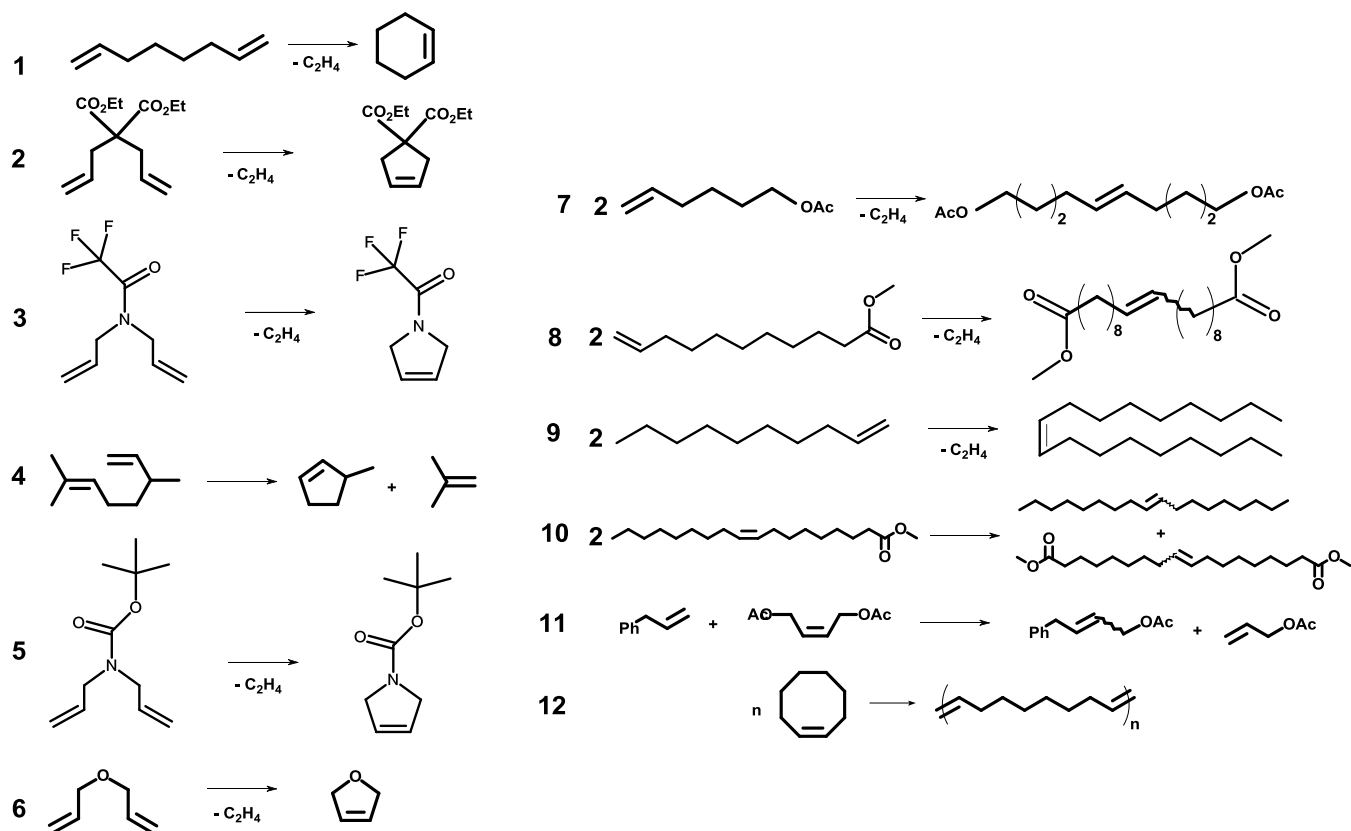
Heterogeneous metathesis catalysts have been prepared by immobilization of the Hoveyda-Grubbs-type catalysts: (i) *via* exchange of the phosphine L ligand; (ii) *via* exchange of alkylidene ligand; or (iii) *via* direct non-covalent interaction. For the immobilization were used different supports: (i) mesoporous molecular sieves SBA-15, SBA-16, MCM-41, and MCM-48; (ii) organosilicates SG-1 and SG-2; and (iii) ordinary Silicagel 40. Resulting heterogeneous catalysts were characterized using various methods and activity of the catalysts was studied in metathesis reactions such as ROMP, RCM, CM, and self-metathesis.

4.3.1. Tested substrates in metathesis reactions

All prepared heterogeneous catalysts were tested with the set of substrates (Scheme 4.1.) included (i) RCM substrates: **1** - 1,7-octadiene, **2** – DEDAM (diethyl diallylmalonate), **3** – DAF (*N,N*-diallyl-2,2,2-trifluoroacetamide), **4** – DAC (*tert*-butyl *N,N*-diallylcarbamate), **5** – (-)- β -citronellene and **6** – allyl ether (ii) Self-metathesis substrates: **7** – 5-hexenyl acetate, **8** – methyl 10-undecenoate, **9** – 1-decene, and **10** – methyl oleate; (iii) Cross-metathesis substrates: **11** - allylbenzene with DAB; (iv) ROMP substrate: **12** - *cis*-cyclooctene.

4.3.2. Hoveyda-Grubbs type catalysts immobilized *via* exchange of L ligand

A new type of heterogeneous metathesis catalysts was prepared by the immobilization of the Hoveyda-Grubbs 1st generation-type catalyst (**RC-304**) on the mesoporous molecular sieves SBA-15, SBA-16, MCM-41, and MCM-48 modified with molecules bearing dicyclohexylphosphine groups (PCy₂) on the surface (**M1** - **M4**). The prepared catalysts were tested in various metathesis reactions. Ru leaching, possibility of catalyst reusing and the influence of the support on the catalyst activity were studied.



Scheme 4.1. Metathesis reactions studied with prepared catalysts.

4.3.2.1. Preparation and characterization of the catalysts

Modification of mesoporous molecular sieves was performed using 2-(dicyclohexylphosphino)ethyltriethoxysilane (described in Chapter 3.3.1.). Molecular sieves modified with the PCy₂ (**M1** - **M4**) were studied by elemental analysis (the weight contents of P in the modified molecular sieves were determined). Elemental analysis revealed that **M1** – **M3** contained approximately 1.3 wt. % of P. The average linker density 0.38, 0.41, and 0.39 PCy₂ linkers/nm² for SBA-15, SBA-16, and MCM-48, respectively, was calculated from the weight content of P. SBA-15 modified with the PCy₂ linkers was studied by ²⁹Si CP MAS NMR (Figure 4.12.).

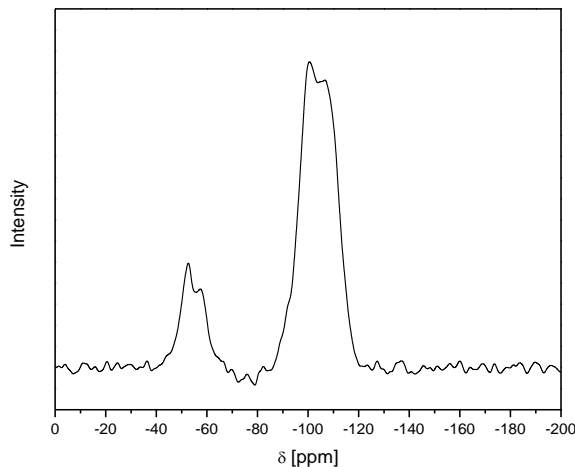


Figure 4.12. ^{29}Si CP MAS NMR spectrum of SBA-15 modified with PCy_2 linkers.

The presence of signals in the range from about -45 ppm to -60 ppm (T^m sites) confirms the attachment of linkers to the surface by siloxane bridges. As for T^m sites [$\text{T}^m = \text{RSi}(\text{OSi})_m(\text{OEt})_{3-m}$, $m = 1,2,3$], the values of chemical shifts corresponding to T^1 , T^2 , and T^3 are -47, -57, and -67 ppm, respectively [175]; in our case the PCy_2 linkers are bound to the surface by T^1 and T^2 sites. With more than one ethoxy group per silane, there are always residual ethoxy groups at the silanes. The number of residual ethoxy groups is independent on the substituent at the triethoxysilane group. The immobilization of PCy_2 linkers (whose T^m sites prevail) is influenced by reaction conditions (silica drying, solvent) [176]. Assuming that linker density is 0.38 linkers per nm^2 and the average OH groups concentration is about 4.2 OH groups/ nm^2 for all sieves [177], only $1/10$ of OH groups was consumed for the reaction with PCy_2 linkers. The possibility of phosphine oxidation by reaction with surface OH groups was suggested by Fontaine *et al.* [178].

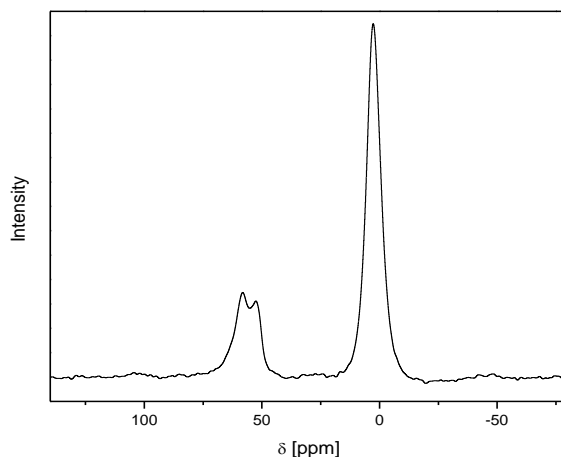
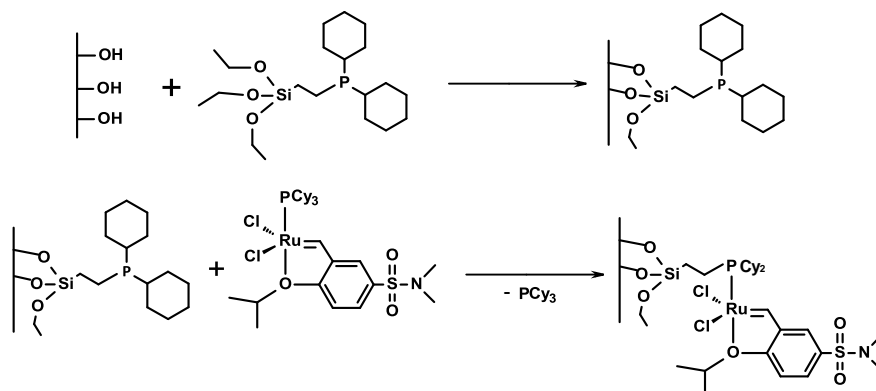


Figure 4.13. ^{31}P MAS NMR spectrum of SBA-15 modified with PCy_2 linkers.

The ^{31}P MAS NMR spectrum of **M1** (Figure 4.13.) really shows resonances in the region 50-60 ppm, which can be ascribed to oxidized P product(s). Nevertheless, the dominant singlet at 2.6 ppm proved that the majority of P is in the phosphine state being able to react with Ru alkylidene by phosphine ligand exchange.

New catalysts **C01** – **C04** were prepared by immobilization of the complexes **RC-304** on **M1** – **M4** (Scheme 4.2). The immobilization did not proceed quantitatively. Under conditions applied, different fractions of the starting amounts of complexes **RC-304** were transferred into catalysts **C01**, **C02**, **C03**, and **C04** (0.83, 0.48, 0.78, and 0.82, respectively). The reason of non-quantitative immobilization of the Ru complexes is the equilibrium caused by the competitive nucleophilic substitution between free ligand (PCy_3) and the linkers (PCy_2 linker). As a result, different amounts of **RC-304** had to be used to obtain the catalysts of approximately same Ru loading (1 wt. %).



Scheme 4.2. Immobilization of **RC-304** on SBA-15, SBA-16, MCM-41, and MCM-48 modified with PCy_2 linker (**M1** – **M4**).

The analysis of nitrogen adsorption isotherms of modified sieve and prepared catalyst (Figure 4.14.) and XRD patterns showed that mesoporous character and the regular architecture of the supports used were preserved during the preparation of the catalysts. However, the strong decrease in the BET area S_{BET} and void volume V_{ME} was observed for prepared catalyst (S_{BET} decreased from 766 m²/g for parent SBA-15 to 474 m²/g for **C01**, and V_{ME} decreased from 1.03 cm³/g for parent SBA-15 to 0.71 cm³/g for **C01**). Decreased S_{BET} and V_{ME} were also observed for **C02** – **C04** catalysts. On the other hand, average pore size diameter D_{ME} did not change. It is in the range from 3.9 nm to 5.9 nm (see Table 4.3.). Narrow pore size distribution of used supports was also preserved during preparation of new heterogeneous catalysts. As expected, the introduction of organic linkers into the pores of supports resulted in decreased nitrogen adsorption capacity. It is reflected by significantly lower S_{BET} values and reduced pore volumes as compared with the parent supports. Subsequent immobilization of complex **RC-304** led only

to small changes in textural parameters, because of a low amount of complex introduced. For catalyst function it is important that the changes of average pore diameter are rather small (for SBA-15 and MCM-41 nearly negligible).

Table 4.3. Textural characteristics of prepared catalysts.

| Material | S_{BET} (m^2/g) | V_{ME} (cm^3/g) | D_{ME} (nm) |
|------------|---|---|-------------------------|
| C01 | 474 | 0.71 | 5.9 |
| C02 | 341 | 0.23 | 3.7 ^a |
| C03 | 523 | 0.61 | 5.2 |
| C04 | 701 | 0.64 | 3.9 |

^a Pore entrance diameter.

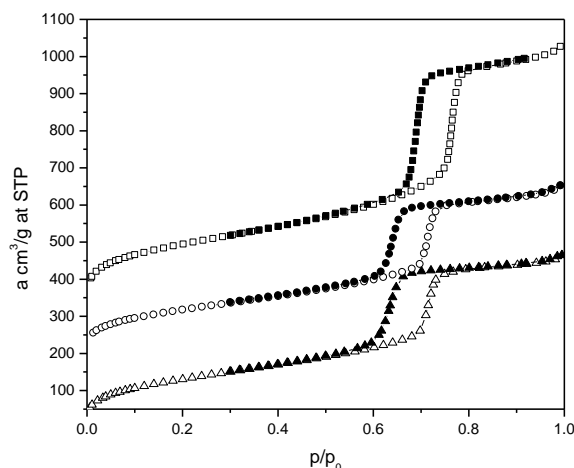


Figure 4.14. Nitrogen adsorption and desorption isotherms of parent SBA-15 (■), **M1** (●), and **C01** (▲). For clarity 300 and 200 cm^3/g (STP) was added to the adsorption isotherms of SBA-15 and **M1** respectively. Open symbols are used for adsorption branches of the isotherms, filled symbols for desorption branches of the isotherms.

The XPS results are in agreement with immobilized **RC-304**, according to Scheme 4.2. The stoichiometry for **M1** and for catalyst **C01** calculated from XPS was $\text{Si}_{1.0}\text{O}_{1.97}\text{P}_{0.042}\text{C}_{0.92}$ and $\text{Si}_{1.0}\text{O}_{1.95}\text{Ru}_{0.008}\text{Cl}_{0.015}\text{P}_{0.046}\text{C}_{0.99}$, respectively. The Ru/P ratio shows the excess of P, indicating that only about 20 % of P linkers participated in the Ru immobilization. According to Scheme 4.2, Si/P ratios for modified support and catalyst should be the same. A slight increase in the P concentration in the catalyst might be connected with a partial trapping of liberated PCy_3 in the sieves as it was recently described [177]. The XPS binding energies for complexes **RC-304**, **M1**, and catalyst **C01** are provided in Table 4.4. Binding energies for complex **RC-304** are in

agreement with the values of Jarzemska *et al.* [179] (taking into account the difference in values of C1s binding energy used for spectra calibration).

The increase in the binding energy of P 2s for **C01** in comparison with **RC-304** can be ascribed to the dominating contribution of free P linkers in **C01**. A lower value of binding energy of Ru 3d_{5/2} electrons in **C01** in comparison with that in the free complex **RC-304** may be connected with the changes in the geometry of Ru coordination sphere as a result of the immobilization. Similar changes have been observed for the immobilization of Grubbs 2nd generation catalyst on mesoporous molecular sieves *via* phosphine ligand exchange [104].

Table 4.4. XPS binding energies (± 0.2 eV) for complexes and catalysts used ^a.

| Sample | Ru 3d _{5/2} | C 1s | Cl 2p | P 2s |
|---------------|----------------------|-------|-------|-------|
| RC-304 | 281.2 | 284.8 | 198.2 | 188.5 |
| M1 | - | 284.8 | - | 189.7 |
| C01 | 280.4 | 284.8 | 198.3 | 189.5 |

^a The line C 1s (284.8 eV) was used as a reference for spectra calibration.

4.3.2.2. Catalytic activity - influence of reaction conditions

At first, we checked if some particular reaction condition, such as stirring or temperature, influenced the catalyst behaviour during the catalytic cycle in metathesis reactions. For this reason, we ran several RCM reactions in order to find the optimal condition for our new heterogeneous catalysts (**C01** – **C04**).

Figure 4.15. displays the influence of the speed of the stirring during the reaction of catalyst **C01** in RCM of 1,7-octadiene. Two stirring speeds have been chosen (250 *rpm* and 1000 *rpm*) to evaluate whether the external mass transfer played an important role during the reaction. Results suggested that the reactions proceeded with these two different speeds of stirring with slight difference in the initial reaction rate (TOF₅ in case of 250 *rpm* was 0.033 s⁻¹, and in the case of faster stirring of 1000 *rpm* was TOF₅ = 0.046 s⁻¹), while shapes of conversion curves do not differ significantly, and final conversions were in both cases identical Results showed that low/high speed of stirring (external diffusion of substrate to the pores of heterogeneous catalyst) did not influence the catalytic activity.

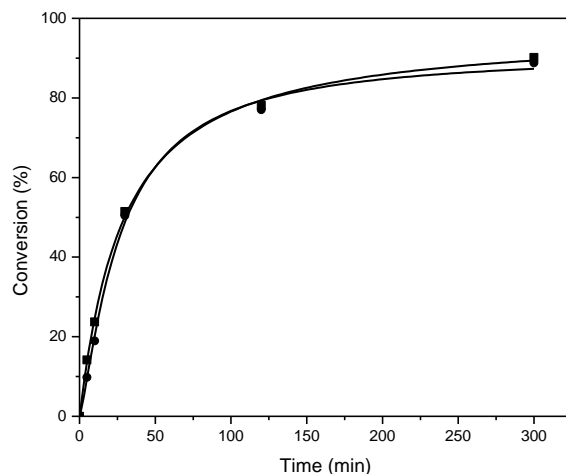


Figure 4.15. Influence of different speed of stirring in RCM of 1,7-octadiene with **C01**. 30 °C, c^0 (1,7-octadiene) = 0.15 mol/L, molar ratio Ru/1,7-octadiene = 1:100, toluene, 250 rpm (●) and 1000 rpm (■).

Effect of different catalyst concentration on the catalyst activity in RCM of DEDAM (Figure 4.16.) was examined. The reaction proceeded according to Eq. 2 in Scheme 4.1., and no other products than the expected diethyl cyclopent-3-ene-1,1-dicarboxylate were observed. With decreasing **C01** concentration, the initial reaction rate decreased. Expressed in terms of TOF values after 5 min (TOF_5) increased in the order of Ru/DEDAM molar ratio 1:500 ($\text{TOF}_5 = 0.042 \text{ s}^{-1}$) < 1:250 ($\text{TOF}_5 = 0.081 \text{ s}^{-1}$) < 1:100 ($\text{TOF}_5 = 0.089 \text{ s}^{-1}$). It was also demonstrated that with reducing catalyst concentration lower final conversion of DEDAM was observed. At molar ratio Ru/DEDAM = 1:100 (the highest catalyst concentration used), DEDAM conversion after 5 h approached the same final conversion reached with alkylidene **RC-304** as a homogeneous catalyst. Initial reaction rate increased in the order **C01** ($\text{TOF}_5 = 0.089 \text{ s}^{-1}$) < **RC-304** ($\text{TOF}_5 = 0.25 \text{ s}^{-1}$). The slower reaction rate of heterogeneous catalyst will be discussed in Chapter 4.3.2.3. Reaction with molar ratio Ru/DEDAM = 1:250 ($\text{TOF}_5 = 0.081 \text{ s}^{-1}$) proceeded more slowly than for Ru/DEDAM = 1:100 ($\text{TOF}_5 = 0.089 \text{ s}^{-1}$) and did not reach high conversion; substrate conversion reached only 40 % after 5 h. At molar ratio Ru/DEDAM = 1:500, catalyst concentration was not sufficient enough to reach high substrate conversion under conditions applied only 10 % of the substrate was converted to RCM products.

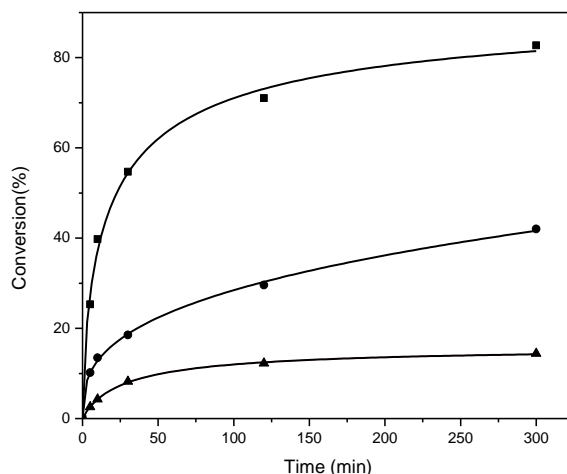
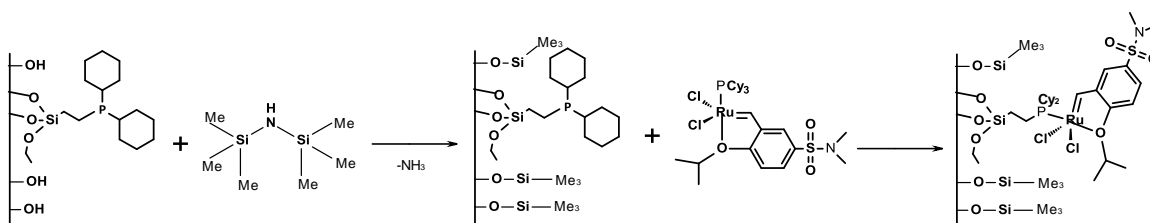


Figure 4.16. Influence of catalyst concentration on conversion in RCM of DEDAM with catalyst **C01**. 80 °C, c^0 (DEDAM) = 0.15 mol/L, toluene, molar ratio Ru/DEDAM = 1:100 (■) molar ratio Ru/DEDAM = 1:250 (●); molar ratio Ru/DEDAM = 1:500 (▲).

We also evaluated the influence of the hydrophilic/hydrophobic properties of the support surface on the catalyst activity of the prepared catalyst. Catalyst **C01a** was prepared in the same way as **C01** only difference was that after modification of SBA-15 with PCy₂ linkers hexamethyldisilazane was used as a capping agent (trimethylsilylating reagent) to cover remaining surface OH groups (Scheme 4.3). Capping of surface OH groups diminishes the surface silanol density and provides more hydrophobic environment for the metathesis reactions. IR spectra of silylated materials showed greatly decreased intensity of isolated silanol groups (not illustrated), which testified the capping treatment. Immobilization of **RC-304** on modified **M1** resulted in 0.83 wt. % of trapped Ru (23 % less Ru was immobilized than without capping treatment).



Scheme 4.3. Immobilization of **RC-304** on SBA-15 with capped surface OH groups.

C01a catalyst was tested in RCM of DEDAM, DAF, and DAC, and in self-metathesis of 5-hexenyl acetate, and methyl 10-undecenoate. Improvement of the substrate conversion by OH group capping was not observed. In all cases, the capping effect on substrates conversion was negative. In RCM of DAF substrate conversion decreased from 92 % to 29 %; in RCM of DAC decreased from 84 % to 76 %; in SM of 5-hexenyl acetate substrate conversion decreased from

75 % to 42 %; and in SM of methyl 10-undecenoate substrate conversion decreased from 63 % to 27 %. Only in the case of RCM of DEDAM (Figure 4.17.), substrate conversion was slightly higher (89 % vs. 83 %), and the initial reaction rate was better. Expressed in terms of TOF values, after 5 min of the reaction (TOF_5) the catalyst **C01a** was approximately twice as good ($\text{TOF}_5 = 0.14 \text{ s}^{-1}$) as catalyst **C01** ($\text{TOF}_5 = 0.078 \text{ s}^{-1}$). This result could be due to the fact that the hydrophilic substrate can diffuse more easily inside the hydrophobic pores. Based on these results, OH groups capping was not used in further experiments.

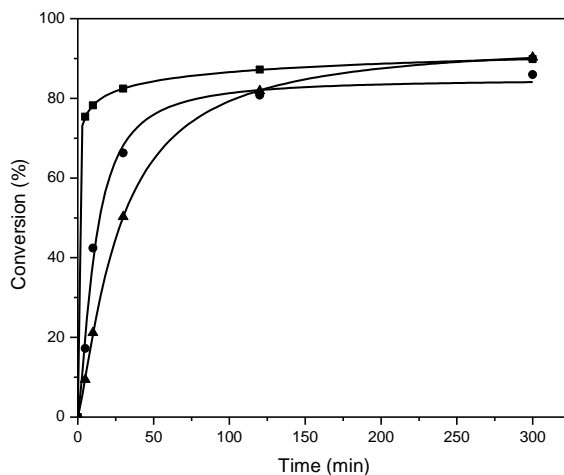


Figure 4.17. RCM of DEDAM over **RC-304** (■), **C01** (●), and **C01a** (▲). 80 °C, toluene, molar ratio Ru/DEDAM = 1:100, c^0 (DEDAM) = 0.15 mol/L

All manipulations with the catalysts (preparation, catalysts tests) were usually carried out under argon atmosphere. We tried to perform so-called endurance test of parent homogeneous Ru alkylidene **RC-304** and catalyst **C01**. **RC-304** and **C01** were exposed to air for 10 days. After that both catalysts were tested in RCM of 1,7-octadiene (Figure 4.18.).

Reactions carried out with **RC-304** as a homogeneous catalyst were slightly different from each other in terms of TOF_5 values (TOF_5 for **RC-304** stored under Ar was 0.29 s^{-1} , and TOF_5 for **RC-304** exposed to air was 0.31 s^{-1}). It is because Ru alkylidenes are more stable towards oxygen and water than Mo, and W alkylidenes [180, 181]). TOF_5 for **C01** stored under the argon atmosphere was 0.16 s^{-1} , TOF_5 for exposed **C01** decreased to 0.043 s^{-1} in comparison with properly stored **C01**. The gap between the activity of heterogenized catalysts was considerably bigger. Exposed supported catalyst probably adsorbed water from the air, which caused: (i) a certain deactivation of the Ru alkylidene, and (ii) slower diffusion inside the pores system resulting in a slower initial reaction rate compared with supported catalyst stored under argon atmosphere. In order to get better conversion of metathesis substrates, the argon atmosphere is advisable to use.

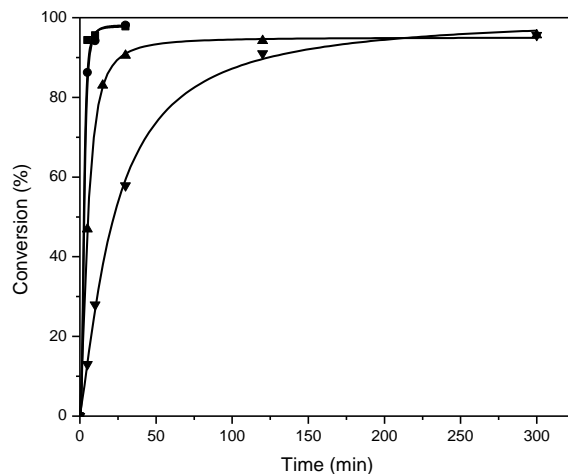


Figure 4.18. RCM of 1,7-octadiene over catalyst **RC-304** stored under Ar (■), **RC-304** exposed to air (●), **C01** stored under Ar (▲), and **C01** exposed to air (▼). 40 °C, c^0 (1,7-octadiene) = 0.15 mol/L, molar ratio Ru/1,7-octadiene = 1:100, toluene.

4.3.2.3. Catalysts activity in metathesis reactions of different types

All catalysts were tested in RCM of 1,7-octadiene, DEDAM, DAF, and DAC, in self-metathesis of 1-decene, 5-hexenyl acetate, and methyl 10-undecenoate, in cross-metathesis (CM) of allylbenzene with DAB, and in ROMP of cyclooctene (Scheme 4.1.), which all belong to the standard metathesis reactions used for comparison and evaluation of new metathesis catalysts [182]. The results achieved with prepared heterogeneous catalysts are summarized in Table 4.5.

Ring closing metathesis

Figure 4.19. shows conversion curves for RCM of 1,7-octadiene with Ru alkylidene **RC-304** and heterogenized catalysts **C01 – C04** at the temperature of 0 °C. The initial reaction rate of reaction promoted by **RC-304** expressed in TOF_5 values was 0.143 s^{-1} , the full substrate conversion was achieved in 2 h. In the case of the reaction catalysed with **C01 – C04** catalysts, the initial reaction rate expressed in TOF_{30} values, increased in the order **C04** ($TOF_{30} = 0.002 \text{ s}^{-1}$) \leq **C02** ($TOF_{30} = 0.004 \text{ s}^{-1}$) $<$ **C03** ($TOF_{30} = 0.010 \text{ s}^{-1}$) \leq **C01** ($TOF_{30} = 0.012 \text{ s}^{-1}$). Conversions obtained in 5 h increased in the same order. The drop of activity by changing the homogeneous systems for heterogeneous ones may originate from the low substrate concentration in the early reaction stage due to the diffusion of substrate into catalyst channels.

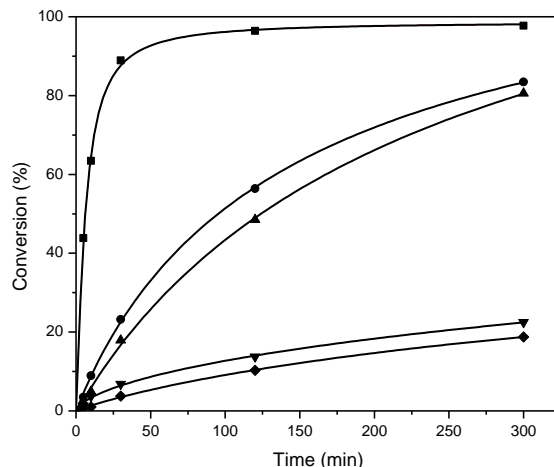


Figure 4.19. RCM of 1,7-octadiene over **RC-304** (■), **C01** (●), **C02** (▼), **C03** (▲), and **C04** (◆). 0 °C, Ru/1,7-octadiene = 1:100, toluene, c^0 (1,7-octadiene) = 0.15 mol/L.

The different behaviour of immobilized catalysts can be explained by the effect of supports used. As concerns immobilized Ru alkylidenes, it was found that the activity increased with the pore size for RCM of (-)- β -citronellene [125] and for the metathesis of methyl oleate [104]. In addition, three-dimensional pore systems (MCM-48, SBA-16) can be more advantageous for molecular diffusion than one-dimensional channel-like pore systems (MCM-41 and SBA-15) [183]. Locating Hoveyda–Grubbs alkylidene into confined space of cage-like system contributed to catalyst stability and prolonged its life time [184]. In our case, when the pore size seems to be decisive, catalyst activity increased with the increasing pore entrance diameter. For SBA-16 the entrance diameter (4.7 nm) was more important for catalyst activity than the cage diameter (7.4 nm) since the initial reaction rate over **C02** (pore diameter 3.7 nm) did not exceed too much the initial reaction rate over **C04** (pore diameter 3.9 nm). Similarly, the reaction rates and final conversions over **C03** (pore diameter 5.2 nm) and **C01** (pore diameter 5.9 nm) were close to each other, despite having different dimensionality of pore systems.

The effect of increasing pore size on conversion was also observed in RCM of DAF (Figure 4.20.), and DAC (Figure 4.21.). Conversions after 5 h reaction increased in the order **C04** < **C02** < **C03** \leq **C01** \leq **RC-304** for DAF, and **C04** < **C02** = **C03** < **C01** \leq **RC-304** for DAC. This order practically followed the increasing pore size similarly as for 1,7-octadiene at 0 °C.

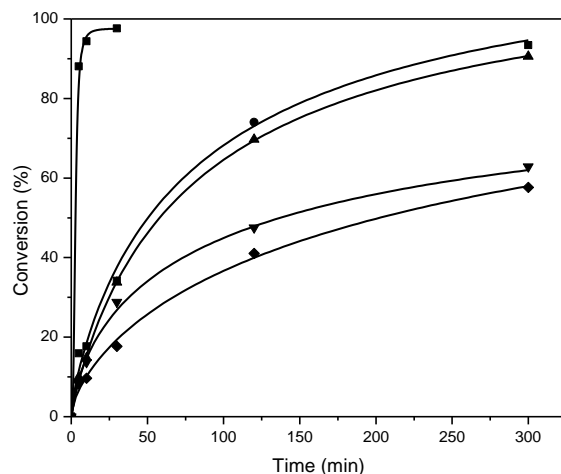


Figure 4.20. RCM of *N,N*-diallyl-2,2,2-trifluoroacetamide (DAF) over **RC-304** (■), **C01** (●), **C02** (▼), **C03** (▲), and **C04** (◆). 30 °C, Ru/DAF = 1:100, toluene, c^0 (DAF) = 0.15 mol/L.

RCM of DAF and DAC catalysed with **C01** and/or **C03** exhibited conversions over 90 % which is close to those reached by **RC-304**. Catalysts **C02** and **C04** reached in RCM of DAF and DAC conversion about 50 %. In both RCM reactions performed with heterogeneous catalysts, high retardations of reaction rates occurred. The low catalysts activity can be explained by deactivation of heterogeneous catalysts during the reaction. The catalyst deactivation can occur due to: (i) decomposition of immobilized carbene species, described for example in ref. [185], and (ii) accumulation of substrate molecules or reaction products in the pores due to slow diffusion inside the catalysts pores. In our case, most likely the second pathway become important with decreasing pore size (in the case of catalysts **C02** and **C04**).

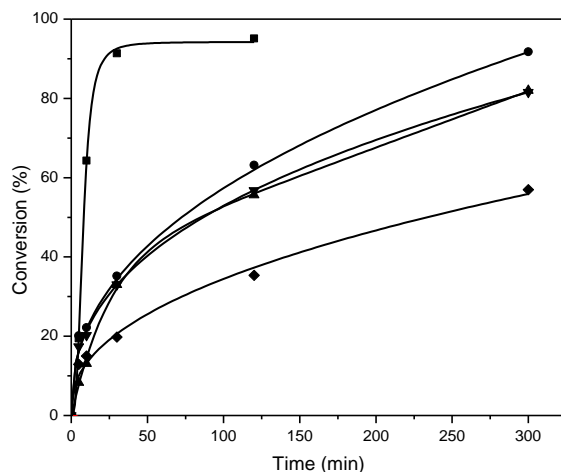


Figure 4.21. RCM of *tert*-butyl diallylcarbamate (DAC) over **RC-304** (■), **C01** (●), **C02** (▼), **C03** (▲), and **C04** (◆). 30 °C, Ru/DAC = 1:100, toluene, c^0 (DAC) = 0.15 mol/L.

Figure 4.22. shows conversion curve for RCM of DEDAM for all tested catalysts. In this reaction conversion increased in different order than for previous substrates (**C02** < **C03** < **C04** < **C01** < **RC-304**). The most active heterogeneous catalyst in RCM of DEDAM was **C01** (hexagonal architecture). On the other hand, catalyst **C04** (hexagonal architecture), which was the least active catalyst among all in other tested reactions, showed to be the second best heterogeneous catalyst in RCM of DEDAM. The catalysts **C02** and **C03** with the cubic architecture of supports were the two least active. The reason for this behaviour can be that in this reaction the pore entrance of heterogeneous catalyst did not play crucial role for the diffusion rate of DEDAM to the catalytically active sites in the pores and/or diffusion rates of products from the catalysts pores, while the support architecture (hexagonal vs. cubic) influenced the reaction. The effect of support architecture was earlier observed by Shinde *et. al.* for RCM of (-)- β -citronellene with Ru alkylidene supported on SBA-15 and MCM-48 [116]. In comparison with other RCM substrates, conversion of DEDAM did not reach conversion of 99 % found in literature with both homogeneous (**RC-304**) and heterogeneous (**C01 – C04**) catalysts [186].

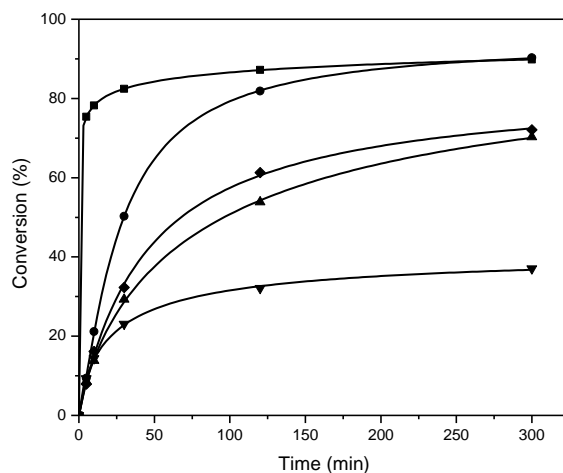


Figure 4.22. RCM of DEDAM over **RC-304** (■), **C01** (●), **C02** (▼), **C03** (▲), and **C04** (◆).
80 °C, Ru/DEDAM = 1:100, toluene, c^0 (DEDAM) = 0.15 mol/L.

Selectivity in all RCM reactions was 95–100 %, see Table 4.5. The products of cycloisomerization (diethyl 3-methyl-4-methylenecyclopentane-1,1-dicarboxylate for DEDAM, 1-(trifluoroacetyl)-3-methyl-4-methylenepyrrolidine for DAF) were observed as the only side products (Figure 4.23.). The side product of RCM of DAC was not identified.

Table 4.5. Olefin metathesis reactions promoted with **C01** catalyst.

| Reactant | Conditions | Conversion | Selectivity |
|--|---------------------|------------------------------------|--------------------|
| diethyl diallylmalonate | t = 80 °C | 90 % | 95 % |
| 1,7-octadiene | t = 0 °C (30 °C) | 84 % (98 %) | 100 % |
| N,N-diallyl-2,2,2-trifluoroacetamide | t = 30 °C | 93 % | 98 % |
| tert-butyl N,N-diallylcarbamate | t = 30 °C | 92 % | 98 % |
| 1-decene | t = 80 °C | 57 % | 97 % |
| methyl 10-undecenoate | t = 80 °C | 64 % | 98 % |
| 5-hexenyl acetate | t = 80 °C | 77 % | 95 % |
| allylbenzene with <i>cis</i> -1,4-diacetoxy-2-butene | a) t = 80 °C | 33 % to AllB and 23 % to DAB | 79 % ^{b)} |
| cyclooctene | c) t = 80 °C | polymer yield = 74 % | - |

reaction conditions: toluene, Ru/substrate = 1:100, c^0 (substrate) = 0.15 mol/L, reaction time 5 h

^{a)} c^0 (DAB) = 0.3 mol/L, c^0 (AllB) = 0.2 mol/L, Ru/DAB+AllB = 1:100

^{b)} selectivity was calculated with respect to CM products, ^{c)} Ru/COE = 1:500, c^0 (COE) = 0.8 mol/L, reaction time 3h

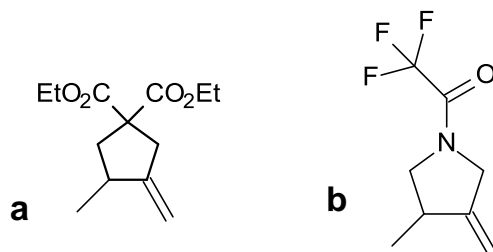


Figure 4.23. Cycloisomerization products of DEDAM (a) and DAF (b).

Cross-metathesis

The effect of increasing pore size of support on conversions was observed also in CM of AllB with DAB (Figure 4.24.). Conversions after 5 h were in the order **C03** (5.2 nm) \leq **C01** (5.9 nm) \leq **RC-304**. Excess of DAB (molar ratio AllB : DAB = 1:1.5) was used to obtain higher selectivity to CM products. In 120 min, 30 % conversion of AllB was reached at 80 °C with the catalyst **C01**. In the same time, conversion of AllB with catalyst **C03** was only 18 %. Selectivity of the reactions to CM products was 79 % for both catalysts. The main by-product was formed by self-metathesis of allyl-benzene (1,4-diphenyl-2-butene).

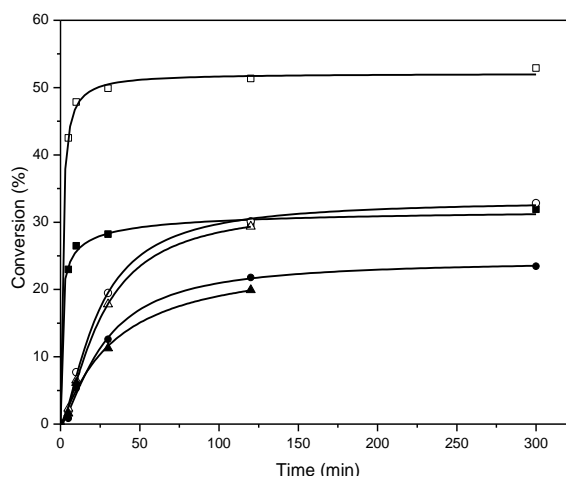


Figure 4.24. CM of AllB (open symbol) and DAB (filled symbol) over **RC-304** (■), **C01** (●), and **C03** (▲). 80 °C, toluene, Ru/AllB molar ratio = 1:40, c^0 (AllB) = 0.2 mol/L, Ru/DAB molar ratio = 1:60, c^0 (DAB) = 0.3 mol/L.

Self-metathesis reactions

In the case of self-metathesis of 5-hexenyl acetate (Figure 4.25.), 1-decene, and methyl 10-undecenoate with catalyst **C01**, it was observed lower conversion at 5 h than expected (77 %, 57 %, and 64 % respectively), due to literature reported conversion is higher than 90 % [116].

The order of increasing TOF of the heterogeneous catalysts was the same like for RCM reactions for all three substrates ($C04 < C02 < C03 \leq C01$). On the other hand, homogeneous catalyst **RC-304** achieved the same final conversion after 5 h as the most active heterogeneous catalyst **C01**. The shape of conversion curves for **RC-304** shows a strong retardation of the reactions at prolonged reaction times suggesting a gradual catalyst deactivation. The inherent deactivation of Hoveyda–Grubbs catalyst was described and deactivation mechanisms were outlined [187]. As concerns selectivity, double bond shift isomerization followed by cross-metathesis is responsible for the formation of small amounts of by-products (heptadecene, 1,9-diacetoxynonene, dimethyl 1,19-nonadecenedioate for metathesis of 1-decene, 5-hexenyl acetate, and 10-undecenoate, respectively).

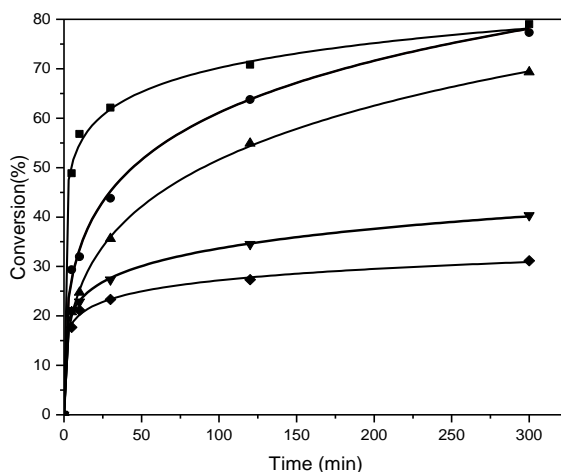


Figure 4.25. Self-metathesis of 5-hexenyl acetate over **RC-304** (■), **C01** (●), **C02** (▼), **C03** (▲), and **C04** (◆). 80 °C, Ru/5-hexenyl acetate = 1:100, toluene, c^0 (5-hexenyl acetate) = 0.15 mol/L.

ROMP of COE

In ROMP of COE, catalyst **C01** provided high molecular weight polymer ($M_w = 160,000$, $M_n = 84,000$) in 74 % yield (reaction conditions: 3 h, 80 °C, Ru/COE = 1:500, c^0 (COE) = 0.8 mol/L). Ethyl vinyl ether was used as a quenching reagent to stop the reaction propagation and produce an olefin-capped polymer chain.

4.3.2.4. Filtration test, catalyst leaching and reusing

Filtration tests are often used for the examination of heterogeneity in transition metal catalysed reactions [188]. The results of filtration test for RCM of 1,7-octadiene over **C01** in toluene is shown in Figure 4.26. 5 minutes after the beginning of the reaction, half of the liquid phase was filtered off at the reaction temperature and transferred into a parallel reactor, where it

was kept under the same conditions as the parent reaction mixture in the original reactor. The reaction continued in the original reactor, reaching nearly 100 % of conversion, whereas in the reactor with separated liquid phase, the reaction stopped immediately. It evidenced that the solid catalyst was responsible for the catalytic activity in RCM of 1,7-octadiene. Similar results were obtained for **C01** in dichloromethane.

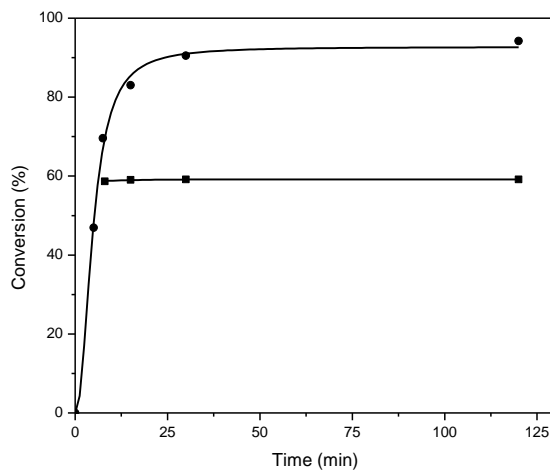


Figure 4.26. Filtration experiment for RCM of 1,7-octadiene with catalyst **C01**. Liquid phase in contact with solid catalyst (circles), liquid phase after filtration (squares), toluene, 40 °C, molar ratio Ru/1,7-octadiene = 1:250, c^0 (1,7-octadiene) = 0.15 mol/L.

For the catalyst **C01**, Ru leaching in the course of RCM of 1,7-octadiene in toluene (40 °C, 5 h, Ru/1,7-octadiene = 1:250, c^0 (1,7-octadiene) = 0.15 mol/L) was 0.1 % of the original Ru content in the catalyst, which corresponds to the maximum product contamination equal to 5.6 ppm of Ru. It should be noted that it is below the upper limit prescribed by European Medicines Agency for pharmaceutical products (10 ppm) [189]. On the other hand, the Ru leaching increased to 2.2 % of starting Ru amounts in the catalyst, when the reaction was carried out in dichloromethane (under the same temperature and concentrations as for toluene). To show the advantage of covalently immobilized **RC-304** on silica supports *via* phosphine linkers, **C11** catalysts was additionally prepared by simple physisorption of **RC-304** on the non-modified surface of SBA-15. In RCM of 1,7-octadiene under the same conditions, the leaching for **C11** was 1.51 % (75.6 ppm) in toluene and 12.8 % (656 ppm) in dichloromethane. Catalyst **C11** showed leaching one order of magnitude higher than **C01**.

For RCM of DEDAM in toluene (80 °C, Ru/DEDAM = 1:100), the Ru leaching of **C01** was 0.38 % of Ru (8.0 ppm of Ru in the product). It may be noticed that these values are considerably lower than those obtained for Grubbs 2nd generation catalyst immobilized *via* phosphine linkers (5.3 % in toluene, 80 °C, Ru/DEDAM = 1:250 [104]). The reason for higher

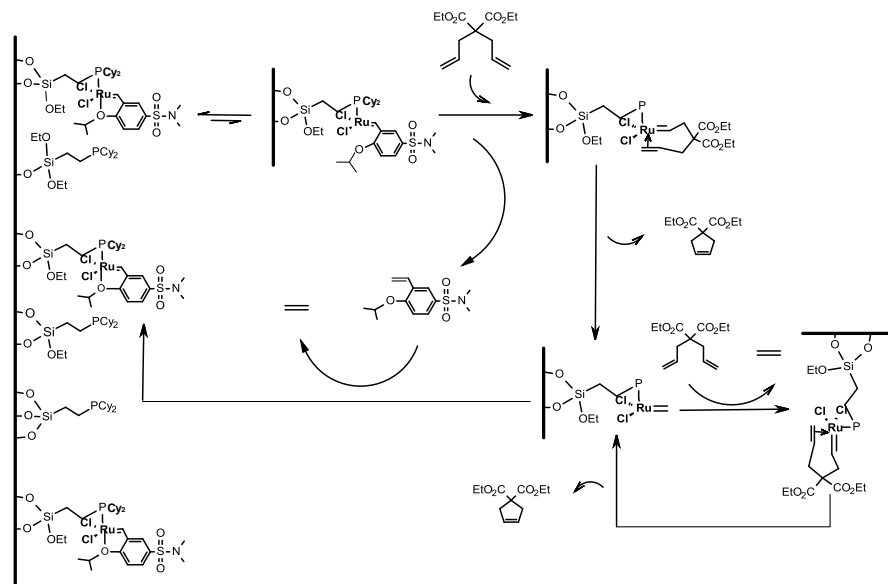
leaching in the case of Grubbs 2nd generation catalyst immobilized *via* phosphine linkers can be explained by the proposed mechanism, which is described in Scheme 4.4. Carbenes such as Hoveyda-Grubbs-type catalysts are converted to the catalytically active 14-electron Ru species by dissociation of the Ru–O chelation bond. Ru–O bond is not as strong as Ru–P bond, and therefore, it does not need the high temperature for dissociation. During the reaction, the catalyst is tightly bound to the wall of mesoporous support. Contrary to it, Grubbs 2nd generation catalyst is immobilized *via* phosphine linkers, which undergo dissociation of Ru–P bond to create catalytically active species. The catalyst is released into the liquid phase contrary to Hoveyda-Grubbs 1st generation catalyst, which stays firmly attached to the surface of used supports. For example, Hoveyda-Grubbs 2nd generation catalyst immobilized *via* non covalent interaction showed strong dependence on the solvent used (4 % in benzene, 14 % in dichloromethane [117]).

Reusing of catalyst **C01** was studied in RCM of 1,7-octadiene (Table 4.6.). After 5 h of the reaction, the catalyst was separated by filtration, washed with toluene, then new portions of toluene, and 1,7-octadiene were added. The catalyst was used 5 times without practically any decrease in the conversion achieved after 5 h (drop in conversion was 6 %). Nevertheless, certain losses in catalyst amount during its separation as well as the possible catalyst deactivation caused a gradual decrease in catalyst activity, which was manifested in the last run.

Table 4.6. Catalyst **C01** reusing in RCM of 1,7-octadiene.

| Runs | 1 | 2 | 3 | 4 | 5 | 6 |
|-----------------------|----------|----------|----------|----------|----------|----------|
| Conversion (%) | 98.0 | 97.9 | 97.9 | 97.7 | 92.0 | 54.1 |

RCM of 1,7-octadiene, 40 °C, 5 h, toluene, Ru/1,7-octadiene = 1:100, c^0 (1,7-octadiene) = 0.15 mol/L.



Scheme 4.4. Proposed reaction mechanism inside the pores of the catalysts for Hoveyda-Grubbs 1st generation catalyst immobilized *via* phosphine linker.

4.3.2.5. Catalyst activity in metathesis reactions in flow reactor

Reactions in flow reactor offer several advantages (faster reaction: excellent mixing and heat transfer cleaner products: better selectivity; reactions can be run at small scale; reactions parameters can be rapidly varied, easier scale-up *etc.*) over traditional batch methods [190]. Because of its catalytic activity, high selectivity, and recyclability **C01** was investigated in a continuous process. For the evaluation of catalyst behaviour under flow conditions, we used RCM of 1,7-octadiene as a model reaction. The tested reaction was run under 3 different flow rates. After 5 h of the reaction, the highest TON of 275 was achieved with the lowest flow rate of 0.04 mL min⁻¹. With the flow rate of 0.07 mL min⁻¹, TON decreased to 93, and with the flow rate of 0.1 mL min⁻¹ TON decreased to 32. To check the experimental error of our flow reactor, the RCM experiment was repeated 3 times and the absolute error in the determination of conversion was $\pm 5\%$. Figure 4.27 shows the effect of different WHSV values on conversion of the used substrate. At WHSV of 1.2 h⁻¹, conversion of 1,7-octadiene after 30 min of reaction was 88%. Then the decrease in the conversion occurred (the drop between maximal and ending conversion was about 20%). When higher WHSV 3 h⁻¹ was applied, lower substrate conversion was achieved. Maximal conversion in 30 min was 64%, than the same decrease of conversion occurred. For reaction with WHSV 6 h⁻¹, the conversion drop from maximal achieved conversion 85% to 10% at the end of the reaction. The reason for such fast catalyst deactivation at WHSV 6 h⁻¹ is probably that the increasing WHSV values in the reaction lead to a decrease of the conversion indicating catalyst deactivation. The deactivation of the catalyst cannot be explained

by the leaching of the Ru alkylidene, because under given condition ($50\text{ }^{\circ}\text{C}$, $c = 0.15\text{ mol/L}$, $\text{WHSV} = 1.2\text{ h}^{-1}$), leaching was only 0.35 % of original content in the heterogeneous catalyst. To preserve catalytic activity in flow systems, efficient removal of ethylene is crucial. In the case of reaction with $\text{WHSV } 6\text{ h}^{-1}$, high concentration of ethylene was evaluated at the beginning of the reaction and ruthenium methylidenes were subsequently involved in the unproductive metathesis of ethylene which ultimately must lead to their decomposition [191].

Catalyst **C01** proved to be active under flow condition also in RCM of DAF, and DAC. Under condition applied ($50\text{ }^{\circ}\text{C}$, $c = 0.15\text{ mol/L}$, $\text{WHSV} = 1.2\text{ h}^{-1}$), the shape of the conversion curve was similar like in RCM of 1,7-octadiene. Maximal conversions achieved after 30 min for DAF and DAC were 97 % and 86 %, respectively. After 5 h of the reactions, conversions slightly decreased from 97 % to 92 % for DAF and from 86 % to 75 % for DAC.

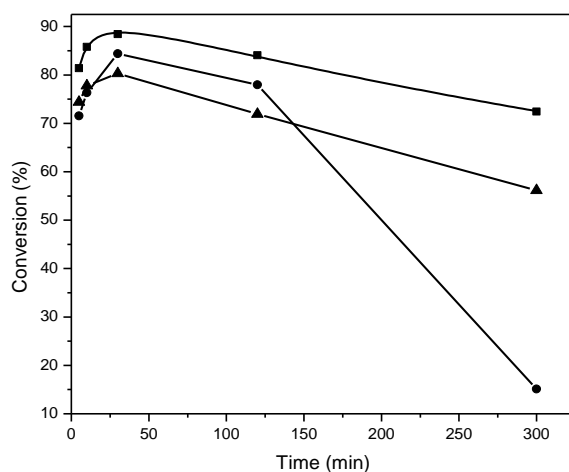


Figure 4.27. Effect of different WHSV on conversion in RCM of 1,7-octadiene with catalyst **C01** in flow system, toluene, $50\text{ }^{\circ}\text{C}$, $c^0(1,7\text{-octadiene}) = 0.15\text{ mol/L}$, flow rate = 0.04 mL/min , $\text{WHSV} = 1.2\text{ h}^{-1}$ (■), 3 h^{-1} (▲), 6 h^{-1} (●).

Stability of the catalyst **C01** was tested in RCM of 1,7-octadiene under optimal conditions (50 and $30\text{ }^{\circ}\text{C}$, flow rate = 0.04 mL/min , $\text{WHSV} = 1.2\text{ h}^{-1}$). The reaction time was nine times longer (45 h ; Figure 4.28.). Substrate conversion during the time sharply decreased from maximal conversions (89% and 63%) after 30 min to approximately 15% for both temperatures. Nevertheless, the cumulative TON of the reaction was 1505 . In contrast, maximal TON for catalyst **C01** in the reusing experiment in the batch reactor for the same system was 446 .

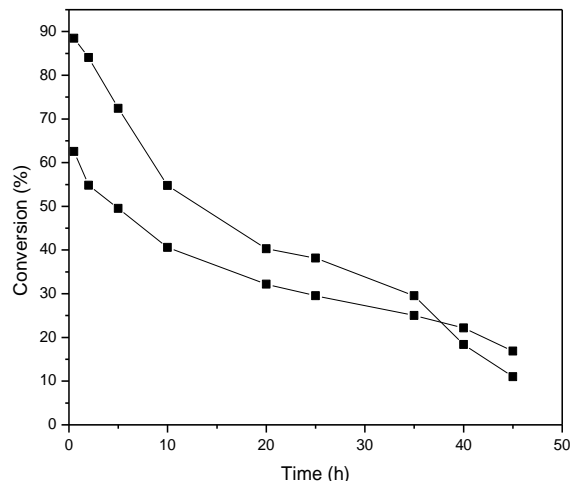


Figure 4.28. Effect of prolonged time of flow reaction on catalyst activity of **C01** in RCM of 1,7-octadiene. Toluene, c^0 (1,7-octadiene) = 0.15 mol/L, flow rate = 0.04 mL/min, WHSV = 1.2 h^{-1} , 50 °C (■) and 30 °C (●).

Finally, to show the advantage of immobilization of Hoveyda-Grubbs 1st generation catalyst *via* phosphine linker, **C01**, and **C12** catalysts were compared in RCM of 1,7-octadiene (Figure 4.29.). Conversion of 1,7-octadiene in the reaction catalysed by **C01** dropped from the maximal conversion of 96 % to 78 % after 5 hours of reaction. Conversion in the case of the reaction catalysed by **C12** dropped significantly from maximal 50 % to final 12 %. The behaviour of catalyst **C12** can be explained as follows: 16 electron pre-catalyst (Figure 4.30. **a**) is converted to 14 electron species active in metathesis reactions (Figure 4.30. **b**) by reversible dissociation of phosphine ligand, which provides space on ruthenium for coordination of olefinic substrate molecules to form a ruthenacyclobutane intermediate (Figure 4.30. **c**). This means that **C12** catalyst immobilized *via* phosphine linker has to be turned into catalytically active species by releasing from the surface of the support into a liquid phase. Ru alkylidene is leaching out with the flow of reaction mixture from the flow reactor. Bek *et al.* in ref. [104] showed that **C12** catalyst in reactions carried out in batch reactor exhibited filtration test which manifested heterogeneous character of **C12** (reaction conditions: DEDAM, 80 °C, $c = 0.15$ mol/L, molar ratio Ru/DEDAM = 1:250, toluene) with Ru leaching of 5.3 % (for **C01** at the same experimental condition the leaching was 0.38 %), with respect to the starting content of Ru in the catalyst (reactions conditions: DEDAM, 100 °C, $c = 0.15$ mol/L, molar ratio Ru/DEDAM = 1:250, toluene). These data were explained as follows that Ru alkylidenes remained captured in the pores by repeating dissociation - association process (boomerang catalyst).

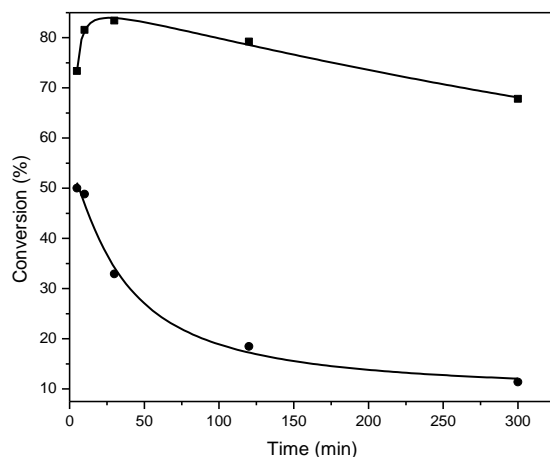


Figure 4.29. RCM of 1,7-octadiene with **C01** (■) and **C12** (●) under flow conditions. Toluene, 50 °C, c^0 (1,7-octadiene) = 0.15 mol/L, WHSV = 1.2 h⁻¹.

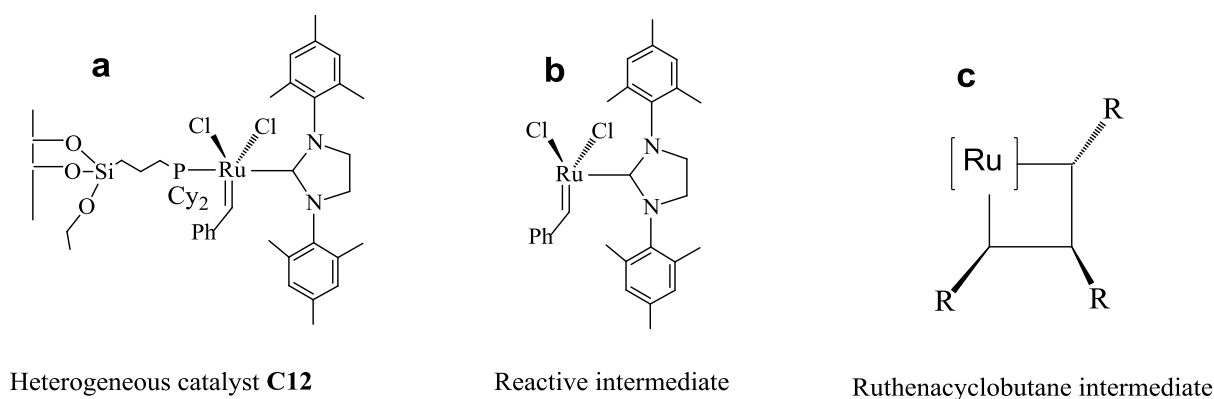


Figure 4.30. Different states of catalyst **C12** during metathesis reaction.

The leaching of **C12** in our flow reactor was approximately twice as high (14.92 % of original Ru content) as it was in the batch reactor. With respect to leaching this high and decrease in activity, so-called boomerang mechanism seems to be questionable. This mechanism can sufficiently explain the behaviour of catalysts like **C12** under batch conditions, but not under flow conditions. On the other hand, only 0.35 % of original Ru content in the catalyst was washed out in the case of catalyst **C01** with a different activation step. Activation step, in which metathetically inactive 16 electron species (Figure 4.31. **a**) turns into 14 electron species active in metathesis reactions (Figure 4.31. **b**), involve dissociation or interchange mechanism (discussed in theoretical part) of isopropoxystyrene. Therefore **C01** type catalyst proved strong heterogeneity of this type of immobilization in both batch and flow reactors.

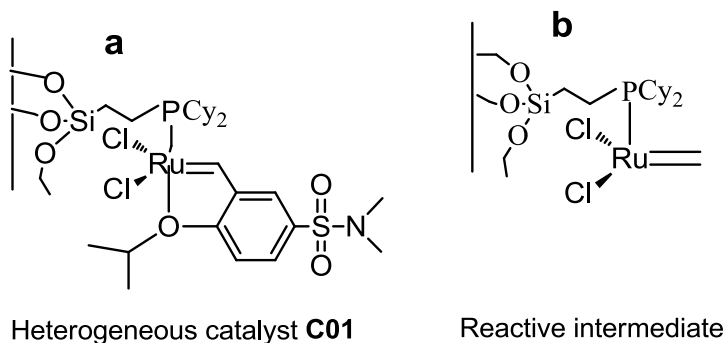


Figure 4.31. Different states of catalyst **C01** during metathesis reaction.

4.3.3. Grubbs type alkylidenes immobilized *via* exchange of L ligand

In addition to above mentioned **C12** catalyst, a new heterogeneous metathesis catalyst (**C13**) was prepared by immobilization of Grubbs 2nd generation type alkylidenes on **M1** support, in which *N*-mesityl groups were replaced by mono-*ortho*-substituted phenyls (*e.g.*, tolyls) (**GII-tolyl**). The prepared catalyst was tested in RCM and self-metathesis reactions. Ru leaching and possibility of catalyst reusing were also studied.

GII-tolyl was originally designed to make RCM of tetrasubstituted olefins easier in comparison with classical Grubbs 2nd generation catalyst. It also showed high activity in RCM reactions that generate di- and trisubstituted olefins. The free *ortho* position on phenyl groups in *N*-heterocyclic carbene ligand leaves space around the ruthenium atom for hindered substrates [192].

4.3.3.1. Preparation and characterization of the catalyst

The modification of the mesoporous molecular sieves was performed in the same way as described in Chapter 4.3.2. using 2-(dicyclohexylphosphino)ethyltriethoxysilane. New catalyst **C13** was prepared by immobilization of the complex **GII-tolyl** on SBA-15 modified with PCy₂ linkers (**M1**). The immobilization did not proceed quantitatively. Under conditions applied, only half of the starting amount of complex **GII-tolyl** was transferred into catalyst **C13** (corresponding to 0.66 wt. % of Ru in the catalyst).

The analysis of nitrogen adsorption isotherms and XRD patterns showed that mesoporous character and regular architecture of the supports used were preserved during the preparation of the catalysts. However, the strong decrease in the area S_{BET} and void volume V_{ME} was associated with the catalyst preparation (S_{BET} decreased from 701 m²/g for parent SBA-15 to 452 m²/g, and V_{ME} decreased from 0.98 cm³/g for parent SBA-15 to 0.65 cm³/g). The average pore size

diameter D_{ME} did not change and narrow pore size distribution was preserved. The same trend was observed also in previous cases (catalysts **C01** – **C04**).

4.3.3.2. Catalyst activity in metathesis reactions

The catalyst **C13** was tested in RCM of DEDAM, 1,7-octadiene, diallyl ether, and (-)- β -citronellene, as well as in self-metathesis of 5-hexenyl acetate, methyl oleate, and methyl 10-undecenoate (Scheme 4.1.). It was tested in batch reactor only. Despite high activity of **GII-tolyl** reported in the literature [193], in our experiment **GII-tolyl** did not react at all with methyl oleate, methyl 10-undecenoate, diallyl ether, and (-)- β -citronellene. On the other hand, heterogenized **GII-tolyl** showed better substrate conversion than our previous catalysts in RCM of DEDAM and self-metathesis of 5-hexenyl acetate.

In self-metathesis of 5-hexenyl acetate (Figure 4.32) **C13** catalyst showed significant stabilization of Ru alkylidene after immobilization on **M1** surface. Initial reaction rate was high for both homogeneous catalyst **GII-tolyl** ($\text{TOF}_5 = 0,66 \text{ s}^{-1}$) and heterogeneous catalyst **C13** ($\text{TOF}_5 = 0.39 \text{ s}^{-1}$), but in the case of **GII-tolyl** the reaction stopped when 50 % of substrate was converted to products, while with heterogeneous catalyst **C13** the reaction reached conversion 90 % after 300 min. The observed stabilization effect in this reaction was probably due to catalyst bimolecular decomposition suppressed by losing the mobility in the immobilized **GII-tolyl**.

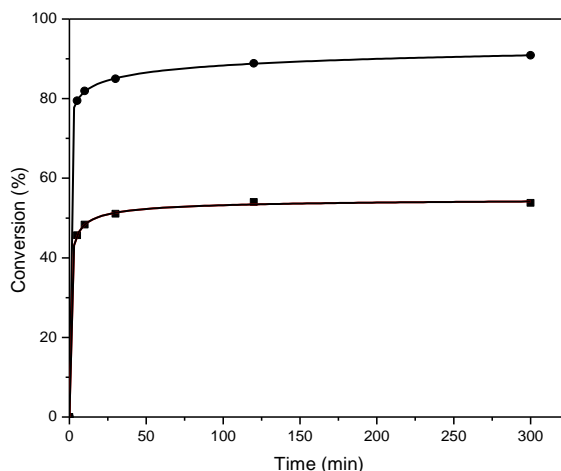


Figure 4.32. Self-metathesis of 5-hexenyl acetate over **GII-tolyl** (■), **C13** (●). 80 °C, Ru/5-hexenyl acetate = 1:250, toluene, c^0 (5-hexenyl acetate) = 0.15 mol/L.

Afterward, we tested the catalytic activity of **C13** in RCM of DEDAM. 97 % conversion of DEDAM was reached in 30 min. In contrast, Hoveyda-Grubbs catalyst **C01** and Grubbs 2nd generation catalyst **C12** immobilized in the same way exhibited considerably lower conversions (45 % and 36 %, respectively) under the same reaction conditions. The explanation for the

different catalytic activity of the mentioned heterogeneous catalysts may lie in their nature. Hoveyda-Grubbs 1st generation catalyst immobilized on SBA-15 *via* exchange of phosphine ligand (**C01**) is fully heterogeneous catalyst. On the other hand, Grubbs 2nd generation catalyst immobilized on SBA-15 *via* exchange of phosphine ligand (**C12**, **C13**) must be released into the liquid phase to start the catalyst cycle (*vide supra*). Figure 4.33 shows that conversion curves of DEDAM catalysed by **C01** and **C12** possessed almost the same shape despite **C01** and **C12** having different kind of Ru alkylidene and different way of initiation. However, the big difference was observed between activities of the catalysts **C12** and **C13**, which probably operate by the same catalyst initiation mechanism, but differ in NHC ligand. **C12** catalyst contains Grubbs 2nd generation catalyst with *N*-mesitylen groups, and **C13** contains Grubbs 2nd generation catalyst with *N*-tolyl groups. Results suggested that under applied conditions, *N*-tolyl groups in **C13** catalyst play an important role during the catalyst cycle probably due to the reducing the steric bulkiness of the NHC ligand in Ru alkylidene, which increases the catalyst activity in metathesis reactions (being more sterically favourable for coordinating the substrate molecule).

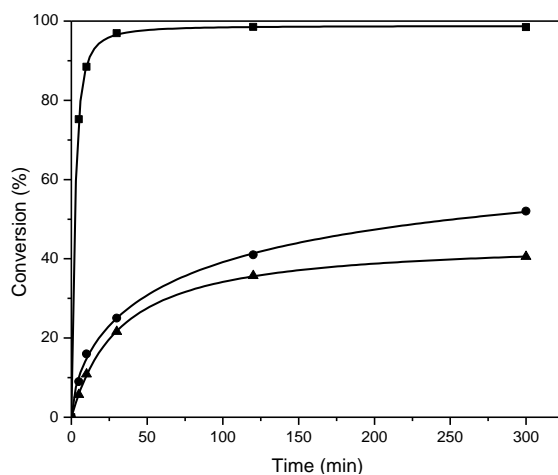


Figure 4.33. RCM of DEDAM over **C13** (■), **C12** (●), and **C01** (▲). 80 °C, Ru/DEDAM = 1:250, toluene, c^0 (DEDAM) = 0.15 mol/L.

Filtration test for RCM of DEDAM over **C13** in toluene is shown in Figure 4.34. The result showed that heterogeneous catalyst is fully responsible for the catalytic activity in the RCM of 1,7-octadiene. However, reusability of the catalyst in RCM of 1,7-octadiene (70 °C, $c = 0.15$ mol/L, molar ratio Ru/1,7-octadiene = 1:250) was very poor, conversion after the first run was 93 %, after the second run only 33 %. The drop of the substrate conversion after the first run was not due to leaching of catalytically active species out of the pores system, which was confirmed by both filtration test and Ru leaching (only 2.4 % Ru was leached out with respect to the starting content of Ru in the catalyst). Therefore, the loss of a considerable catalyst activity during the reusing experiment can occur by several factors: (i) impurities in the solvent and

substrate; (ii) oxygen and water can partially deactivate the heterogeneous catalyst during the regeneration; (iii) leaching of Ru species; and (iv) decompositions of immobilized carbene species.

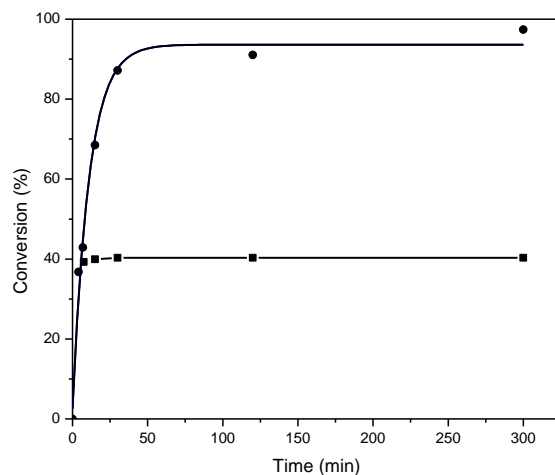


Figure 4.34. Filtration test in RCM of 1,7-octadiene with catalyst **C13**. 70 °C, molar ratio Ru/1,7-octadiene = 1:250, toluene, c^0 (1,7-octadiene) = 0.15 mol/L; suspension (●), filtrate (■).

In summary, unexpected results were observed with **GII-tolyl** alkylidene possessing more open steric environment around the ruthenium centre, which should make the alkylidene more active in sterically demanding reactions. However, the **GII-tolyl** proved to be active only in RCM of DEDAM, and 1,7-octadiene, and self-metathesis of 5-hexenyl acetate. Heterogenization of **GII-tolyl** showed to be beneficial due to the stabilization of highly active but less stable Ru alkylidene. Improved stability of **C13** was observed in RCM of DEDAM as well as in self-metathesis of 5-hexenyl acetate.

4.3.4. Hoveyda–Grubbs alkylidenes immobilized on organic-inorganic hybrid silica material

We tried to prepare heterogeneous metathesis catalyst by immobilization of **RC-304** via exchange of alkylidene ligand on mesoporous silica support modified with linker molecules prepared by sol-gel method. As the linker molecules, triethoxyvinylsilane (support SG-1) and styrylethyltrimethoxysilane (support SG-2) were used. The IR spectra of prepared materials showed weak peaks at 2924 and 2834 cm^{-1} from the stretching vibration of C-H bonds and vibration at 1625 cm^{-1} which may indicate the presence of C=C double bond. IR spectra suggested the presence of linker molecules in prepared mesoporous materials. The N_2 adsorption isotherms of SG-1 and SG-2 are representative for materials with a broad distribution of mesopores; the pore diameter distribution is centred at 5 and 7 nm in the case of SG-1 and SG-2, respectively. The BET areas of both supports were around 650 m^2/g . After immobilization of the

RC-304 on these materials, the BET area decreased to 437 m²/g, and 462 m²/g for **SG01** and **SG02**, respectively. Under the conditions applied, only about 30 % of the starting amount of **RC-304** was transferred into catalysts **SG01** and **SG02** (corresponding to 0.34, and 0.38 wt. % of Ru in the catalysts, respectively). The low loading of **RC-304** onto the supports materials was probably due to the poor availability of linker molecules.

The catalysts **SG01** and **SG02** were tested in RCM of 1,7-octadiene (25 °C, Ru/1,7-octadiene = 1:250, c^0 (1,7-octadiene) = 0.15 mol/L). High initial reaction rates were observed in both cases. TOF₅ values were 0.274 s⁻¹ and 0.279 s⁻¹ for catalysts **SG01**, and **SG02**, respectively. The conversions after 5 h were the same for both catalysts (98 %) with high selectivity to desired products (99 %).

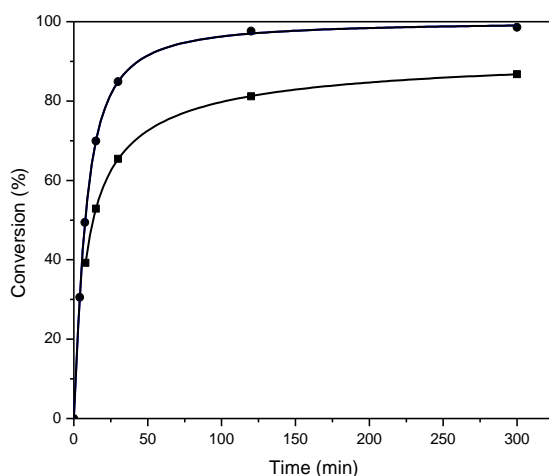


Figure 4.35. Filtration experiment in RCM of 1,7-octadiene with catalyst **SG02**. Liquid phase in contact with solid catalyst (circles), liquid phase after filtration (squares), toluene, 25 °C, molar ratio 1,7-octadiene/Ru = 250, c^0 (1,7-octadiene) = 0.15 mol/L.

In next step, we focused on the evaluation of the heterogeneity of prepared catalysts in filtration test (Figure 4.35.). Unfortunately, this test showed that, more or less, catalytically active species are leached out from the support material into liquid phase for both catalysts. The low heterogeneity of the prepared catalysts was supposedly caused by decomposition of linker molecule during the synthesis of the sol-gel material, which resulted in weak direct non-covalent immobilization interaction of **RC-304** the sol-gel materials [194]. After those negative results, we stopped further research on this topic. The preparation of heterogeneous catalysts by immobilization of **RC-304** on directly prepared support material with linker molecules (SG-1, SG-2) was in accord with the results published by Plaixats group, which has been interested in the preparation of heterogeneous metathesis catalyst using sol-gel approach for several years [152, 195]. On the other hand, to the best of our knowledge, catalysts prepared by Plaixats group

were not characterized by filtration experiments or by amount of ruthenium leached out from the catalysts. Question arises, if this method really leads to the true heterogeneous catalysts.

4.3.5. Immobilization of Ru complexes *via* non-covalent interaction

Another strategy for immobilization of highly active Ru alkylidenes on the surface of mesoporous molecular sieves is the immobilization *via* direct non-covalent interactions of Ru alkylidenes with surface OH groups of the used supports. For this purpose, we used highly ordered SBA-15, MCM-41, and conventional Silicagel 40 as support materials. As Ru alkylidene, we used commercially available **CI-HG-II** catalyst bearing quaternary ammonium groups placed in NHC ligand and its new analogues with different counter-ions **X-HG-II** (X = I, BF₄⁻ and PF₆⁻) (see Figure 3.1.). Textural properties of the prepared catalysts **C05** – **C07** were determined using several characterization methods (N₂ adsorption, XRD, XPS, ICP-MS), and activity of the catalysts was studied in various types of metathesis reactions such as RCM, CM, and self-metathesis.

4.3.5.1. Preparation and characterization of the catalysts

Immobilization of the **CI-HG-II** on to SBA-15, and MCM-41 proceeded almost quantitatively, as 99 % of initial amount of **CI-HG-II** was immobilized (Ru content in catalyst = 1.17 wt. % of Ru). In the case of amorphous Silicagel 40, only 75 % of initial **CI-HG-II** was immobilized due to the lower accessibility of surface of amorphous Silicagel 40, which resulted in lower Ru alkylidene immobilization (Ru content in catalyst = 0.92 wt. % of Ru).

The analysis of nitrogen adsorption isotherms (Figure 4.36. for **C05** as an example) showed that mesoporous character and regular architecture of the supports used were preserved during the preparation of the catalysts. However, the strong decrease in the BET area and void volume was associated with the catalyst preparation (S_{BET} decreased from 739 m²/g for parent SBA-15 to 492 m²/g, and V_{ME} decreased from 1.15 cm³/g for parent SBA-15 to 0.92 for **C05**). Concerning catalysts **C06** on MCM-41 and **C07** on Silicagel 40 the same trend of decreasing of textural parameters was observed (see Table 4.7.). Effect of decreasing textural parameters after immobilization of Ru alkylidene on the surface of silica supports was observed earlier [137]. However, pore size diameters did not change as a result of complex deposition and narrow pore size distribution was preserved as well.

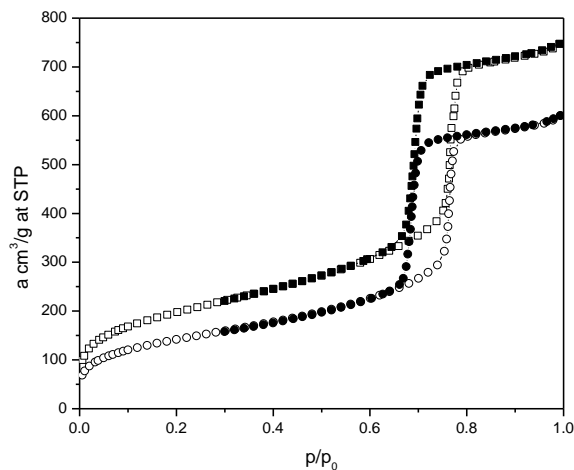


Figure 4.36. Nitrogen adsorption and desorption isotherms of SBA-15 (■), and prepared catalyst C05 (●). Open symbols are used for adsorption branches of the isotherms, filled symbols for desorption branches of the isotherms.

Table 4.7. Textural parameters of supports and catalysts.

| Material | S_{BET} (m^2/g) | V_{ME} (cm^3/g) | D_{ME} (nm) |
|---------------------|--------------------------|--------------------------|------------------|
| SBA-15 | 739 | 1.15 | 6.7 |
| C05 | 492 | 0.92 | 6.6 |
| MCM-41 | 972 | 1.14 | 4.0 |
| C06 | 640 | 0.68 | 3.9 |
| Silicagel 40 | 559 | 0.47 | 4.6 |
| C07 | 387 | 0.45 | 4.5 |

All catalysts were tested in the RCM of 1,7-octadiene, (-)- β -citronellene, and DAF, and in self-metathesis of methyl oleate (Scheme 4.1.). All reactions belong to the standard metathesis reactions used for the comparison and evaluation of new metathesis catalysts [196]. Application of new heterogeneous catalysts is summarized in Table 4.9.

4.3.5.2. Catalytic activity – influence of support

Prepared catalysts C05, C06, and C07 were tested in RCM of (-)- β -citronellene and 1,7-octadiene and in self-metathesis of methyl oleate (Scheme 4.1.) to evaluate the effect of different supports used.

For comparison with ordered silica materials SBA-15, and MCM-41 with narrow pore size distribution, **CI-HG-II** was also immobilized on Silicagel 40. In RCM of 1,7-octadiene (Figure 4.37.) the initial reaction rate increased in the order **C07** = **C06** < **C05** < **CI-HG-II**. Differences of substrate conversions depend on the pore size of supports used and show the advantage of the SBA-15 as a support. It is attributed to the regular mesoporous structure of SBA-15 with the largest pore diameter among all used supports. The positive effects of pore size of catalyst was also observed in RCM of (-)- β -citronellene and self-metathesis of methyl oleate. Also, in these reactions, the initial reaction rates decreased with the type of catalysts in the following order: **CI-HG-II** > **C05** > **C06** > **C07**. The **C05** proved to be the most active heterogeneous catalyst, producing the initial reaction rate almost as high as that observed for homogeneous **CI-HG-II** (in RCM of (-)- β -citronellene TOF_{10} was 3.06 s^{-1} for **CI-HG-II** and 3 s^{-1} for **C05**; in self-metathesis of methyl oleate TOF_{10} was 0.188 s^{-1} for **CI-HG-II** and 0.154 s^{-1} for **C05**). With all catalysts, reactions proceeded selectively to methylcyclopentene and dimethyl octadecenylidiate, respectively, as the only reaction products. The drop of the initial reaction rate of the heterogeneous catalysts compared to the homogeneous ones is connected with the diffusion of the reactant to the catalytically active species inside of the pores of support materials.

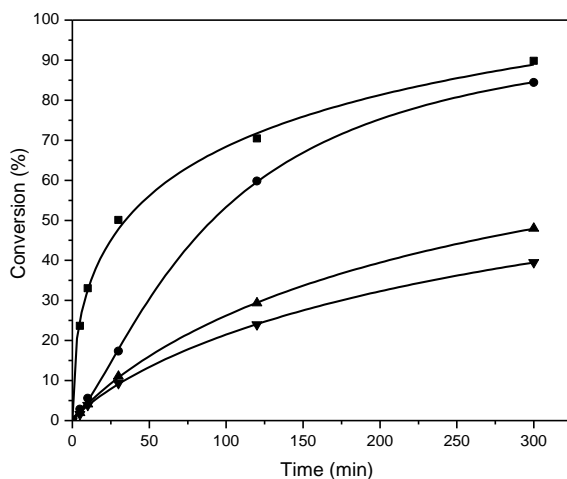


Figure 4.37. RCM of 1,7-octadiene with catalysts **CI-HGII** (■), **C05** (●), **C06** (▲), and **C07** (▼). 0 °C, molar ratio Ru/1,7-octadiene = 1:250, toluene, $c^0(1,7\text{-octadiene}) = 0.15 \text{ mol/L}$.

To confirm the heterogeneity of prepared catalyst **C05**, the standard filtration test was carried out (RCM of 1,7-octadiene at 40 °C - Figure 4.38.). Ruthenium leaching in this experiment was only 2.6 % of the initial amount of Ru which corresponds to the maximum 17 ppm of Ru in the product. The values of substrate conversion in the filtrate (Figure 4.38.) suggested that Ru species that were leached into the liquid phase could not catalyse metathesis reactions. The heterogeneity of the **C05** was also confirmed by additional experiment, in which **C05** was stirred in highly polar THF for 24 h. With such treated catalyst, RCM of (-)- β -

citronellene was carried out. The TON was without change in comparison with reaction promoted with fresh portion of catalyst. The treatment with THF affected the initial reaction rate. The TOF_5 decreased from 0.43 s^{-1} to 0.31 s^{-1} .

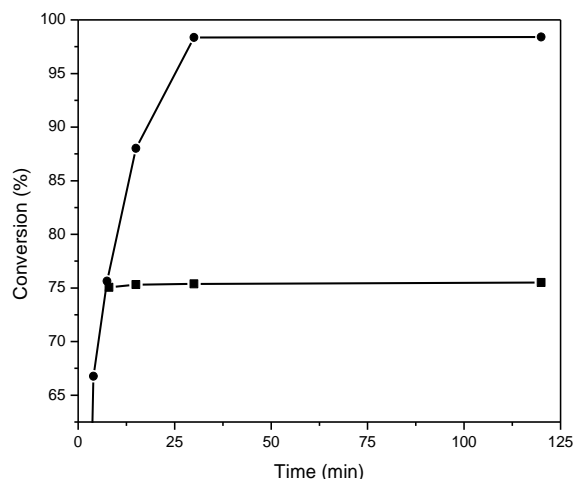


Figure 4.38. Filtration test in RCM of 1,7-octadiene. $40 \text{ }^\circ\text{C}$, molar ratio $\text{Ru}/1,7\text{-octadiene} = 1:250$, toluene, $c^0(1,7\text{-octadiene}) = 0.15 \text{ mol/L}$; suspension (●), filtrate (■).

4.3.5.3. Catalytic activity - influence of counter-anion

The influence of counter-anions on catalyst activity of ammonium tagged ruthenium alkylidenes has been already reported for olefin metathesis in water [197]. The authors of this report found that higher anion hydrophilicity led to a higher catalyst activity. Contrary to our system, ammonium tags were located on the alkylidene ligand. To see, if the counter-anion affects the immobilization process and the activity of the catalysts in the reactions, three more analogues of **Cl-HG-II** were prepared with counter-anions Γ^- , BF_4^- and PF_6^- .

Immobilization of **I-HG-II**, **BF₄-HG-II**, and **PF₆-HG-II** on to SBA-15 proceeded almost quantitatively, as 95 %, 97 %, and 99 % of initial homogeneous Ru alkylidene was immobilized, respectively. It corresponds to 1.12, 1.15, and 1.09 wt. % of Ru, respectively. The immobilization process showed to be independent on the kind of counter-anion.

All prepared alkylidenes **X-HG-II** ($X = \text{Cl}^-$, Γ^- , BF_4^- , and PF_6^-) were tested in homogeneous reactions RCM of (-)- β -citronellene, 1,7-octadiene, and DAF as well as in the reactions over heterogeneous catalysts immobilized on SBA-15: **C05**, and **C08 – C10** (Figures 4.39. – 4.41.).

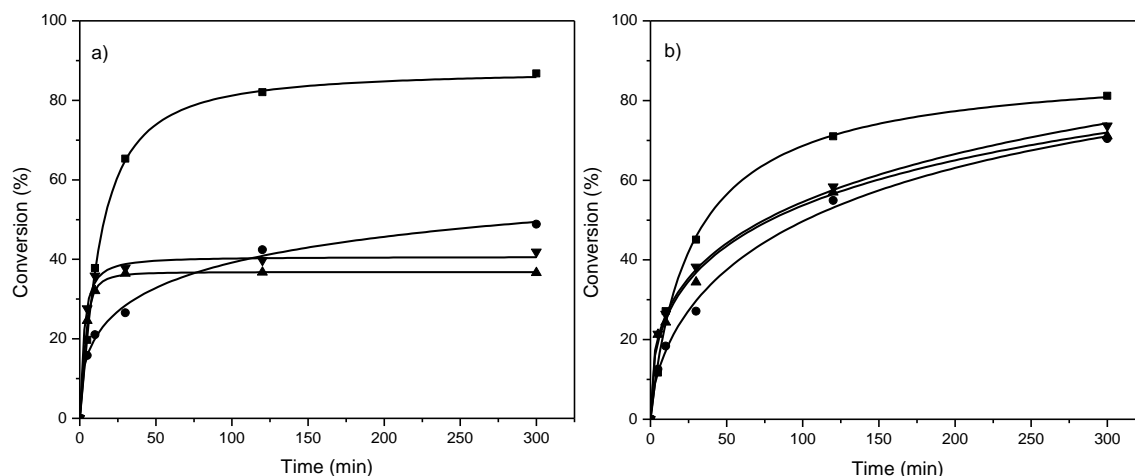


Figure 4.39. Influence of counter-ion X: Cl^- (■), I^- (●), BF_4^- (▲), and PF_6^- (▼) on conversion of (-)- β -citronellene with catalyst **X-HG-II** Fig. a) and **X-HG-II/SBA-15** Fig b). 60 °C, toluene, c^0 ((-)- β -citronellene) = 0.15 mol/L, molar ratio Ru/(-)- β -citronellene = 1:2000.

It turned out that the kind of counter-anion used affected homogeneous metathesis much more than the heterogeneous one. In RCM of (-)- β -citronellene, and 1,7-octadiene **Cl-HG-II** was the most active homogeneous catalyst of **X-HG-II**, the order in the catalytic activity of other **X-HG-II** alkylidenes was different for these two substrates. In the RCM of (-)- β -citronellene TON decreased in the order **Cl-HG-II** (1740) > **I-HG-II** (980) > **PF₆-HG-II** (800) > **BF₄-HG-II** (700). In the RCM of 1,7-octadiene TON decreased in the order **Cl-HG-II** (220) > **I-HG-II** (143) > **BF₄-HG-II** (105) > **PF₆-HG-II** (65).

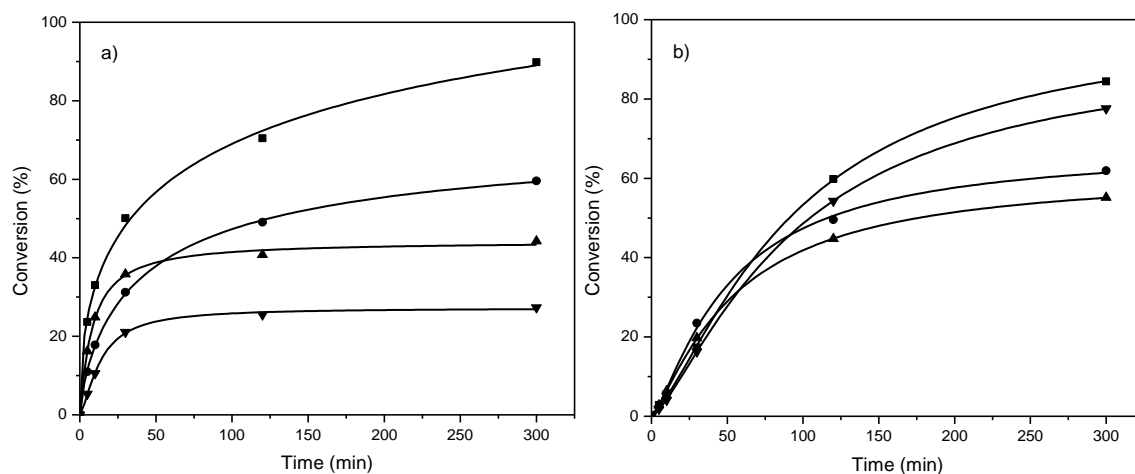


Figure 4.40. Influence of counter-ion X: Cl^- (■), I^- (●), BF_4^- (▲), and PF_6^- (▼) on the conversion of 1,7-octadiene with catalyst **X-HG-II** Fig. a) and **X-HG-II/SBA-15** Fig b). 0 °C, toluene, c^0 (1,7-octadiene) = 0.15 mol/L, molar ratio Ru/1,7-octadiene = 1:250.

It was found, that over heterogeneous catalysts **C08**, **C09**, and **C10** higher final conversions were reached than with **X-HG-II** alkylidenes. This behaviour was probably connected with the stabilization of Ru alkylidenes by immobilization on the surface of SBA-15. Stabilization effect of immobilization of Ru complexes was already described [198]. Only **Cl-HG-II** showed higher initial reaction rates and higher final conversions than its heterogeneous analogue. The catalyst **C05** was the most active among all heterogeneous catalysts for these two tested substrates (1,7-octadiene, (-)- β -citronellene). The order of conversion of the other three heterogeneous catalysts is different in each RCM. In the RCM of (-)- β -citronellene final conversion decreased in the order **Cl-HG-II/SBA-15** (80 %) > **PF₆-HG-II/SBA-15** (72 %) > **BF₄-HG-II/SBA-15** (69 %) = **I-HG-II/SBA-15** (69 %). In the RCM of 1,7-octadiene final conversion decreased in the order **Cl-HG-II/SBA-15** (84 %) > **PF₆-HG-II/SBA-15** (79 %) > **I-HG-II/SBA-15** (61 %) > **BF₄-HG-II/SBA-15** (55 %).

The results from RCM of DAF (Figure 4.41.) exhibited, that **Cl-HG-II** was the least active catalyst among all homogeneous and heterogeneous catalysts. Supposedly, the loss of activity of **Cl-HG-II** is due to a higher polarity of substrate DAF. Stabilization effect of supported catalysts was confirmed also in this case, where **C05**, **C08**, **C09**, and **C10** reached higher final conversions than the homogeneous catalysts. Difference between **X-HG-II** and heterogeneous analogues were: **Cl-HG-II** (48 %) – **C05** (80 %), **I-HG-II** (65 %) – **C08** (70 %), **BF₄-HG-II** (67 %) – **C09** (71 %), **PF₆-HG-II** (61 %) – **C10** (80 %). The kind of counter-anion had no effect on catalyst selectivity: in all homogeneous as well as heterogeneous RCM of (-)- β -citronellene, 1,7-octadiene, and DAF methylcyclopentene, cyclohexene, and *N*-(trifluoroacetyl)-3-pyrroline were found as the only products, respectively.

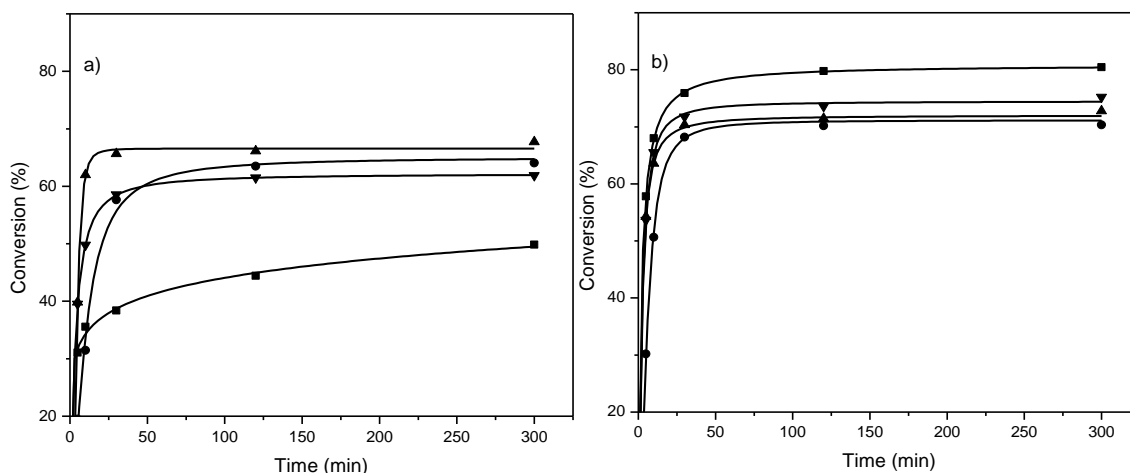


Figure 4.41. Influence of counter-ion X: Cl⁻ (■), I⁻ (●), BF₄⁻ (▲), and PF₆⁻ (▼) on conversion of DAF with catalyst **X-HG-II** Fig. a) and **X-HG-II/SBA-15** Fig b). 60 °C, toluene, c⁰(DAF) = 0.15 mol/L, molar ratio Ru/DAF = 1:250.

Stability of the homogeneous catalyst **CI-HG-II** was tested in RCM of (-)- β -citronellene (Figure 4.42.). One reaction was carried out as usual. In the case of the two others, the catalyst was kept under reaction condition for 2, and 5 h. After this period, a portion of the substrate was added to the reactor. Substrate conversion significantly dropped down in the reactions where substrate was added after 2 and 5 h. In the case, when substrate was added after 5 h, substrate conversion decreased from 85 % to 15 %. Stability of catalyst **CI-HG-II** in RCM of (-)- β -citronellene was studied by UV-VIS spectroscopy (Figure 4.42. b). All spectra exhibited the same band at 380 nm which reflected d-d transition of the Ru(II) atom [199]. The intensity of the peak decreased with time suggested that catalyst start to decompose (dissolution of Ru alkylidene allows ligand dissociation and formation of more reactive 14-electron species, which is more sensitive to decomposition; therefore Ru alkylidene became inactive in the metathesis reaction).

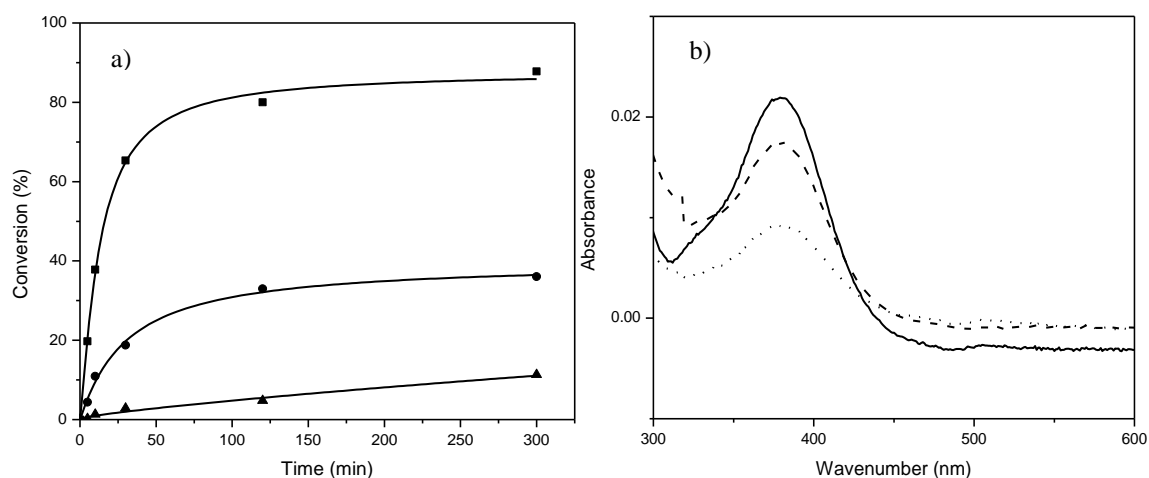


Figure 4.42. a) Stability of the **CI-HG-II** in RCM of (-)- β -citronellene, 60 °C, c^0 ((-)- β -citronellene) = 0.15 mol/L, toluene, molar ratio Ru/(-)- β -citronellene = 1:2000. Substrate was added after 0 h (■), 2 h (●), and 5 h (▲); b) Corresponding UV-VIS spectra in toluene ($c = 0.06$ mol/L, $l = 0.1$ cm) after 0 h (full line), 2 h (dashed line), and 5 h (dotted line).

4.3.5.4. Catalytic activity - influence of reaction conditions

Catalyst **C05** proved to be the best heterogeneous catalyst tested. In accordance with evaluation of good heterogeneous catalyst for particular reaction (activity, stability, and reusability) we decided to check the influence of reaction conditions in order to increase maximal TON. RCM of (-)- β -citronellene was taken as a model reaction.

Figure 4.43. shows the effect of decreasing concentration of catalyst **C05** (and consequently increasing molar ratio Ru:(-)- β -citronellene from 250 to 4000). Initial reaction rate expressed in term of TOF_{30} increased from 0.125 s^{-1} for molar ratio Ru/(-)- β -citronellene 1:250

to 0.53 s^{-1} for molar ratio Ru/(-)- β -citronellene 1:4000. Maximal conversion (99 %) of (-)- β -citronellene was achieved with molar ratio up to Ru/(-)- β -citronellene 1:1000. However, maximal TON = 1623 was accomplished with molar ratio Ru/(-)- β -citronellene 1:2000, despite incomplete conversion (81 %) of used substrate. Further decrease in the catalyst concentration did not lead to increased TON number (Ru/(-)- β -citronellene 1:4000; TON = 1399). 100 % selectivity to methylcyclopentene was observed in all experiments.

The catalyst **C05** also turns out to be reusable in RCM of (-)- β -citronellene not only at high catalyst concentration Ru/(-)- β -citronellene 1:250, but also when lower concentration of catalyst was applied (Ru/(-)- β -citronellene 1:1000) (Table 4.8.). In the first case, **C05** was able to sufficiently accomplish four runs in RCM of (-)- β -citronellene with conversion of the substrate over 90 %.

In the next run, conversion drops from 90 % to 47 %, which indicates a partial deactivation of the catalyst. The cumulative TON in this experiment reached 1069. Decreased concentration of the catalyst (Ru/(-)- β -citronellene 1:1000) allowed to get higher cumulative TON of 2110 in the three consecutive runs before conversion dropped below 10 % in the fourth run.

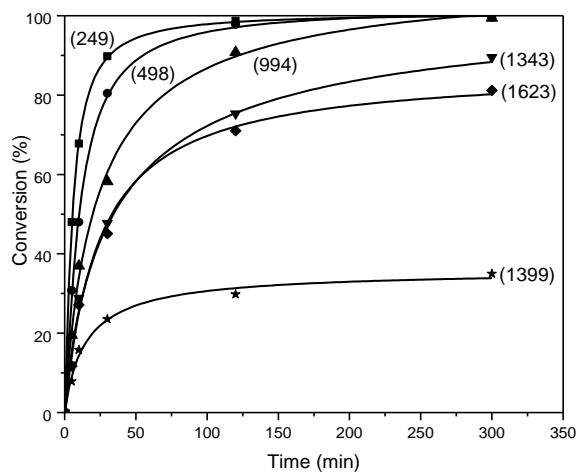


Figure 4.43. RCM of (-)- β -citronellene over **C05** loading dependence. $60 \text{ }^\circ\text{C}$, c^0 ((-)- β -citronellene) = 0.15 mol/L , toluene, molar ratio Ru/(-)- β -citronellene = 1:250 (■), 1:500 (●), 1:1000 (▲) 1:1500 (▼), 1:2000 (◆), and 1:4000 (★). Maximum TONs achieved are given in brackets.

Table 4.8. Reusing of C05 in RCM of (-)- β -citronellene.

| Run | 1 | 2 | 3 | 4 | 5 |
|------------------------------|---------------------|--------|--------|--------|--------|
| Conversion (%) ^{a)} | 99 | 97 | 94 | 90 | 47 |
| | (248) ^{c)} | (491) | (726) | (951) | (1069) |
| Conversion (%) ^{b)} | 94 | 79 | 38 | 8 | 3 |
| | (940) | (1730) | (2110) | (2118) | (2121) |

a) 60 °C, 5 h, Ru/(-)- β -citronellene = 1:250, toluene, c^0 ((-)- β -citronellene) = 0.15 mol/L

b) 60 °C, 5 h Ru/(-)- β -citronellene = 1:1000, toluene, c^0 ((-)- β -citronellene) = 0.15 mol/L

c) cumulative TON is given in brackets

The influence of temperature on TON and TOF in RCM of (-)- β -citronellene (Figure 4.44.) was determined. Reactions were carried out using the same concentration c^0 ((-)- β -citronellene) = 0.15 mol/L and molar ratio Ru/(-)- β -citronellene = 1:2000. As expected, increasing temperature had a positive influence on the reaction rates and final TONs and the best result was obtained at 80 °C (TON 1880, TOF 1.3 s⁻¹). Nevertheless, reasonable activity was still observed at 40 °C. Arrhenius plot was linear in the studied region of temperature and apparent activation energy determined from it was 31.1 kJ/mol. Similar values of apparent activation energy were found for supported Hoveyda-Grubbs catalysts recently (42 kJ/mol for self-metathesis of methyl oleate and 36.8 kJ/mol for RCM of (-)- β -citronellene) [200].

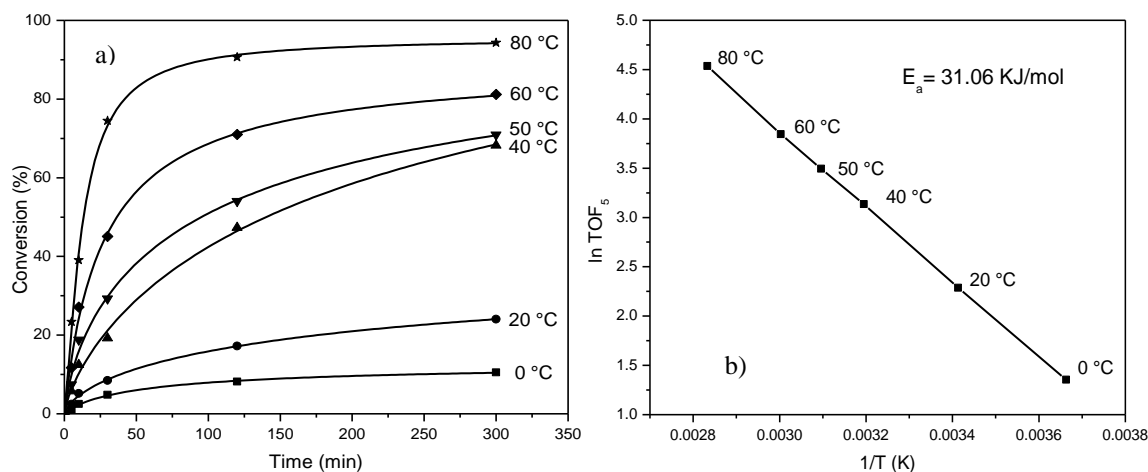


Figure 4.44. a) Influence of temperature on conversion in RCM of (-)- β -citronellene. c^0 ((-)- β -citronellene) = 0.15 mol/L, toluene, molar ratio Ru/(-)- β -citronellene = 1:2000, T = 0 (■), 20 (●), 40 (▲), 50 (▼), 60 (◆), and 80 °C (★). b) Arrhenius plot calculated from Fig. a).

Then, RCM of (-)- β -citronellene at 60 °C with molar ratio Ru/(-)- β -citronellene = 1:2000 at different substrate concentrations was performed. Increased substrate concentration from 0.15 mol/L to neat substrate resulted in higher TON and especially in higher TOF. Maximum TON and TOF in reaction carried out at 0.15 mol/L reached 1623 (5 h reaction time) and 0.93 s⁻¹ (TOF calculated after 10 min), respectively. In contrast, at 1 mol/L concentration TON 2000 (5 h) and TOF₁₀ 3.1 s⁻¹ were found. Reaction performed in neat substrate exhibited the highest TON and TOF, but with distinctive drop of selectivity over 70 %. The drop of selectivity towards RCM product was due to RCM substrates at high reaction concentration can form ADMET oligomers [201].

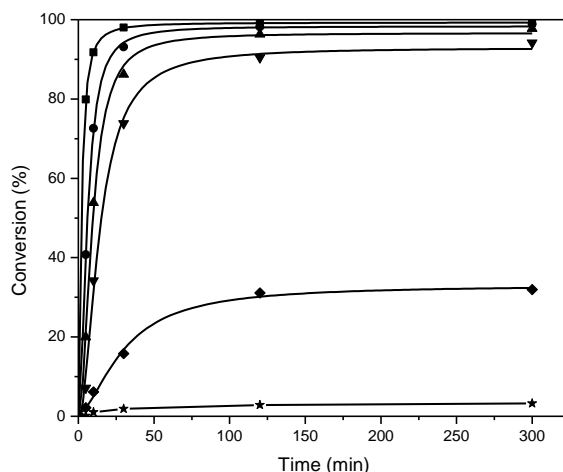


Figure 4.45. RCM of (-)- β -citronellene over **C05** loading dependence. Toluene, c⁰((-)- β -citronellene) = 1 mol/L, 60 °C, molar ratio Ru/(-)- β -citronellene = 1:2000 (■), 1:4000 (●), 1:8000 (▲), 1:12000 (▼), 1:16000 (◆), 1:24000 (★).

It turned out that substrate concentration of 1 mol/L (Figure 4.45.) is convenient to get maximal TON with selective formation of ring closing metathesis products. Reactions with molar ratio Ru/substrate in the range 1:2000 to 1:12000 showed similar final conversions. The initial reaction rate expressed in TOF₃₀ values increased in the order 1:2000 (TOF₃₀= 1.05 s⁻¹) < 1:4000 (TOF₃₀= 2.04 s⁻¹) < 1:8000 (TOF₃₀= 3.86 s⁻¹) < 1:12000 (TOF₃₀= 4.8 s⁻¹). Conversion in reaction with Ru/molar ratio 1:12000 reached to 94 %, which corresponds to excellent TON of 11300. Subsequent decrease in the catalyst concentration to molar ratio 1:16000 caused decrease in substrate conversion (final conversion was 32 %). However, at temperature 80 °C, catalyst promoted full conversion of (-)- β -citronellene with achieved TON = 16000. When molar ratio 1:24000 was applied almost no activity was observed.

Despite low selectivity of RCM of neat (-)- β -citronellene, reactions with further decreasing catalyst amount were carried out to estimate what maximal molar ratio Ru/substrate

can be used to get reasonable TON. Molar ratio Ru/catalyst in RCM of (-)- β -citronellene was decreased up to 1:48000. Achieved conversion was 70 %, which corresponds to TON = 33451 (Figure 4.46.). But the selectivity to the ring closing products was only 30 %, it reduced maximal TON to productive TON ~ 11000. Isolation of by-products followed by GC-MS analysis allowed for identification of a dimer and two trimers formed in acyclic diene metathesis (ADMET) and two cyclic olefins – products of cycloisomerization reaction (Scheme 4.5.).

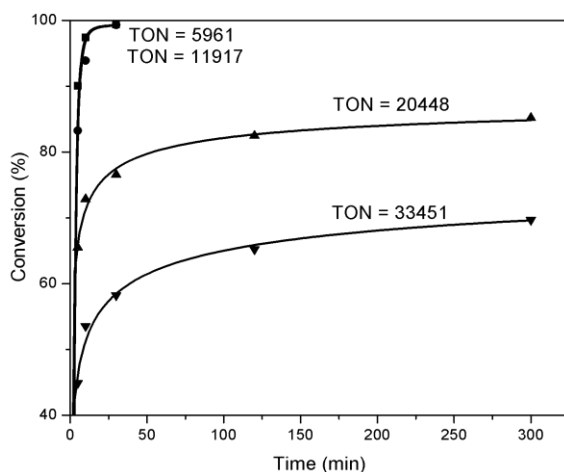
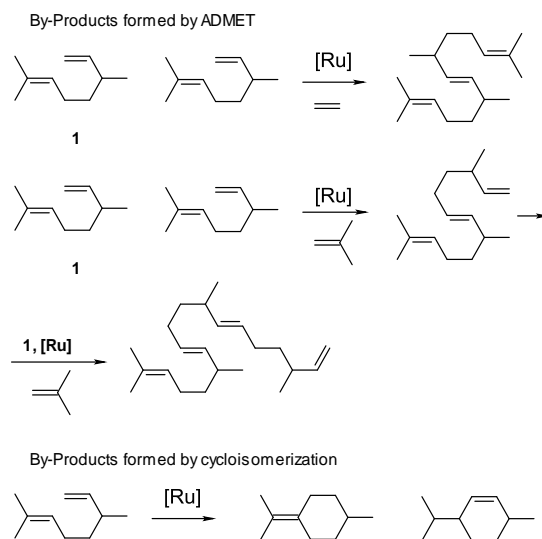


Figure 4.46. RCM of (-)- β -citronellene with **C05** in neat substrate, 60 °C, molar ratio Ru/(-)- β -citronellene = 1:6000 (■), 1:12000 (●), 1:24000 (▲), 1:48000 (▼).



Scheme 4.5. By-products detected after RCM of (-)- β -citronellene carried out in neat substrate.

4.3.5.5. Catalytic activity – influence of solvent

The catalyst **C05** was tested in RCM of (-)- β -citronellene (Figure 4.47.), 1,7-octadiene (Figure 4.48.), and self-metathesis of methyl oleate (Figure 4.49.) in different solvents (toluene, CH₂Cl₂, ethyl acetate, and THF) due to the growing interest in using more environmentally friendly solvents in industry (especially ethyl acetate, which was recently reported to be exceptionally good solvent for homogeneous metathesis [202]). The initial reaction rate and conversion after 300 min in all tested systems increased in order THF < CH₂Cl₂ < ethyl acetate < toluene. The catalyst **C05** showed one exception, in RCM of 1,7-octadiene in ethyl acetate, the initial reaction rate was higher than for toluene (Table 4.9). The experiments revealed the possibility of replacement of the solvent from toluene to more environmentally and user friendly ethyl acetate due to TON and TOF not changing significantly in the reactions carried out in toluene and ethyl acetate (Table 4.9).

Table 4.9. **C05** TOFs and TONs in reactions with toluene and ethyl acetate.

| Substrate | Solvent | TON | TOF ₃₀ |
|----------------------------|---------------|------|-----------------------|
| (-)- β -citronellene | Toluene | 1080 | 0.16 s ⁻¹ |
| | Ethyl acetate | 960 | 0.11 s ⁻¹ |
| 1,7-octadiene | Toluene | 207 | 0.025 s ⁻¹ |
| | Ethyl acetate | 185 | 0.041 s ⁻¹ |
| methyl oleate | Toluene | 137 | 0.036 s ⁻¹ |
| | Ethyl acetate | 125 | 0.033 s ⁻¹ |

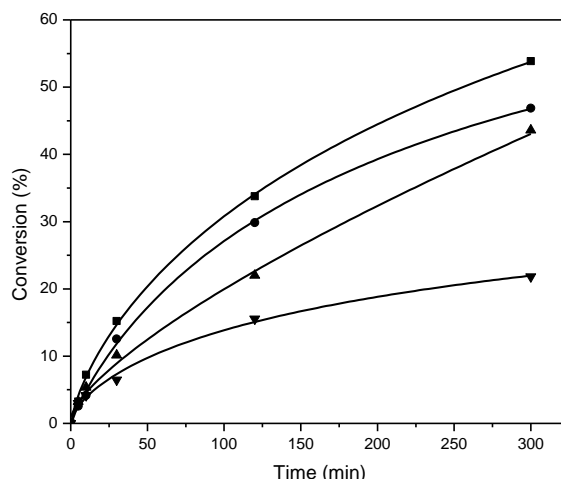


Figure 4.47. Influence of solvent on the catalytic activity of **C05** in RCM of (-)- β -citronellene. 40 °C, molar ratio Ru/(-)- β -citronellene = 1:2000, c^0 ((-)- β -citronellene) = 0.15 mol/L, toluene (■), CH₂Cl₂ (●), ethyl acetate (▲), and THF (▼).

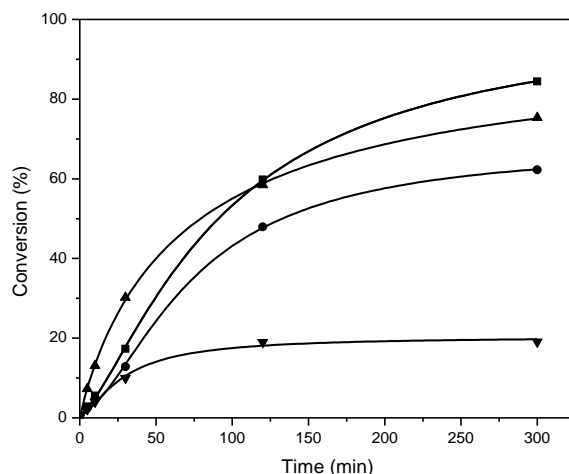


Figure 4.48. Influence of solvent on catalyst activity of **C05** in RCM of 1,7-octadiene. 0 °C, molar ratio Ru/1,7-octadiene = 1:250, c^0 (1,7-octadiene) = 0.15 mol/L, toluene (■), CH₂Cl₂ (●), ethyl acetate (▲), and THF (▼).

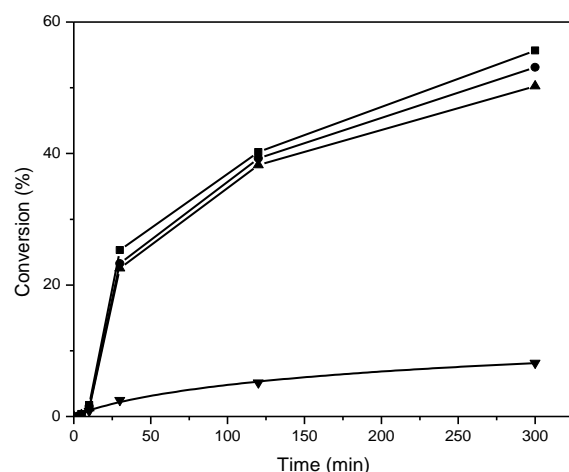


Figure 4.49. Influence of solvent on catalyst activity of **C05** in self-metathesis of methyl oleate. 30 °C, molar ratio Ru/ methyl oleate = 1:250, c^0 (methyl oleate) = 0.15 mol/L, toluene (■), CH₂Cl₂ (●), ethyl acetate (▲), and THF (▼).

To explain the low activity of catalyst **C05** in very polar solvent THF for all three substrates, the separate experiment was done. The catalyst **C05** catalyst was stirred in THF for 24 h, than it was recovered by filtration and by vacuum drying. Such treated catalyst was used in RCM of (-)- β -citronellene in toluene. Catalytic activity of aged catalyst was almost the same as for the fresh catalyst used under the same conditions. The reduced activity of catalyst **C05** in reactions done in THF was probably not due the decomposition of such catalyst, but most probably the coordination of etheric oxygen from THF to the catalytically active species occurred as already reported in the literature [203].

Ru leaching in RCM of (-)- β -citronellene in all tested solvents was very low (0.96, 1.04, 0.87 wt. % from original amount of Ru used in reaction for ethyl acetate, DCM, and THF respectively).

4.3.6. Metathesis summary

Heterogeneous catalysts for olefin metathesis were prepared by immobilization of commercially available Hoveyda-Grubbs type alkylidene complex **RC-304** on mesoporous molecular sieves SBA-15, SBA-16, MCM-41, and MCM-48 having the surface modified with PCy₂ linkers. The mesoporous character and narrow pore size distributions of supports were preserved in prepared heterogeneous catalysts. The catalysts (1 wt. % of Ru) proved their activity and high selectivity in RCM of 1,7-octadiene, DEDAM, DAF, and DAB; in self-metathesis of 1-decene, 5-hexenyl acetate, and methyl 10-undecenoate; and in cross-metathesis of allylbenzene with *cis*-1,4-diacetoxy-2-butene. Significant effect of the support pore size on heterogeneous catalyst activity was found in RCM of 1,7-octadiene, DAF, and DAB. The initial reaction rates and/or conversions achieved were found to decrease with decreasing pore size of catalyst supports. Filtration tests confirmed that the solid catalyst was fully responsible for the catalytic activity during the reaction. Catalysts could be easily separated from the reaction mixture, in contrast to the corresponding homogeneous system, and can be used repeatedly. The Ru leaching was very low (0.1 % of starting Ru amounts in catalyst for 1,7-octadiene at 40 °C and 0.38 % for DEDAM at 80 °C), about 1 order of magnitude lower than that of catalysts prepared by the immobilization of Grubbs 2nd generation catalyst on mesoporous molecular sieves through phosphine linkers. In ROMP of COE high-molecular-weight polymer was obtained in good yield.

New heterogeneous metathesis catalysts were prepared by immobilizing Hoveyda-Grubbs type alkylidenes with quaternary ammonium tagged *N*-heterocyclic ligands (**X-HG-II**, **X** = Cl, I, PF₆, BF₄) on silica (Silicagel 40) and siliceous mesoporous molecular sieves SBA-15 and MCM-41. In dependence on the support used, the catalyst activity was found to increase in the order Silicagel 40 < MCM-41 < SBA-15. The filtration test indicated that the heterogeneous catalyst was fully responsible for the catalytic activity. The counter-anion had a significant effect on catalyst activity in tested RCM reactions. Rapid deactivation leading to incomplete conversions was observed for **X** = I, PF₆, and BF₄, especially in homogeneous systems. Heterogenization by supporting on SBA-15 led to certain stabilization and higher final conversions in RCM over **X-HG-II/SBA-15** were achieved than in corresponding homogeneous systems (for **X** = I, PF₆, and BF₄). **C05** catalyst (*i.e.* **Cl-HG-II** on **SBA-15**) exhibited the highest activity from all heterogeneous catalysts prepared. In RCM of (-)- β -citronellene in toluene high TONs (up to 16 000) and 100 % selectivity to methylcyclopentene were achieved at substrate

concentration 1 mol/L and elevated temperatures. In the case of neat (-)- β -citronellene, a drop in selectivity to methylcyclopentene was observed in favour of ADMET products and cycloisomers. **C05** also exhibited high activity and selectivity in a series of RCM of different substrates, in self-metathesis of unsaturated esters, in enyne-metathesis, and in cross-metathesis with methyl acrylate, giving rise to the products with very low content of residual Ru (less than 10 ppm in most cases). In addition to toluene, ethyl acetate can be also used, especially in processes requiring more environmentally friendly solvent.

5. Conclusions

Silicate mesoporous materials have received widespread interest because of their high BET areas combined with large and uniform pore sizes. Their potential applications are: (i) supports for catalytically active species in various organic reactions; (ii) adsorbents for gas separation, and purification; (iii) adsorbents for removal of pollutants from liquid phase. Mesoporous molecular sieves were used for functionalizations to develop new materials for adsorption of CO₂ and for preparation of new highly active heterogeneous metathesis catalysts.

Novel method was introduced to prepare mesoporous molecular sieves with MgO promoted with potassium carbonate without causing collapse of their mesoporous structure. Such modification enhanced their CO₂ adsorption capacity.

The main part of the thesis was devoted to the preparation of new heterogeneous metathesis catalysts evidencing that mesoporous molecular sieves represent progressive supports for new heterogeneous catalysts for olefin metathesis. As supports, conventional silica (Silicagel 40), mesoporous molecular sieves (SBA-15, SBA-16, MCM-41, and MCM-48) or sol-gel materials (SG-1, SG-2) were used. Used Ru alkylidenes were immobilized *via* linker or *via* direct non-covalent interaction with the surface of the used solids. The prepared heterogeneous catalysts exhibited high activity and selectivity in metathesis reactions of different types (RCM, CM, self-metathesis, and ROMP) with various types of olefinic substrates. Despite lower reaction rate of the reactions promoted by heterogeneous catalysts in comparison with those promoted by homogeneous Ru alkylidene catalysts, the most important advantages of the heterogenized catalysts were confirmed: (i) the prepared catalysts show low Ru leaching; and (ii) can be used repeatedly. The activity of prepared catalysts depends on the catalysts support. Independently on used Ru alkylidenes and methods of their immobilization, the SBA-15 proved to be the best support material for new heterogeneous metathesis catalysts. Taking into account the economical and environmental considerations, handling of immobilized Ru alkylidenes presents many advantages in comparison with Ru alkylidenes as homogeneous catalysts.

6. References

- [1] V. L. Zholobenko, A. Y. Khodakov, M. Imperor-Clerc, D. Durand, I. Grillo, *Adv. Colloid Interface Sci.*, 142 (2008) 67
- [2] A. Zukal, J. Mayerová, J. Čejka, *Phys. Chem. Chem. Phys.*, 12 (2010) 5240
- [3] H. Balcar, J. Čejka, *Coord. Chem. Rev.*, 257 (2013) 3107
- [4] Y. Deng, J. Wei, Z. Sun, D. Zhao, *Chem. Soc. Rev.*, 42 (2013) 4054
- [5] S. H. Wu, C. Y. Moua, H. P. Lin, *Chem. Soc. Rev.*, 42 (2013) 3862
- [6] C. T. Kresge, M. E. Leonowicz, W. J. Roth, J. C. Vartuli, J. S. Beck, *Nature*, 359 (1992) 710
- [7] K. Schumacher, P. I. Ravikovitch, A. Du Chesne, A. V. Neimark, K. K. Unger, *Langmuir*, 16 (2000) 4648
- [8] M. Kruk, M. Jaroniec, C. H. Ko, R. Ryoo, *Chem. Mater.*, 12 (2000) 1961
- [9] D. Zhao, Q. Huo, J. Feng, B. F. Chmelka, G. D. Stucky, *J. Am. Chem. Soc.*, 120 (1998) 6024
- [10] M. Thommes, *Chemie Ingenieur Technik*, 82 (2010) 1059
- [11] W. J. J. Stevens, K. Lebeau, M. Mertens, G. V. Tendeloo, P. Cool, E. F. Vansant, *J. Phys. Chem. B* 110 (2010) 9183
- [12] L. A. Solovyov, *Chem. Soc. Rev.*, 42 (2013) 3708
- [13] S. Lowell, J. E. Shields, M. A. Thomas, M. Thommes, *Characterization of Porous Solids and Powders: Surface Area, Pore Size and Density*. Kluwer Academic Publishers, Dordrecht, Netherlands, 2004
- [14] A. Taguchi, F. Schuth, *Microporous Mesoporous Mater.*, 77 (2005) 1
- [15] B. Yilmaz, U. Muller, *Top. Catal.*, 52 (2009) 888
- [16] D. Schneider, D. Kondrashova, R. Valiullin, A. Bunde, J. Kärger, *Chem. Ing. Tech.*, 87 (2015) 1794
- [17] C. Perego, R. Millini, *Chem. Soc. Rev.*, 42 (2013) 3956
- [18] https://www.ipcc.ch/pdf/special-reports/srccs/srccs_annex1.pdf (accessed September 26, 2016)
- [19] http://www.ipcc.ch/publications_and_data/ar4/syr/en/spm.html (accessed September 26, 2016)
- [20] M. Marquis, P. Tans, *Science*, 320 (2008) 460

- [21] Current Greenhouse Gas Concentrations, http://cdiac.ornl.gov/pns/current_ghg.html (accessed September 26, 2016)
- [22] S. Choi, J. H. Drese, C. W. Jones, *ChemSusChem.*, 2 (2009) 796
- [23] H. Yang, Z. Xu, M. Fan, R. Gupta, R. B. Slimane, A. E. Bland, I. Wright, *J. Environ. Sci.*, 20 (2008) 14
- [24] America's Climate Choices: Panel on Advancing the Science of Climate Change; National Research Council, *Advancing the Science of Climate Change*, The National Academies Press, Washington, DC, USA.
- [25] J. Kothandaraman, A. Goeppert, M. Czaun, G. K. S. Prakash, G. A. Olah, *J. Am. Chem. Soc.*, 138 (2016), 778
- [26] OECD/IEA. *Tracking Industrial Energy Efficiency and CO₂ Emissions*; International Energy Agency: Paris, 2007
- [27] Q. Wang, J. Luo, Z. Zhong, A. Borgna, *Energy Environ. Sci.*, 4 (2011) 42
- [28] A. Corma, *Chem. Rev.*, 97 (1997) 2373
- [29] R. Xu, W. Pang, Q. Huo, *Modern inorganic synthetic chemistry*, Elsevier, Amsterdam, Netherlands, 2011
- [30] J. Weitkamp, L. Puppe, *Catalysis and zeolites: fundamentals and application*, Springer, Heidelberg, Germany, 1999
- [31] S. Fujita, T. Kanai, Y. Oumi, T. Sano, *Stud. Surf. Sci. Catal.*, 158 (2005) 191
- [32] J. Zhu, X. Meng, F. Xiao, *Front. Chem. Sci. Eng.*, 7 (2013) 233
- [33] W. J. Roth, P. Nachtigall, R. E. Morris, J. Čejka, *Chem. Rev.*, 114 (2014) 4807
- [34] J. Wang, L. Huang, R. Yang, Z. Zhang, J. Wu, Y. Gao, Q. Wang, D. O'Hare, Z. Zhong, *Energy Environ. Sci.*, 7 (2014) 3478
- [35] S. Kulprathipanja, *Zeolites in Industrial Separation and Catalysis*, Wiley: Weinheim, Germany, 2010, Vol. 1
- [36] C. P. Cabello, P. Rumori, G. T. Palomino, *Microporous Mesoporous Mater.*, 190 (2014) 234
- [37] H. Frost, R. Q. Snurr, *J. Phys. Chem. C.*, 111 (2007), 18794
- [38] Z. Yong, V. Mata, A. E. Rodrigues, *Sep. Purif. Rev.*, 26 (2002) 195
- [39] M. T. Arpin, S. Yusup, *Can. J. Pure Appl. Sci.*, 5 (2011) 1391

- [40] A. M. Ruminski, K. J. Jeonx, J. J. Urban, *J. Mater. Chem.*, 21 (2011) 11486
- [41] T. K. Kim, K. J. Lee, J. Y. Cheon, J. H. Lee, S. H. Joo, H. R. Moon, *J. Am. Chem. Soc.*, 135 (2013) 8940
- [42] Y. Ding, G. Song, X. Zhu, R. Chen, Q. Liao, *RSC Adv.*, 5 (2015) 30929
- [43] Y. G. Ko, S. S. Shin, U. S. Choi, *J. Colloid Interface Sci.*, 361 (2011) 594
- [44] F. Shakerian, K. H. Kim, J. E. Szulejko, J. W. Park, *Applied Energy*, 148 (2015) 10
- [45] J. A. Cecilia, E. Vilarrasa-García, C. García-Sancho, R. M. A. Saboya, D. C. S. Azevedo, C. L. Cavalcante Jr., E. Rodríguez-Castellón, *Int. J. Greenh. Gas Control*, 52 (2016) 344
- [46] N. Linares, A. M. Silvestre-Albero, E. Serrano, J. Silvestre-Albero, J. Garcia-Martinez, *Chem. Soc. Rev.*, 43 (2014) 7681
- [47] A. Vinu, K. Ariga, S. Saravanamurugan, M. Hartmann, V. Murugesan, *Microporous Mesoporous Mater.*, 76 (2004) 91
- [48] H. K. Song, K.W. Cho, K. H. Lee, J. Non, *Cryst. Solids*, 242 (1998) 69
- [49] M. Bhagiyalakshmi, J. Y. Lee, H. T. Jang, *Int. J. Greenh. Gas Con.*, 4 (2010) 51
- [50] J. Fernandez, F. Gonzalez, C. Pesquera, C. Blanco, M. J. Renedo, *Ind. Eng. Chem. Res.*, 49 (2010) 2986
- [51] H. Zhao, W. Yan, Z. Bian, J. Hu, H. Liu, *Solid State Sci.*, 14 (2012) 250
- [52] L. Qiming, M. Juanjuan, Z. Yuan, W. Tianhe, *Wuhan Univ. J. Nat. Sci.*, 19 (2014) 111
- [53] Y. Bang, S. J. Han, S. Kwon, V. Hiremath, I. K. Song, J. G. Seo, *J. Nanosci. Nanotechnol.*, 14 (2014) 8531
- [54] D. P. Harrison, *Greenhouse Gas Control Technologies* 7, 2 (2005) 1101
- [55] J. Cossy, S. Arseniyadis, C. Meyer, *Metathesis in natural product synthesis: strategies, substrates and catalysts*, Wiley: New Jersey, USA, 2010; Vol. 1
- [56] K. Grela, *Olefin Metathesis: Theory and Practise*, Wiley: New Jersey, USA, 2014; Vol. 1
- [57] K. J. Ivin, J. C. Mol, *Olefin Metathesis and Metathesis Polymerization*, Academic Press, London, 1997
- [58] L. Delaude, A. F. Noels, 2005. Metathesis. Kirk-Othmer Encyclopedia of Chemical Technology.
- [59] J. L. Herisson, Y. Chauvin, *Makromol. Chem.*, 141 (1971) 161
- [60] D. Astruc, *New J. Chem.*, 29 (2005) 42

- [61] K. Tanaka, K. Miyahara, *J. Chem. Soc., Chem. Commun.*, (1979) 314
- [62] P. Sledz, M. Mauduit, K. Grela, *Chem. Soc. Rev.*, 37 (2008) 2433
- [63] R. H. Grubbs, *Handbook of Metathesis*; Wiley: Weinheim, Germany, 2003; Vol. 3
- [64] K. B. Wagener, F. J. Gomez, *Encyclopedia of Materials: Science and Technology*, 2008, 48
- [65] S. Blechert, S. J. Connon, *Angew. Chem. Int. Ed.*, 42 (2003) 1900
- [66] A. K. Chatterjee, T. Choi, D. P. Sanders, R. H. Grubbs, *J. Am. Chem. Soc.*, 125 (2003) 11360
- [67] N. Holub, S. Blechert, *Chem. Asian J.*, 2 (2007) 1064
- [68] A. M. Lozano-Vila, S. Monsaert, A. Bajek, F. Verpoort, *Chem. Rev.*, 110 (2010) 4865
- [69] S. Monsaert, A. L. Vila, R. Drozdak, P. V. Der Voort, F. Verpoort, *Chem. Soc. Rev.*, 38 (2009) 3360
- [70] R. H. Grubbs, *Handbook of Metathesis*; Wiley: Weinheim, Germany, 2003; Vol. 1
- [71] J. C. Mol, *Catal. Today*, 51 (1999) 289
- [72] K. Ziegler, E. Holzkamp, H. Breil, H. Martin, *Angew. Chem.*, 16 (1955) 67
- [73] H. S. Eleuterio, German Pat. 1072811, Du Pont de Nemours & Co, 1960
- [74] G. Natta, G. Dall'Asta, L. Porri, *Makromol. Chem.*, 81 (1965) 253
- [75] G. Natta, *Angew. Chem., Int. Ed. Engl.*, 3 (1964) 723
- [76] G. P. Chiusoli, P. M. Maitlis, Eds.; *Metal-catalysis in Industrial Organic Processes*; Royal Society of Chemistry: Cambridge, United Kingdom, 2006
- [77] J. C. Mol, *J. Mol. Catal. A*, 213 (2004) 39
- [78] R. R. Schrock, *J. Am. Chem. Soc.*, 96 (1974) 6796
- [79] R. R. Schrock, S. M. Rocklage, J. H. Wengrovius, G. Rupprecht, J. Feldmann, *J. Mol. Catal.*, 8 (1980) 73
- [80] J. H. Wengrovius, R. R. Schrock, M. R. Churchill, J. R. Missert, W. J. Youngs, *J. Am. Chem. Soc.*, 102 (1980) 4515
- [81] B. M. Novak, R. H. Grubbs, *J. Am. Chem. Soc.*, 110 (1988) 7542
- [82] S. T. Nguyen, L. K. Johnson, R. H. Grubbs, *J. Am. Chem. Soc.*, 114 (1992) 3974
- [83] R. R. Schrock, A. H. Hoveyda, *Angew. Chem. Int. Ed.*, (2003) 4592
- [84] T. Trnka, R. H. Grubbs, *Acc. Chem. Res.*, 34 (2001) 18
- [85] R. R. Schrock, C. Czekelius, *Adv. Synth. Catal.*, 349 (2007) 55

- [86] S. Kotha, M. K. Dipak, *Tetrahedron*, 68 (2012) 397
- [87] S. S. Zhu, D. R. Cefalo, J. Y. Jamieson, W. M. Davis, A. H. Hoveyda, R. R. Schrock, *J. Am. Chem. Soc.*, 121 (1999) 8251
- [88] R. Singh, R. R. Schrock, P. Muller, A. H. Hoveyda, *J. Am. Chem. Soc.*, 129 (2007) 12654
- [89] I. Ibrahim, M. Yu, R. R. Schrock, A. H. Hoveyda, *J. Am. Chem. Soc.*, 131 (2009) 3844
- [90] A. H. Hoveyda, R. R. Schrock, *Nature*, 471 (2011) 461
- [91] G. C. Fu, R. H. Grubbs, *J. Am. Chem. Soc.*, 114 (1992) 5426
- [92] G. C. Fu, S. T. Nguyen, R. H. Grubbs, *J. Am. Chem. Soc.*, 115 (1993) 9856
- [93] V. Dragutan, I. Dragutan, A. T. Balaban, *Platinum Metals Rev.*, 44 (2000) 112
- [94] P. Schwab, M. B. France, J.W. Ziller, R. H. Grubbs, *Angew. Chem., Int. Ed.*, 34 (1995) 2039
- [95] K. A. Burdett, L. D. Harris, P. Margl, B. R. Maughon, T. Mokhtar-Zadeh, P. C. Saucier, E. P. Wasserman, *Organometallics*, 23 (2004) 2027
- [96] T. Nicola, M. Brenner, K. Donsbach, P. Kreye, *Org. Process Res. Dev.*, 9 (2005) 513
- [97] M. Scholl, S. Ding, Ch. W. Lee, R. H. Grubbs, *Org. Lett.*, 1 (1999) 953
- [98] J. Cossy, S. Arseniyadis, C. Meyer, *Metathesis in natural product synthesis*, Wiley-VCH: Weinheim, Germany, 2010
- [99] E. Colacino, J. Martinez, F. Lamaty, *Coord. Chem. Rev.*, 251 (2007) 726
- [100] M. S. Sanford, M. Ulman, R. H. Grubbs, *J. Am. Chem. Soc.*, 123 (2001) 749
- [101] J. A. Love, J. P. Morgan, T. M. Trnka, R. H. Grubbs, *Angew. Chem. Int. Ed.* 41 (2002) 4035
- [102] J. S. Kingsbury, J. P. A. Harrity, P. J. Bonitatebus, Jr., A. H. Hoveyda, *J. Am. Chem. Soc.*, 121 (1999) 791
- [103] A. H. Hoveyda, D. G. Gillingham, J. J. Van Veldhuizen, O. Kataoka, S. B. Garber, J. S. Kingsbury, J. P. A. Harrity, *Org. Biomol. Chem.*, 2 (2004) 8
- [104] D. Bek, H. Balcar, N. Žilková, A. Zukal, M. Horáček, J. Čejka, *ACS Catal.*, 1 (2011) 709
- [105] T. Vorfalt, K. J. Wannowius, H. Plenio, *Angew. Chem., Int. Ed.*, 49 (2010) 5533
- [106] I. W. Ashworth, I. H. Hillier, D. J. Nelson, J. M. Percy, M. A. Vincent, *Chem. Commun.*, 47 (2011) 5428
- [107] J. M. Bates, J. A. M. Lummiss, G. A. Bailey, D. E. Fogg, *ACS Catal.*, 4 (2014) 2384

- [108] J. A. Love, M. S. Sanford, M. W. Day, R. H. Grubbs, *J. Am. Chem. Soc.*, 125 (2003) 10103
- [109] K. Skowerski, J. Pastva, S. J. Czarnocki, J. Janošková, *Org. Process Res. Dev.*, 19 (2015) 872
- [110] S. B. Garber, J. S. Kingsbury, B. L. Gray, A. H. Hoveyda, *J. Am. Chem. Soc.*, 122 (2000) 8168
- [111] S. Gessler, S. Randl, S. Blechert, *Tetrahedron Lett.*, 41 (2000) 9973
- [112] K. M. Kuhn, J. B. Bourg, C. K. Chung, S. C. Virgil, R. H. Grubbs, *J. Am. Chem. Soc.*, 131 (2009) 5313
- [113] J. M. Basset, R. Psaro, D. Roberto, R. Ugo (Eds), *Modern Surface Organometallic Chemistry*, Wiley-VCH, Weinheim, 2009
- [114] D. C. Sherrington, A. P. Kybett, *Supported Catalysts and Their Applications*, Royal Society of Chemistry, Cambridge, U.K., 2001
- [115] B. Van Berlo, K. Houthoofd, B. F. Sels, P. A. Jacobs, *Adv. Synth. Catal.*, 350 (2008) 1949
- [116] T. Shinde, N. Žilková, V. Hanková, H. Balcar, *Catal. Today*, 179 (2012) 123
- [117] H. Balcar, T. Shinde, N. Žilková, Z. Bastl, *Beilstein J. Org. Chem.*, 7 (2011) 22
- [118] P. H. Deshmukh, S. Blechert, *Dalton Trans.*, (2007) 2479
- [119] K. Vehlow, S. Maechling, K. Kohler, S. Blechert, *J. Organomet. Chem.*, 691 (2006) 5267
- [120] P. Nieczypor, W. Buchowicz, W. J. N. Meester, F. P. J. T. Rutjes, J. C. Mol, *Tetrahedron Lett.*, 42 (2001) 7103
- [121] K. H. Park, S. Kim, Z. K. Chung, *Bull. Korean Chem. Soc.*, 29 (2008) 2057
- [122] A. Monge-Marcet, R. Pleixats, X. Cattoën, M. W. C. Man, *Tetrahedron*, 69 (2013) 341
- [123] X. Elias, R. Pleixats, M. W. C. Man, J. J.E. Moreau, *Adv. Synth. Catal.*, 349 (2007) 1701
- [124] L. Jafarpour, M. P. Heck, C. Baylon, H. M. Lee, C. Mioskowski, S. P. Nolan, *Organometallics*, 21 (2002) 671
- [125] D. Fischer, S. Blechert, *Adv. Synth. Catal.*, 347 (2005) 1329
- [126] A. Dewaele, B. Van Berlo, J. Dijkmans, P. A. Jacobs, B. F. Sels, *Catal. Sci. Technol.*, 6 (2016) 2580
- [127] H. Balcar, D. Bek, J. Sedlaček, J. Dědeček, Z. Bastl, M. Lamač, *J. Mol. Catal. A: Chem.*, 332 (2010) 19

- [128] A. Michrowska, K. Mennecke, U. Kunz, A. Kirschning, K. Grela, *J. Am. Chem. Soc.*, 128 (2006) 13261
- [129] A. Kirschning, K. Harmrolfs, K. Mennecke, J. Messinger, U. Schon, K. Grela, *Tetrahedron Lett.*, 49 (2008) 3019
- [130] Special issue: Adamski, J., Ed.; The International Workshop on 11 β and 17 β Hydroxysteroid Dehydrogenases. *Mol. Cell. Endocrinol.*, 248 (2006) 1
- [131] D. Astruc, *Organometallic Chemistry and Catalysis*, Springer-Verlag, Berlin, Germany, 2007
- [132] J. O. Krause, S. Lubbad, O. Nuyken, M. R. Buchmeiser, *Adv. Synth. Catal.*, 345 (2003) 996
- [133] L. Yang, M. Mayr, K. Wurst, M. R. Buchmeiser, *Chem. - Eur. J.*, 10 (2004) 5761
- [134] T. S. Halbach, S. Mix, D. Fischer, S. Maechling, J. O. Krause, C. Sievers, S. Blechert, O. Nuyken, M. R. Buchmeiser, *J. Org. Chem.*, 70 (2005) 4687
- [135] D. C. Braddock, K. Tanaka, D. Chadwick, V. P. W. Bohm, M. Roeper, *Tetrahedron Lett.*, 48 (2007) 5301
- [136] B. Marciniak, S. Rogalski, M. J. Potrzebowski, C. Pietraszuk, *ChemCatChem.*, 3 (2011) 904
- [137] D. Bek, N. Žilková, J. Dědeček, J. Sedláček, H. Balcar, *Top Catal.*, 53 (2010) 200
- [138] D. Bek, R. Gawin, K. Grela, H. Balcar, *Catal. Commun.*, 21 (2012) 42
- [139] M. Gruttadauria, F. Giacalone, R. Noto, *Green Chem.*, 15 (2013) 2608
- [140] M. Ahmed, A. G. M. Barrett, D. C. Braddock, S. M. Cramp, P. A. Procopiou, *Tetrahedron Lett.*, 40 (1999) 8657
- [141] J. S. Kingsbury, A. H. Hoveyda, *J. Am. Chem. Soc.*, 127 (2005) 4510
- [142] M. Bieniek, A. Michrowska, D. L. Usanov, K. Grela, *Chem. Eur. J.*, 14 (2008) 806
- [143] T. Vorfalt, K. J. Wannowius, V. Thiel, H. Plenio. *Chem. Eur. J.*, 16 (2010) 12312
- [144] M. L. H. Green, *J. Organomet. Chem.*, 500 (1995) 127
- [145] F. Wanga, L. Liua, W. Wanga, S. Li, M. Shi, *Coord. Chem. Rev.*, 256 (2012) 804
- [146] S. C. Schurer, S. Gessler, N. Buschmann, S. Blechert, *Angew. Chem. Int. Ed.*, 112 (2000) 4062

- [147] M. Mayr, B. Mayr, M. R. Buchmeiser, *Angew. Chem. Ind. Ed.*, 113 (2001) 3957; M. Mayr, D. Wang, R. Kroll, N. Schuler, S. Pruhs, A. Furstner, M. R. Buchmeiser, *Adv. Synth. Catal.*, 347 (2005) 484
- [148] M. Mayr, M. R. Buchmeiser, K. Wurst, *Adv. Synth. Catal.*, 344 (2002) 712
- [149] S. Pruhs, C.W. Lehmann, A. Furstner, *Organometallics*, 23 (2004) 280
- [150] J. P. Gallivan, J. P. Jordan, R. H. Grubbs, *Tetrahedron Lett.*, 46 (2005) 2577
- [151] X. Elias, R. Pleixats, M. Wong Chi Man, J. J. E. Moreau, *Adv. Synth. Catal.*, 348 (2006) 751
- [152] A. Monge-Marceta, R. Pleixats, X. Cattoenb, M. W. C. Man, *J. Mol. Catal. A: Chem.*, 357 (2012) 59
- [153] K. Mennecke, K. Grela, U. Kunz, A. Kirschning, *Synlett*, 19 (2005) 2948
- [154] S. T. Nguyen, R. H. Grubbs, *J. Organomet. Chem.*, 497 (1995) 195
- [155] K. Melis, D. De Vos, P. Jacobs, F. Verpoort, *J. Mol. Catal. A: Chem.*, 169 (2001) 47
- [156] H. Balcar, J. Čejka, *Macromol. Symp.*, 293 (2010) 43
- [157] T. Ookoshi, M. Onaka, *Chem. Commun.*, (1998) 2399
- [158] P. Topka, H. Balcar, J. Rathouský, N. Žilková, F. Verpoort, J. Čejka, *Microporous Mesoporous Mater.*, 96 (2006) 44
- [159] D. J. Nelson, S. Manzini, C. A. Urbina-Blanco, S. P. Nolan, *Chem. Commun.*, 50 (2014) 10355
- [160] A. Zukal, M. Thommes, J. Čejka, *Microporous Mesoporous Mater.*, 104 (2007) 52
- [161] J. M. Kim, S. K. Kim, R. Ryoo, *Chem. Commun.*, 2 (1998) 259
- [162] C. Z. Yu, B. Z. Tian, J. Fan, G. D. Stucky, D. Y. Zhao, *J. Am. Chem. Soc.*, 124 (2002) 4556
- [163] H. Yan, C. Blanford, B.T. Holland, W. Smyrl, A. Stein, *Chem. Mater.*, 12 (2000) 1134
- [164] S. Lowell, J. E. Shields, M. A. Thomas, M. Thommes, *Characterization Of Porous Solids And Powders: Surface Area, Pore Size And Density*, Kluwer Academic Publisher, Dordrecht, 2004, Springer
- [165] Y. L. Wei, Y. Cao, J. H. Zhu, X. W. Yan, *Chin. J. Inorg. Chem.*, 19 (2003) 233
- [166] M. Kruk, M. Jaroniec, A. Sayari, *Langmuir*, 13 (1997) 6267
- [167] S. W. Bian, J. Baltrusaitis, P. Galhotra, V. H. Grassian, *J. Mater. Chem.*, 20 (2010)

- [168] I. G. Shenderovich, G. Buntkowsky, A. Schreiber, E. Gedat, S. Sharif, J. Albrecht, N. S. Golubev, G. H. Findenegg, H. H. Limbach, *J. Phys. Chem. B*, 107 (2003) 11924
- [169] A. Zukal, H. Šiklova, J. Čejka, *Langmuir*, 24 (2008) 9837
- [170] A. Zukal, J. Jagiello, J. Mayerová, J. Čejka, *Phys. Chem. Chem. Phys.*, 13 (2011) 15468
- [171] D. Nachtigallová, O. Bludský, C. O. Arean, R. Bulanek, P. Nachtigall, *Phys. Chem. Chem. Phys.*, 8 (2006) 4849
- [172] P. Nachtigall, M. R. Delgado, D. Nachtigallová, C. O. Arean, *Phys. Chem. Chem. Phys.*, 14 (2012) 1552
- [173] B. Aziz, G. Zhao, N. Hedin, *Langmuir*, 27 (2011) 3822
- [174] A. Zukal, A. Pulido, B. Gil, P. Nachtigall, O. Bludský, M. Rubeš, J. Čejka, *Phys. Chem. Chem. Phys.*, 12 (2010), 6413
- [175] V. Dufaud, M. E. Davis, *J. Am. Chem. Soc.*, 125 (2003) 9403
- [176] J. Blumel, *Coordin. Chem. Rev.*, 252 (2008) 2410
- [177] P. Topka, Ph.D. Thesis, Charles University, Prague, 2008
- [178] H. Staub, R. Guillet-Nicolas, N. Even, L. Kayser, F. Kleitz, F.-G. Fontaine, *Eur. J. Chem.*, 17 (2011) 4254
- [179] K. Jarzemska, S. Seal, K. Wozniak, A. Szadkowska, M. Bieniek, K. Grela, *Chem-CatChem.*, 1 (2009) 144
- [180] R. R. Schrock, J. S. Murdzek, G. C. Bazan, J. Robbins, M. Di Mare, M. O'Regan, *J. Am. Chem. Soc.*, 112 (1990) 3875
- [181] M. Scholl, T. M. Trnka, J. P. Morgan, R. H. Grubbs, *Tetrahedron Lett.*, 40 (1999) 2247
- [182] T. Ritter, A. Hejl, A. G. Wenzel, T. W. Funk, R. H. Grubbs, *Organometallics*, 25 (2006) 5740
- [183] S. B. Pu, J. B. Kim, M. Seno, T. Inui, *Microporous Mater.*, 10 (1997) 25
- [184] H. Yang, Z. Ma, Y. Wang, Y. Wang, L. Fang, *Chem. Commun.*, 46 (2010) 8659
- [185] S. Polarz, B. Volker, F. Jeremias, *Dalton Trans.* 39 (2010) 577
- [186] A. Kabro, G. Ghattas, T. Roisnel, C. Fischmeister, Ch. Bruneau, *Dalton Trans.*, 41 (2012) 3695

- [187] S. B. Garber, J. S. Kingsbury, B. L. Gray, A. H. Hoveyda, *J. Am. Chem. Soc.*, 122 (2000) 8168
- [188] N. T. S. Phan, M. Van Der Sluys, C. W. Jones, *Adv. Synth. Catal.*, 348 (2006) 609
- [189] Guideline on the specification limits for residues of metal catalysts or metal reagents, Europea] A. Kabro, G. Ghattas, Thierry Roisnel, C. Fischmeister, Ch. Bruneau, *Dalton Trans.*, 41 (2012) 3695n Medicines Agency; http://www.ema.europa.eu/docs/en_GB/document_library/Scientific_guideline/2009/09/WC500003586.pdf (accessed September 26, 2016)
- [190] J. Wegner, S. Ceylan, A. Kirschning, *Chem. Commun.*, 47 (2011) 4583
- [191] A. Tracz, M. Matczak, K. Urbaniak, K. Skowerski, *Beilstein J. Org. Chem.*, 11 (2015) 1823
- [192] I. C. Stewart, T. Ung, A. A. Pletnev, J. M. Berlin, R. H. Grubbs, Y. Schrodi, *Organic Lett.*, 9 (2007) 1589
- [193] F. Grisi, A. Mariconda, C. Costabile, V. Bertolasi, P. Longo, *Organometallics*, 28 (2009) 4988
- [194] J. C. Chadwick, R. Duchateau, Z. Freixa, P. W. N. M. van Leeuwen, *Homogeneous catalysts: Activity – Stability – Deactivation*, Wiley: Weinheim, Germany, 2011; Vol. 1
- [195] X. Elias, R. Pleixats, M. Wong Chi Man, *Tetrahedron*, 64 (2008) 6770
- [196] T. Ritter, A. Hejl, A. G. Wenzel, T. W. Funk, R. H. Grubbs, *Organometallics*, 25 (2006) 5740
- [197] V. Dragutan, A. Demonceau, I. Dragutan, E. Finkelshtein, Eds.; Springer Science Netherlands, (2010) 49
- [198] Y. Zhang, J. Fei, Y. Yu, X. Zheng, *Catal. Commun.*, 5 (2004) 643
- [199] A. B. P. Lever, *Inorganic electronic spectroscopy*; Elsevier: Amsterdam, 1984
- [200] J. Zelin, A. F. Trasarti, C. R. Apesteguía, *Catal. Commun.*, 42 (2013) 84
- [201] E. B. Pentzer, T. Gadzikwa, S. T. Nguyen, *Org.Lett.*, 10 (2008) 5613
- [202] K. Skowerski, J. Białecki, A. Tracz, T. K. Olszewski, *Green Chem.*, 16 (2014) 1125
- [203] M. Smolen, M. Kędziołek, K. Grela, *Catal. Comm.*, 44 (2014) 80

7. Enclosures

- 1) Arnošt Zukal, Jakub Pastva, Jiří Čejka.
MgO-modified mesoporous silica's impregnated by potassium carbonate for carbon dioxide adsorption.
Microporous and Mesoporous Materials 167 (2013) 44 – 50.
- 2) Jakub Pastva, Jiří Čejka, Naděžda Žilková, Oto Mestek, Mojca Rangus, Hynek Balcar.
Hoveyda-Grubbs first generation type catalyst immobilized on mesoporous molecular sieves.
Journal of Molecular Catalysis A: Chemical 378 (2013) 184 – 192.
- 3) Jakub Pastva, Stefan J. Czarnocki, Jiří Čejka, Naděžda Žilková, Krzysztof Skowerski, Hynek Balcar.
Ru based complexes immobilized on mesoporous silica via quaternary ammonium tag.
ACS Catalysis 4 (2014) 3227 – 3236.